Aerial Optical Fibres in Telecommunication Systems: SOP and PMD Monitoring, and Tolerance of Modulation Formats

Winston Tumps Ireeta

Submitted to the Faculty of Science, Nelson Mandela Metropolitan University, in fulfillment of the requirements for the degree of

PHILOSOPHIAE DOCTOR

Promoter: Prof. Andrew W. R. Leitch

Optical Fibre Research Unit, Department of Physics
Nelson Mandela Metropolitan University
South Campus
Lower Ground, Building 13
6031, Port Elizabeth
SOUTH AFRICA

November 2010

DECLARATION

I, **Winston Tumps Ireeta** with student number **209091059**, hereby declare that this thesis for my Ph.D. qualification is my own work and that it has not previously been submitted for assessment to another University or for another qualification.

Signature:……..

Date:…….

To my beloved dad, Jonathan Bihondo Ireeta (RIP), and sister, Jacqueline Tumwebaze Abooki (RIP).

"I know we shall meet again"

ACKNOWLEDGEMENTS

Like within almost any research group, I have not been working alone. Quite a number of people have been of tremendous help in this particular project and hence deserve a great deal of recognition. I would like to first of all thank my promoter, Prof. Andrew W. R. Leitch, for accepting me as a Ph.D. student and for all his guidance and support. I also owe Dr. Lorinda Wu, who was my co-promoter before she left for greener pastures, a debt of gratitude for all her help and for the many interesting discussions we had during this study. Special thanks to Prof. Andrea Galtarossa of the University of Padova, Italy, for the lectures he administered to our research group during his visit to South Africa. The research articles you gave us plus those lectures helped a lot to better my understanding of the PMD topic.

I would also like to extend my sincere gratitude to Prof. Ernest van Dyk of the Department of Physics, NMMU, for his presentation made during his visit to Makerere University, Kampala, Uganda in 2008. It was from this presentation that I picked interest in coming down here to NMMU and study. Acknowledgements are also extended to all other members of staff in the Department of Physics for all their support during my stay in Port Elizabeth. I am very thankful to Mrs. Alta Beer for the excellent administrative support she rendered me during my stay at NMMU.

The encouragements I received from Prof. E. J. K. B. Banda, Dr. F. M. D'Ujanga (HOD), Prof. Y. Kaahwa, all of the Department of Physics, and Prof. J. Y. T. Mugisha (Dean, Science) of Makerere University cannot go unappreciated.

I am grateful to Telkom SA staff for their invaluable support towards field work data collection for this project especially at St. Albans transmission exchange station in Port Elizabeth. Sincere thanks to the South African Weather Service for the supply of weather information.

Financial support of the project funders: Telkom South Africa (Pty) Ltd, African Laser Centre (ALC), National Research Foundation (NRF), National Laser Centre (NLC), the Technology and Human Resources for Industry Program (THRIP), Ingoma Communication Services (Pty) Ltd, Hezeki Contracting (Pty) Ltd, and Dartcom (Pty) Ltd is sincerely appreciated as well as the bursary I received from NMMU and funding from the Department of Staff Development, Makerere University.

I also thank my colleagues in the Optical Fibre Research Unit as well as all the rest in the Department of Physics for providing a friendly and stimulating environment for me. Sincere thanks to Dr. Willy Okullo, Hassan Ddumba and David Ssevviiri, all from Uganda, with whom I was with during my studies at NMMU. We comforted one another during those times we missed our families. Cannot forget the online chats I had on the "kimeeza" with BSK, JK, GK, JMK, MKN, HN, CSS, GIM and DDW. They used to make me feel as though I was home.

The daily prayers of my mum, Mrs. Gladys Norah Ireeta, are appreciated. The support from my sister, Sharon Nabasa Ireeta, and brother, Edson Munanura Ireeta, during my stay away from home is also appreciated.

Last but not least, special thanks to my wife, Mrs. Doreen Karungi Ireeta, and my son, Jonathan Asbjørn Atuhaire. I am indebted for the loneliness caused during my stay away from you during this research.

Winston Tumps Ireeta
Port Elizabeth, South Africa
30 November 2010 (winston.ireeta@live.nmmu.ac.za)

SUMMARY

The topic of this thesis is aerial optical fibres in telecommunication systems: state of polarization (SOP) and polarization mode dispersion (PMD) monitoring and tolerance of modulation formats. Errors in optical fibre telecommunication systems are introduced when these polarization effects (SOP and PMD) change. These changes are so intense especially in aerial optical fibres. Part of the backbone of South Africa's national grid includes long distances of aerial optical fibre between transmission exchange stations. The work in this thesis can be divided into three parts which all deal with the major aspects of PMD in deployed aerial optical fibres: characterization, environmental effects plus other perturbations, and tolerance of different modulation formats.

In our work, SOP and PMD field measurements revealed that they both fluctuate more rapidly in deployed aerial optical fibres especially on windy and hot days. The SOP and PMD changes in the aerial optical fibres showed a significant correlation with these environmental parameters.

SOP and PMD are stochastic in nature due to changes in the properties of the optical fibres and its positions because of both intrinsic and extrinsic perturbations. In our work, with only 184 PMD values measured and obtained by use of the FTB-5700 single-ended dispersion analyzer, the predicted theoretical Gaussian fit was obtained with a mean of 0.47 ps and standard deviation of 0.08 ps. This small standard deviation was justification for its robustness and accuracy. The statistical distributions for first-order polarization mode dispersion (FO-PMD) and second-order polarization mode dispersion (SO-PMD) for the first time were experimentally confirmed when measured using the FTB-5700 single-ended dispersion analyzer instrument for deployed aerial optical fibres. We were also able to determine the time scale over which to compensate FO-PMD in deployed aerial fibres using the directional time drift autocorrelation function method. It is slightly higher than 390 s for SOP measurements made on a particular windy and hot day. This is due to the fact that the changes of the PMD vector are known to be slower than the SOP changes.

We also investigated the theoretical statistical distribution that corresponds to output SOP variations. The SOP variations can either be with wavelength (for buried fibre) or with time (for aerial fibre). Our results showed that the statistics of the relative SOP changes approached the distribution proposed by Foschini *et al.* (2000).

Advanced optical modulation formats have become a key ingredient in the design of modern state-of-the-art wavelength-division-multiplexed (WDM) optical transmission systems. In our work, we investigated which of these advanced modulation formats is best suited for the South African network especially on systems that have links of aerial optical fibres.

Keywords: *aerial optical fibre, polarization mode dispersion (PMD), principal states of polarization (PSP), state of polarization (SOP), first-order PMD, second-order PMD*

Contents

ACKNOWLEDGEMENTS ..... **IV**

SUMMARY ..... **V**

CHAPTER 1: INTRODUCTION **1**

CHAPTER 2: BASIC CONCEPTS OF POLARIZATION **6**

2.1 Polarization Mode Dispersion **6**

2.1.1 Birefringence 6

2.1.2 Polarization Mode Coupling 9

2.2 Polarization of Light **10**

2.2.1 Jones Vectors 11

2.2.2 Stokes Vectors 12

2.3 Principal States Model **15**

2.4 PMD Vector **15**

2.5 Second-Order PMD **19**

2.6 Random Birefringence Modelling **21**

2.7 Concatenation of PMD Vectors **24**

CHAPTER 3: MODULATION FORMATS **28**

3.1 Modulation Formats Classification **28**

3.1.1 Data Modulation Formats 29

3.1.2 Symbol Alphabet Size 29

3.1.3 Pulsed Modulation RZ Vs NRZ 30

3.2 Modulator Technologies **31**

3.3 Intensity Modulation Formats **32**

3.3.1 NRZ-OOK 32

3.3.2 RZ-OOK 34

3.3.3 CS-RZ 36

3.4 Advanced Modulation Formats 37
3.4.1 Correlative Coding and Partial-Response Formats 37
3.4.2 Vestigial Sideband and Single Sideband 38

3.5 Differential Phase Modulation Formats 39
3.5.1 Binary DPSK 39
3.5.2 DQPSK 40

3.6 Advanced Modulation Formats in Optical Networking 42
3.6.1 Loss, Amplification and Noise 42
3.6.2 WDM Crosstalk and Filter Narrowing 43
3.6.3 Chromatic Dispersion 44
3.6.4 Polarization Mode Dispersion 44
3.6.5 Fibre Kerr Nonlinearity 44
3.6.6 Nonlinearities and Modulation Formats 45

CHAPTER 4: PMD AND SOP MEASUREMENT TECHNIQUES 47

4.1 What it takes to describe PMD 47
4.1.1 Measurement Parameters 47
4.1.2 Inherent Uncertainty 48

4.2 Measurement Techniques 49
4.2.1 Time Domain Measurements 49
4.2.1.1 Time of flight technique 50
4.2.1.2 Low Coherence Interferometry 50
4.2.1.3 FTB-5500, FTB-5500B and FTB-5700 53
4.2.2 Frequency Domain Measurements 55
4.2.2.1 Jones Matrix Eigenanalysis 56
4.2.2.2 Müller Matrix Method 58
4.2.2.3 Poincaré Sphere Analysis 58
4.2.2.4 PA, SOP, and PS Techniques 58

CHAPTER 5: PERTURBATIONS AND ENVIRONMENTAL EFFECTS ON OPTICAL FIBRES 60

5.1 Mechanical Perturbations 60

5.2 Bend and Twist-Induced PMD 61

5.3 Interaction of the Aerial Optical Fibre Cable with Wind 63
5.3.1 Vortex Induced Vibrations 63

5.3.2 Cable Galloping 64
5.3.3 Wake Induced Vibrations 65
5.3.4 Wind Gusts 66

5.4 Effects of Temperature 68

5.5 Summary of Results 71

CHAPTER 6: PMD MEASUREMENTS AND COMPENSATION 72

6.1 Statistical Distributions of PMD 72
6.1.1 FO-PMD Statistical Distributions 73
6.1.2 SO-PMD Statistical Distributions 76

6.2 FTB-5700 Versus GINTY 77
6.2.1 First-Order PMD (FO-PMD) 77
6.2.2 First-Order PMD Coefficient 78
6.2.3 Second-Order PMD (SO-PMD) 79

6.3 PMD Variations 80
6.3.1 Fluctuation with Time 81
6.3.2 FO-PMD Fluctuation with Environmental Effects 82

6.4 States of Polarization Monitoring 83
6.4.1 SOP variations for the Patchcords excluding the FUT 85
6.4.2 SOP variations for the complete FUT 86

6.5 PMD Compensation 92

6.6 Summary of results 92

CHAPTER 7: STATISTICAL CHARACTERIZATION OF THE OUTPUT SOP 94

7.1 PMD Statistics 94
7.1.1 FO-PMD Statistics 95
7.1.2 SO-PMD Statistics 96

7.2 Statistical Theory of SOP 97

7.3 SOP Monitoring Experimental Setup 100

7.4 Rate of SOP Change Histograms 101

7.5 Summary of results **104**

CHAPTER 8: TOLERANCE OF DIFFERENT MODULATION FORMATS **105**

8.1 Transmitted Optical Spectra **105**

8.2 Simulation Model **106**

8.3 Performance Metrics for Analysis of Tolerance to PMD **107**

8.3.1 Eye Diagram 108

8.3.2 Bit-Error Rate 109

8.3.3 Q-factor 110

8.4 Modulation Format Tolerance with Change in the Transmission Rates **111**

8.5 Modulation Format Tolerance with Change in the Optical Fibre Length **114**

8.6 Summary of Results **116**

CHAPTER 9: CONCLUDING REMARKS **117**

9.1 Bending, Twisting and Environmental Effects on Optical Fibres **117**

9.2 PMD Monitoring and Compensation **118**

9.3 Output SOP Statistical Characterization **119**

9.4 Modulation Format's Tolerance to PMD **120**

APPENDIX A **122**

APPENDIX B **124**

APPENDIX C **126**

APPENDIX D **128**

REFERENCES **130**

CHAPTER 1

INTRODUCTION

One of the principle needs of people ever since the ancient times has been communication. This need has thus brought about the rapid interest in the development of communication systems for transmitting information from one distant place to another. Over many years, different forms of communications systems have been made. The drive behind all these motivations for each new form of communication system has been either to improve the transmission capacity, or to increase the data rate at which more and more information is sent, or to increase the distance over which information can be transmitted. Up to the nineteenth century, all communication systems operated at very low information rates and they also comprised of only optical or acoustical transmission links, for example, the first 'telegraph,' which was devised by a French engineer Claude Chappe in the 1790s, was an optical telegraph. Here operators at towers relayed signals from one hill top to the next by the movement of the arms of a semaphore (Hecht 1999, p.5).

Communication and access to information are vital necessities for a successful, vibrant economy, and nation. Optical communication systems have proven to be the most suitable method to relay large amounts of information at a low cost over very long distances. These days optical communication systems are the transport medium of almost all long-haul capacity information (Trischitta and Marra 1996). We truly live in the information age after the rapid growth of internet attests. Internet traffic has been growing annually at double-digit percent rates. Most of this growth is due to the growing demand for higher-bandwidth services in both the business and residential sectors: real time video files upload and download, photo sharing, music broadcast and sharing, internet browsing (especially now with the new applications such as Facebook, Twitter, YouTube etc), data exchange, TV live broadcasting and file backups (ECI Telecom 2008). These services, especially video are posing greater challenges for service providers. Single-mode optical fibre, the backbone of telecommunication networks and the internet, has gone through different developmental stages over the last few decades with the aim of overcoming some of these new challenges.

As the demand for communication and information increases, so does the need for reliable and high speed networks for transmission. Previously, optical telecommunications systems were restricted by the following factors; signal attenuation, multimodal dispersion and chromatic dispersion. Advances in technology for example the introduction of dispersion shifted single-mode fibres (DSFs), dispersion compensating fibres (DCFs), the improvement in source technology and the development of the erbium-doped fibre amplifiers (EDFAs) have helped solve these problems. The typical bit rates employed today are 10 to 40 Gb/s per channel (i.e. every channel in wavelength division multiplexing (WDM) systems where the capacity can be increased beyond the channel bit rate by simultaneously transmitting a large number of channels at different wavelengths in a single optical fibre) and the next generation optical transport systems running at 100 Gb/s per channel are ready, at least technically, to be deployed.

However, having overcome these initial challenges, polarization mode dispersion (PMD) has emerged as one of the most significant factors that limit the transmission performance in long-haul telecommunication systems (both on land and at sea) that carry many digitized signals simultaneously over long distances for high data rates operating at 10 Gb/s and above (Gibbon *et al.* 2008). It should be noted that most of the world's legacy fibres, including South Africa's, were deployed before PMD was a major concern. PMD is more pronounced in old ITU-T G.652 optical fibres compared to the newer ITU-T G.652, 653 and 655 optical fibres. Present day manufactured telecommunication optical fibres have PMDs of about $\leq$ 0.1 ps/km$^{1/2}$. However, it is very costly to upgrade the whole telecommunication network to these new optical fibres all at once. So, the operators today have to take a managed-growth approach, opting to upgrade networks incrementally.

Polarization Mode Dispersion is a form of modal dispersion where two different polarizations of light in a waveguide, which normally travel at the same speed, travel at different speeds due to random imperfections and asymmetries, causing random spreading of optical pulses. The origin of PMD lies in the combined effects of both birefringence and mode coupling. Materials which exhibit birefringence are those where the speed of light is not the same in all directions. Within the amorphous matrix of mechanically unstressed pure glass the SiO_2 molecules are randomly distributed. This then makes it a medium which is isotropic in the sense that the physical properties of the glass are uniformly random in all directions. However, when this glass is exposed to some form of stress, it will exhibit birefringence

since this stress will introduce regions of anisotropy within an otherwise amorphous glass matrix. Stress birefringence is due to both intrinsic and extrinsic factors. Intrinsic factors are permanent fibre features that can be introduced during the manufacturing process accidentally for example a non-circular core or non-symmetrical stress fields in the cladding around the core. Extrinsic factors are such stresses introduced during cabling and the deployment process. Environmental factors such as temperature, stress and fibre movement say wind for the case of an aerial optical fibre can also lead to changes in the birefringence (Cameron *et al*. 1998a). These effects cause the fibre PMD to vary stochastically in time making PMD particularly difficult to manage. Also, although amplifiers or other components such as add-drop multiplexers in an optical system may have constant birefringence, variable polarization rotations between them due to the environment cause these components to randomly add to the PMD of the total system (Kogelnik *et al*. 2002) . Within a single mode fibre, there exist random points of perturbation known as mode coupling sites, where energy may couple between the principle modes of adjacent segments. Mode coupling sites are introduced by variations in composition, geometry and strain within the fibre. These could have originated from the fibre preform during the fibre drawing process or even during the cabling process. Stress on the fibre, bends, twists and splices are also other extrinsic sources of mode coupling (Kaminow 1981).

In order to fulfill future capacity demands for next generation optical communication systems, state-of-the-art dispersion management will also be required to minimize nonlinear signal degradation. Advanced modulation formats can be used to improve the transmission performance and to achieve high spectral efficiency. Modulation is the process by which information is imposed onto a light stream. This can be realized by either directly varying the laser drive current with the information stream to produce a varying optical output power, or by use of an external modulator to modify a steady optical power level emitted by the laser. External modulation is needed for high speed streams (> 2.5 Gb/s) to minimize undesirable nonlinear effects such as chirping (Keiser 2000, p.180). Different modulation formats have been used in the recent years. These include: nonreturn-to-zero (NRZ) and return-to- zero (RZ). Recently ‘new’ modulation formats though that were used in radio communication have also been used as alternatives, for example RZ with narrow pulse widths; carrier suppressed return-to-zero (CS-RZ), single side band return-to-zero (SSB-RZ) and duobinary. Also, the recent introduction and use of phase modulation (which represents information as

variations in the instantaneous phase of a carrier wave) such as differential binary phase shift keying (DBPSK) and the four level differential quadrature phase shift keying (DQPSK) have been tested in the laboratories (Tokle 2004, p.118). Different modulation formats have different tolerances in deployed aerial and buried optical fibres of communication systems.

The legacy fibres pose the most serious challenge especially on the South African telecommunication network that has long links of aerial optical fibre and therefore the necessity for PMD mitigation/compensation in addition to accurate PMD and state of polarization (SOP) monitoring. In order to achieve this, we need to do extensive studies on the rate of change of SOPs on an aerial optical fibre link for a long period of time under different environmental conditions so as to track the fast changing SOPS to help determine the rate of PMD compensation for such links. In addition, there is the need for one to conceive, design, realize and test novel signal modulation techniques in a system context, which enable high capacity signal transport in deployed buried and aerial optical fibres with minimal losses for high speed optical telecommunication systems. These important issues will form the basis of this thesis.

Polarization-mode dispersion is a complex subject. However, a number of textbooks on this topic have been written to explain its theory and mathematical interpretations. In chapter 2, the general basic concepts of polarization are highlighted to enable the reader get a feel for this topic. In this chapter, PMD's physical origin is described with a more qualitative approach followed by its complication due to random mode coupling in the optical fibre. Thereafter, chapter 3 describes the different modulation formats used to transmit information/data. In this chapter, different modulation formats' technologies are given as well as the physical attributes of light that are used for information/data to be imposed. Tolerances of the different modulation formats in PMD-induced environments are also described. Chapter 4 presents the PMD and SOP measurement techniques that were used in this study. Both frequency and time domain techniques are described. From chapter 5 to chapter 8, the experimental results of this study are presented. In chapter 5, the bending and twisting effects of an optical fibre on its PMD are described as well as the impact of environmental parameters such as wind speed, wind gusts and temperature on the PMD of an aerial optical fibre on a link on the South African optical fibre network. Measurement of PMD and SOPs using two different interferometric techniques and the determination of the rate of PMD

compensation on an aerial optical fibre link are presented in chapter 6. In chapter 7, the statistical distributions of the rate of change of SOPs with respect to both time and wavelength are presented. A comparison of the tolerance of three modulation formats namely; DQPSK, RZ and NRZ on an aerial optical fibre network is simulated using commercially available software in chapter 8. Finally in chapter 9, a summary of important and vital findings of this study are presented.

CHAPTER 2

BASIC CONCEPTS OF POLARIZATION

2.1 Polarization Mode Dispersion

Polarization mode dispersion (PMD) originates from the small random *birefringences* that exist in optical fibres that arise during the manufacturing process. This *birefringence*, i.e. a polarization-dependent refractive index, arises from small disturbances in the ideal cylindrical symmetry of the optical fibre core (intrinsic factors) and also stresses, twisting and bends that are external to the fibre (extrinsic factors). Along the fibre, the random change of this birefringence leads to random polarization coupling between the modes. For the best description of how PMD arises in optical fibres, a short section of fibre with uniform birefringence within a long fibre span is considered. A concatenation of hundreds or thousands of such arbitrarily oriented birefringent elements is modelled as representation of a single-mode fibre.

2.1.1 Birefringence

The birefringence in optical fibres is expressed as the differential effective refractive index, propagation constant $\Delta\beta$, between the orthogonal polarization modes (Kogelnik *et al.* 2002),

$$\Delta\beta = \beta_S - \beta_f = \frac{\omega\eta_S}{c} - \frac{\omega\eta_f}{c} = \frac{\omega\Delta\eta}{c} = \frac{2\pi}{\lambda}\Delta\eta, \tag{2.1}$$

where ω is the angular optical frequency of the light, c is the speed of light in vacuum and $\Delta\eta = \eta_S - \eta_f > 0$ is the refractive index difference between the slow (s) and fast (f) axes, whereas λ is the light wave wavelength in vacuum. Besides the optical fibre being twisted, which causes circular birefringence (Ulrich and Simon 1979; Kogelnik *et al.* 2002; Galtarossa *et al.* 2009a), all other perturbations will generally create linear birefringence (Galtarossa *et al.* 2008a; Palmieri *et al.* 2010b) for two linearly polarized waveguide modes with their electric field vectors aligned symmetrically to the optical fibre axes.

For light travelling in an optical fibre, its state of polarization (SOP) can be changed because of birefringence as illustrated schematically in figure 2.1.

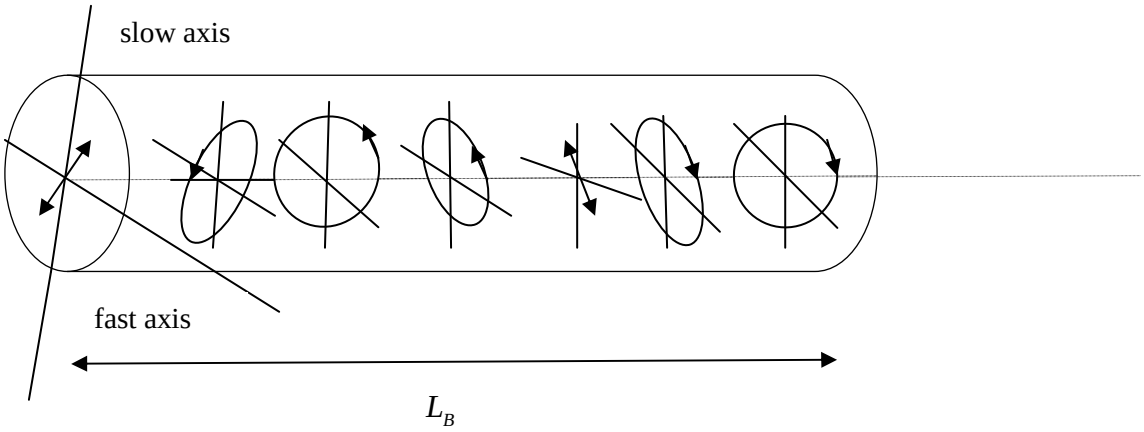

Figure 2.1: A short section of an optical fibre with uniform birefringence showing changes in the polarization state of light from linear to elliptic, circular, elliptic and then back to linear, etc.

In an optical fibre, there exist two orthogonal polarization states (eigenstates) which are not affected by birefringence. A decomposition of any polarization states into these two eigenstates can be done. For the short section/segment of the optical fibre having uniform birefringence we have considered, these eigenstates correspond to the birefringent axes of the segment i.e. the fast and slow axes. In figure 2.1, to ensure that both axes are equally excited, the input light wave was linearly polarized at 45º (Sunnerud 2001, p.6).

Using the differential refractive index together with the optical wavelength, we define a *beat length,* $L_B = \lambda/\eta$, as the propagation distance in which, between the two modes, a 2π phase difference accumulates or, equivalently, the polarization rotates through one periodic cycle. In standard telecommunication single mode fibres, $\Delta\eta$ is approximately 10^{-7}, which gives a beat length of 15.5 m at a wavelength of 1550 nm (Galtarossa *et al.* 2000b). However, polarization-maintaining fibres (PMF) are intentionally manufactured with large $\Delta\eta$ and beat lengths of approximately 3 mm (Kogelnik *et al.* 2002). The input polarizations of light together with the eigenpolarizations of the birefringent media are used to determine the particular states of polarization through which the light cycles. These two factors are generally arbitrary and unknown in a real fibre optic system.

Considering a short segment of optical fibre, in the time domain, the differential group-delay (DGD), $\Delta\tau$, is defined as the time delay between the two orthogonal principal states of polarization (PSP). This is illustrated in figure 2.2 where a pulse launched with equal power

on the two birefringent axes ends up with the two pulse components (that are orthogonal to one another) at the output with a difference in arrival times of (DGD), $\Delta\tau$.

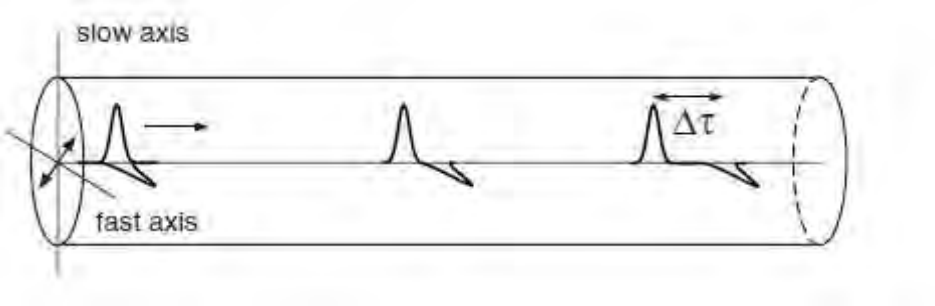

Figure 2.2: A short optical fibre segment showing the time-domain effect of PMD, with a pulse launched with equal power on the two birefringent axes, dispersed due to birefringence. The input state of polarization is oriented at 45º to the axes. At the output, the pulse components are separated by the DGD, $\Delta\tau$.

The DGD, $\Delta\tau$, is obtained by taking the angular frequency derivative of the difference in propagation constants of equation 2.1, i.e.

$$\Delta\tau = \frac{L}{\Delta v_g} = \frac{d}{d\omega}(\Delta\beta)L = \left(\frac{\Delta\eta}{c} + \frac{\omega}{c}\frac{d\Delta\eta}{d\omega}\right)L, \tag{2.2}$$

where Δv_g is the difference in group velocities between the orthogonal modes. The quantity $\Delta\tau/L$, sometimes called *intrinsic* PMD, is often expressed in units of picoseconds per kilometer of optical fibre length when a uniformly birefringent element (for example, a short optical fibre segment) is considered. However, in long fibres, the birefringence is always combined with random polarization mode coupling and hence the PMD will grow with the square root of the optical fibre length. More detailed discussions on this will be given in section 2.1.2.

In the frequency domain, if we consider a uniformly birefringent optical fibre in which linearly polarized light is launched at 45º to the axes, the output phase, $\phi = L\Delta\beta$, determines the output state of polarization. This phase changes with carrier frequency ($\omega_1 < \omega_2 < \omega_3 < \omega_4$) as illustrated in figure 2.3.

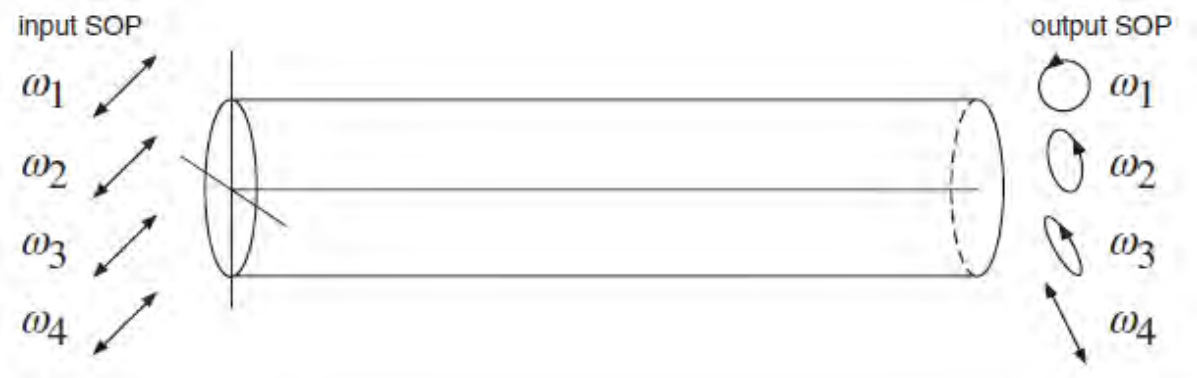

Figure 2.3: The changes in the output state of polarization (SOP) when the angular frequency is changed due to the PMD in the optical fibre. Note that $\omega_1 < \omega_2 < \omega_3 < \omega_4$.

The phase change with angular frequency is given by

$$\frac{\Delta\phi}{\Delta\omega} = \frac{d}{d\omega}(\Delta\beta)L = \Delta\tau . \tag{2.3}$$

Therefore, the PMD in an optical fibre system can be characterized in the frequency/wavelength domain. One of these domains is the Fourier transform of the other. For the polarization state to rotate through one cycle, the frequency separation is: $\Delta\omega = 2\pi/\Delta\tau$, where $\Delta\tau$ is the DGD.

2.1.2 Polarization Mode Coupling

In a short fibre segment, the DGD is easy to determine because the birefringence is additive. However, in today's long-haul high speed optical fibre transmission systems, the fibre lengths are in hundreds or thousands of kilometers and the birefringence ceases being additive. Along the fibre length, there exist random variations in the birefringence axes that cause polarization mode coupling i.e. the fast and slow polarization modes from one segment each decompose into both the fast and slow modes of the next segment, which in general will have different axes (Kogelnik *et al.* 2002). Polarization mode coupling may result from either localized stress during cabling, spooling and deployment, or from splices and components e.g. hinges (Li *et al.* 2010a) or from variations in the optical fibre drawing process or from intentional optical fibre spinning during the drawing process. All these factors will induce mode coupling at meter lengths. Therefore, long optical fibres are normally modelled as a

concatenation of many birefringent sections/segments whose birefringent axes randomly change along the fibre. This is illustrated in figure 2.4.

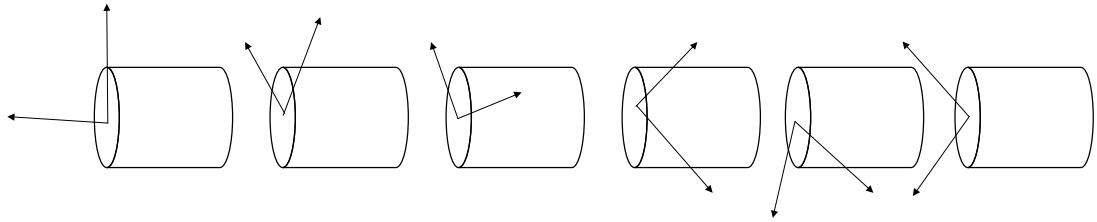

Figure 2.4: A concatenation of birefringent segments along an optical fibre length with their birefringent axes randomly changing.

The birefringence of each optical fibre section can either add or subtract from the total birefringence because of mode coupling and hence the DGD does not accumulate linearly with the fibre length (Rashleigh 1983). It has been shown that for long optical fibre spans, the DGD accumulates as a random walk in three dimensions and on average increases with the square root of the distance (Poole 1988a; Kogelnik *et al.* 2002). Since mode coupling is determined by the optical fibre's environment i.e. variations in, for example, external stresses, its influence on the DGD of the fibre is random. This in turn will lead to DGD of the optical fibre span becoming stochastic in nature and hence a statistical approach to PMD has to be adopted. This will be discussed in detail in chapter 6.

2.2 Polarization of Light

To better understand PMD and its definition, one must first consider polarization of light and how it is described mathematically. Light propagation in an optical fibre can be described by means of transverse electromagnetic waves. Let us consider two perpendicular and linearly polarized light waves that propagate through the same medium in the z direction. In complex notation, the two fields are represented by

$$\begin{aligned} \vec{E}_x(z,t) &= \hat{x}E_o a_x \exp i(\omega t - kz + \phi_x) \\ \vec{E}_y(z,t) &= \hat{y}E_o a_y \exp i(\omega t - kz + \phi_y) \end{aligned} \tag{2.4}$$

where k is the propagation constant and $\phi_y - \phi_x$ is the relative differential phase between the two field components. The resulting optical field is the vectorial sum of these two perpendicular fields in equation 2.4

$$\vec{E}(z,t) = \vec{E}_x(z,t) + \vec{E}_y(z,t) = \left[\hat{x}a_x E_o e^{i\phi x} + \hat{y}a_y E_o e^{i\phi y}\right] e^{i(\omega t - kz)} \tag{2.5}$$

From equation 2.5, the state of polarization of the light is completely determined by the relative amplitudes and phases of these components. Therefore, the focus should only be on the complex amplitude which can be written as a two-element matrix, or *Jones vector*, which we define in the following section.

2.2.1 Jones Vectors

According to Jones (1941), the polarization state of a light wave can be represented in terms of *Jones vectors* as,

$$\vec{j} = \frac{1}{|E_o|}\begin{pmatrix} E_{ox} \\ E_{oy} \end{pmatrix} = \begin{pmatrix} a_x e^{i\phi_x} \\ a_y e^{i\phi y} \end{pmatrix} \tag{2.6}$$

and when divided by $|E_o| = \sqrt{E_{ox}^2 + E_{oy}^2}$ is normalized giving $\sqrt{a_x^2 + a_y^2} = 1$. For illustration, $\vec{j} = \begin{pmatrix} \cos\theta \\ \sin\theta \end{pmatrix}$ represents a linearly polarized light wave with an angle θ to the x-axis and both field components are in phase, meaning that $\phi = \phi_x - \phi_y = 0$. For the right-hand circular polarization, $j = \frac{1}{\sqrt{2}}\begin{pmatrix} 1 \\ -i \end{pmatrix}$ and $\phi = \frac{\pi}{2}$ while the left-hand circular polarization, $j = \frac{1}{\sqrt{2}}\begin{pmatrix} 1 \\ i \end{pmatrix}$ with $\phi = -\frac{\pi}{2}$. These are special cases of the general elliptical polarization states that are given by $j = \begin{pmatrix} \cos\theta \\ \sin\theta e^{-i\phi} \end{pmatrix}$ with the assumption that $\phi_x = 0$. It should be noted that for every polarization state $\vec{j}_1$, there exists an orthogonal polarization state $\vec{j}_2$ such that

$$\vec{j}_1^{\dagger}\vec{j}_2 = 0, \tag{2.7}$$

where $\vec{j}^{\dagger}$ is the conjugate transpose of $\vec{j}$. When a linear optical element is inserted in the path of a propagating light wave, the effect on its polarization state is described mathematically by use of a complex 2×2 Jones matrix, A,

$$\vec{j}_{out} = A\vec{j}_{in}, \tag{2.8}$$

where $\vec{j}_{in}$ and $\vec{j}_{out}$ are the input and output polarization states, respectively.

Considering a birefringent medium in which the polarization dependent losses are negligible, the angular frequency dependent Jones matrix is expressed as

$$A(\omega) = \begin{pmatrix} a(\omega) & b(\omega) \\ -b(\omega) & a^{*}(\omega) \end{pmatrix} \tag{2.9}$$

where $a(\omega)$ and $b(\omega)$ are complex functions of the angular frequency of the light wave and $|a|^2 + |b|^2 = 1$ with $a^{*}(\omega)$ being the complex conjugate of $a(\omega)$.

2.2.2 Stokes Vectors

An arbitrary Jones vector can be described by two degrees of freedom. These two degrees of freedom can be interpreted as coordinates in a spherical coordinate system. Then each state of polarization will correspond to a point that is represented by a *Stokes vector,* $\vec{S} = (s_1, s_2, s_3)^T$, on a unit radius sphere called the Poincaré sphere (defined as a graphical tool or display device for instrumentation which is a convenient three dimensional aid for representing different polarization states of light). The three Cartesian coordinates are defined by (Born and Wolf 1980),

$$\begin{aligned} s_1 &= \frac{|E_x|^2 - |E_y|^2}{|E_o|^2} = \cos 2\theta \\ s_2 &= \frac{2\,\mathrm{Re}\left(E_x E_y^{*}\right)}{|E_o|^2} = \sin 2\theta \cos\phi \\ s_3 &= \frac{2\,\mathrm{Im}\left(E_x E_y^{*}\right)}{|E_o|^2} = \sin 2\theta \sin\phi \end{aligned} \tag{2.10}$$

The Poincaré sphere representation of the states of polarization is shown in figure 2.5.

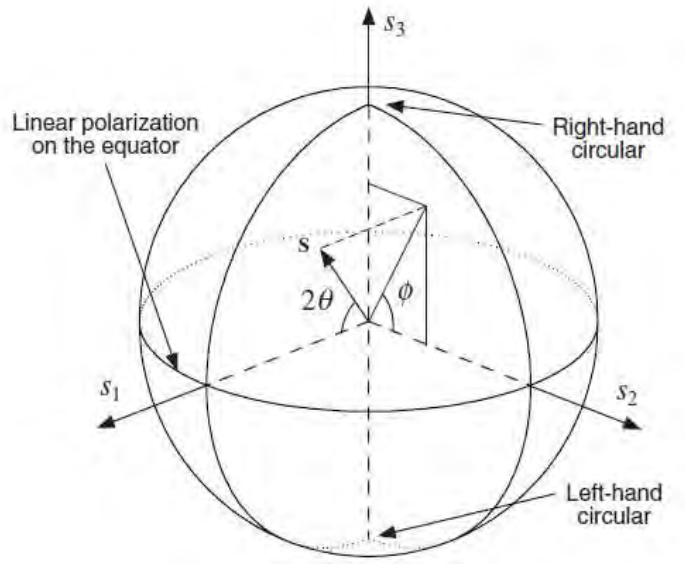

Figure 2.5: Stokes vector representation of the state of polarization of a light wave on a Poincaré sphere.

Along the Equator ($s_3 = 0$), as shown in figure 2.5, we have the linear states of polarization, at the North Pole ($s_3 = 1$), the right-hand circular polarization and at the South Pole ($s_3 = -1$), the left-hand circular polarization. The elliptical states of polarization are distributed continuously between the equator and the poles (Ulrich and Simon 1979; Rashleigh 1983).

In this coordinate system representation of the Stokes vectors, the orthogonal states of polarization have dot product, i.e. $s_1.s_2 = -1$, which means that they are antiparallel. It should also be noted of the existence of a fourth Stokes parameter (optical intensity),

$$s_0 = \frac{\left(|E_x|^2 + |E_y|^2 \right)}{|E_o|^2}, \tag{2.11}$$

that is used in describing non-polarized or partially polarized light.

When the light is completely polarized, we have

$$s_1^2 + s_2^2 + s_3^2 = s_0^2 \tag{2.12}$$

Then the *degree of polarization* (DOP) is defined as

$$DOP = \sqrt{\frac{s_1^2 + s_2^2 + s_3^2}{s_0^2}} \tag{2.13}$$

Like we did for the Jones vectors in section 2.2.1, the effects of a linear optical device on the polarization states of light can also be treated in matrix form in Stokes space. For this case, a Müller rotation matrix, M , multiplies with the input Stokes vectors to give the output Stokes vectors as shown in equation 2.14

$$\vec{s}_{out} = M\vec{s}_{in}. \tag{2.14}$$

For the case of a birefringent medium, M is a real 3×3 matrix that corresponds to a rigid rotation of the Poincaré sphere yet in a polarizing medium, all four Stokes parameters must be used and so M is a 4×4 matrix.

An example is the evolution of the states of polarization shown in figure 2.1 where an SOP that rotates around the sphere is considered. Suppose the input SOP, $\vec{s}_{in} = (0,0,1)^T$, rotates around the $s_1 -$ axis that corresponds to a Müller rotation matrix

$$M = \begin{pmatrix} 1 & 0 & 0 \\ 0 & \cos\phi & -\sin\phi \\ 0 & \sin\phi & \cos\phi \end{pmatrix}, \tag{2.15}$$

then the output SOP ,

$$\vec{s}_{out} = M\vec{s}_{in} = M\begin{pmatrix} 0 \\ 0 \\ 1 \end{pmatrix} = \begin{pmatrix} 0 \\ -\sin\phi \\ \cos\phi \end{pmatrix}. \tag{2.16}$$

2.3 Principal States Model

In a long length optical fibre, the propagation of a pulse/light wave is very complicated because of random polarization mode coupling and pulse splitting at every change in the local birefringent axes of the adjacent segments. However, even for long length fibres, at the optical fibre input there exists two special orthogonal polarization states that result in an output pulse which is not distorted to first order.

The Principal States Model which was first developed by Poole and Wagner (1986) is what is still being used today to characterize PMD. In this model, PMD can be characterized both in the time and in the frequency domain. In the time domain, the difference in arrival times of the decomposed pulses in the two orthogonal birefringent axes is the DGD. Then in the frequency domain, for a given fibre length, there exists a special pair of polarization states for every frequency called the *Principal States of Polarization* (PSPs). So, a PSP is defined as that input state of polarization whose output state of polarization is independent of frequency to first order. Note that this should be over a small frequency range.

PSPs are orthogonal as long as polarization-dependent losses are absent. Then for each pair of input PSPs there exist a corresponding pair of orthogonal PSPs at the optical fibre output. The optical fibre's transmission matrix is used to relate the input and output PSPs, just as any input state of polarization is related to a polarization at the output of an optical fibre. Using the common Stokes vector description of polarization, defined in section 2.2.2, the unit Stokes vectors, $\hat{p}_S$, of the input PSP are related to the output PSP unit Stokes vectors, $\hat{p}$, by the Müller rotation matrix, M as:

$$\hat{p} = M\hat{p}_S \tag{2.17}$$

2.4 PMD Vector

By use of the Principal States Model, the first-order PMD (FO-PMD) is given by the PMD vector (a vector in three-dimensional Stokes space)

$$\vec{\tau} = \Delta\tau\,\hat{p} \tag{2.18}$$

where $\hat{p}$ is the unit Stokes vector pointing in the direction of the fast PSP in Stokes polarization space while the vector $-\hat{p}$ points along the orthogonal slower axis and the magnitude, $\Delta\tau$, is the DGD. These two orthogonal unit Stokes vectors are 180º apart.

The input, $\vec{\tau}_S$, and output, $\vec{\tau}$, PMD vectors for an optical fibre are related by $\vec{\tau} = M\vec{\tau}_S$. It can then be shown that the angular frequency derivative of equation 2.14 will lead directly to the law of infinitesimal rotation,

$$(\vec{s}_{out})_\omega = \frac{d\vec{s}_{out}}{d\omega} = \vec{\tau} \times \vec{s}_{out}, \tag{2.19}$$

where $\vec{\tau}\times = M_\omega M^T$ and M^T is the transpose of M. This means that for a fixed input SOP, the output SOP, $\vec{s}_{out}$, will precess around $\vec{\tau}$ as the angular frequency is changed. The angle of precession is determined by the direction of $\vec{s}_{out}$ relative to $\vec{\tau}$ while the rate at which $\vec{s}_{out}$ precesses around $\vec{\tau}$ is determined by the magnitude, $\Delta\tau$.

As an illustration, if $\vec{s}_{in}$ is launched with equal power along the PSPs, $\left(\vec{s}_{out}\right)_\omega$ will have its largest value and the maximum change in the output state of polarization will occur for a frequency change $\Delta\omega$. The precession angle will have a magnitude $\phi = \Delta\tau\Delta\omega$, with ϕ being the angle of rotation on the Poincaré sphere. Then, if $\vec{s}_{out}$ is aligned with $\pm\vec{\tau}$, there will be no precession and the output state of polarization will not change with angular frequency. This is thus the postulate of a PSP. Therefore, equation 2.19 provides a precise mathematical definition of the PSP and of its length, $\Delta\tau$, the DGD . From this equation, we also note that there are only two PSPs corresponding to the two possible alignments of $\vec{s}_{out}$ with $\pm\vec{\tau}$.

A special fibre, the polarization maintaining fibre (PMF), has a constant PMD vector with its length, the DGD, and the direction $\hat{p}$ not changing with angular frequency. This leads to the output vector $\vec{s}_{out}$ tracing out a circle on the Poincaré sphere as the angular frequency is changed. This is illustrated in figure 2.6.

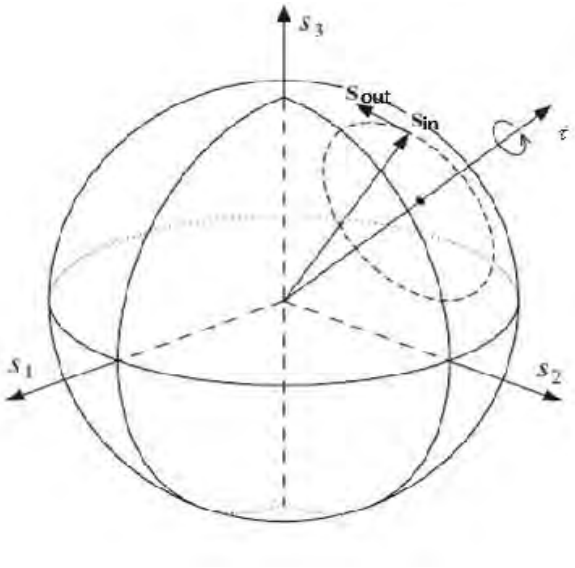

Figure 2.6: Illustration of the frequency domain behaviour of PMD in a short birefringent fibre for the state of polarization evolution versus frequency when the input state of polarization is fixed. It traces out a circle on the surface of the Poincaré sphere.

However, in real telecommunication optical fibres with random polarization mode coupling, the length and direction of the PMD vector changes with angular frequency. Two examples of the output SOP evolution as a function of angular frequency are shown in figure 2.7.

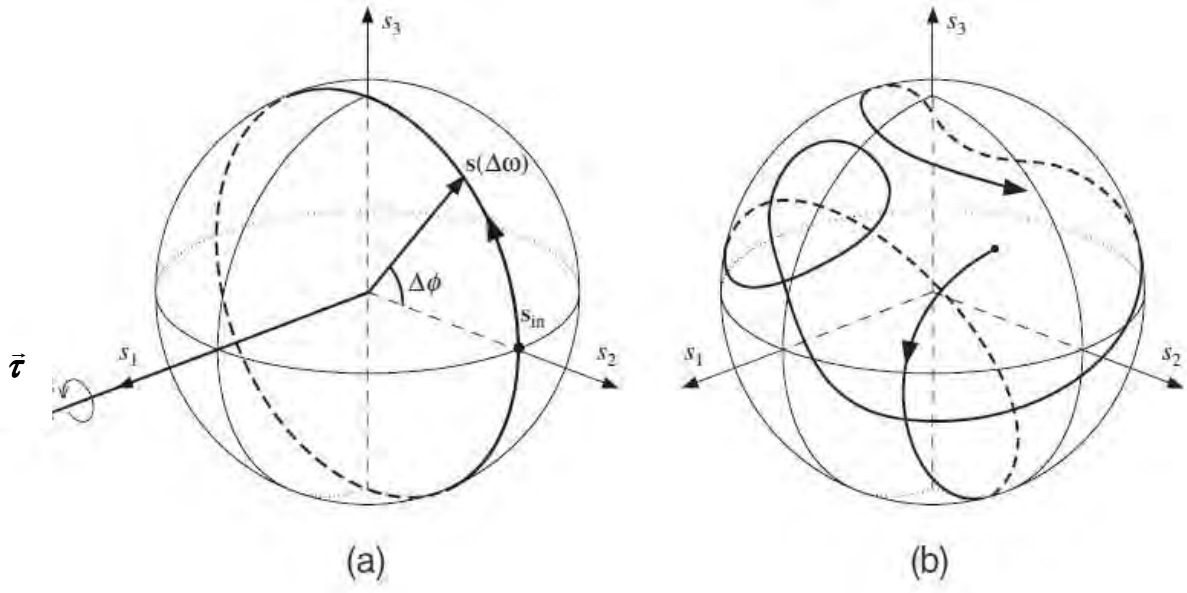

Figure 2.7: The state of SOP evolution as a function of frequency for a short fibre with uniform birefringence (a) and a long fibre with random birefringence and polarization mode coupling (b).

The DGD and the PSPs will vary with frequency/wavelength for a randomly birefringent optical fibre segment, figure 2.7(b). However, they will remain constant for a uniformly birefringent optical fibre segment, figure 2.7(a). Hence, in a small wavelength interval, occupied by a single spectrum, the DGD and the PSPs can be assumed to be constant and defined as first-order PMD effects. This behaviour of real fibres resembles that of the PMF. The DGD at an instant in time for such a wavelength interval is called the "*instantaneous DGD*" and this is different from the average DGD which is obtained by averaging over time or wavelength/frequency. The longer wavelength range motion of the output SOP, $\vec{s}_{out}(\omega)$, around $\vec{\tau}(\omega)$ is more complicated and leads to higher-order PMD. This is illustrated in figure 2.7(b).

Let us now consider what happens in the time domain. In the frequency domain, a continuous wave and PMD view is by single frequency/wavelength. However, in the time domain, it involves pulses. This gives another physical interpretation of the DGD parameter, $\Delta\tau$, to the speed of precession earlier identified. In the time domain, laboratory coordinates are used, i.e. the Jones vectors to characterize polarization and a 2×2 unitary complex transmission matrix, T. The relation between the input ($|s\rangle$) and output ($|t\rangle$) Jones vectors is given by

$$|t\rangle = T|s\rangle \tag{2.20}$$

For the relationship between T and Jones Matrix A, see Appendix A. The PSPs, for this particular case, are characterized by the unit Jones vectors $|p\rangle$ and $|p_-\rangle$ which correspond to the Stokes vectors $\hat{p}$ and $-\hat{p}$. With the PSPs being used as an orthogonal basis set, any input or output state of polarization can be expressed as a vector sum of two components with each aligned with a PSP. Considering an optical fibre with first-order PMD only, the output electric field from it will have the form (Kogelnik *et al.* 2002),

$$\vec{E}_{out}(t) = a|p\rangle E_{in}\left(t-\tau_0-\Delta\tau/2\right)+b|p_-\rangle E_{in}\left(t-\tau_0+\Delta\tau/2\right) \tag{2.21}$$

where a and b are complex weighting coefficients that indicate the field amplitude launched along the slow and fast PSPs, $|p\rangle$ and $|p_-\rangle$, E_{in} is the input electric field and τ_0 is the transmission delay which is independent of polarization. Like earlier discussed, $\Delta\tau$ is the DGD which is identified as the difference in arrival times between the two principal states.

From equation 2.21, it is seen that PMD can cause pulse broadening due to DGD, and also that there is no pulse broadening when the input is aligned with a PSP, i.e. when either a or b is zero. It should be noted that the PMD Stokes vector, $\vec{\tau}$, does not have a vector analog in the laboratory frame as shown in equation 2.21.

Poole *et al.* (1991) derived a dynamical equation for PMD relating the PMD vector to the microscopic birefringence. It describes the evolution of the PMD vector with the optical fibre length.

$$\frac{d\vec{\tau}}{dz} = \frac{d\vec{\beta}}{d\omega} + \vec{\beta} \times \vec{\tau}\,, \tag{2.22}$$

where z is the position along the optical fibre, $\vec{\beta}$ is the three dimensional local birefringence vector of the optical fibre (Eickhoff *et al.* 1981; Galtarossa *et al.* 2000a; Galtarossa and Palmieri 2004b) pointing in the direction of the birefringent axis with a magnitude $\Delta\beta$ proportional to $\Delta\eta$ (Gordon and Kogelnik 2000). Equation 2.22 is the basis for the statistical theory of PMD (Foschini and Poole 1991).

2.5 Second-Order PMD

Since the optical fibre PMD vector varies with the angular frequency, ω, for cases of larger signal bandwidths, a Taylor series expansion of $\vec{\tau}(\omega)$ with $\Delta\omega$ about the carrier frequency ω_0 is used (Foschini and Poole 1991; Gleeson *et al.* 1997; Bülow 1998),

$$\vec{\tau}\left(\omega_0 + \Delta\omega\right) = \vec{\tau}\left(\omega_0\right) + \vec{\tau}_\omega\left(\omega_0\right)\Delta\omega + \ldots \tag{2.23}$$

The second-order PMD (SO-PMD) is obtained by taking the derivative of equation (2.18) with respect to angular frequency (Foschini *et al.* 2000; Ireeta *et al.* 2010a),

$$\vec{\tau}_\omega = \frac{d\vec{\tau}}{d\omega} = \Delta\tau_\omega \hat{p} + \Delta\tau \hat{p}_\omega \tag{2.24}$$

where the subscript ω stands for differentiation with respect to angular frequency. Equation (2.24) has two important terms on the right-hand side. It should be noted that $\hat{p}_\omega$ is not a unit vector and that it is perpendicular to $\hat{p}$, i.e. $\hat{p}_\omega \cdot \hat{p} = 0$. The first term is $\vec{\tau}_{\omega\|}$, the component of $\vec{\tau}_\omega$ that is parallel to $\vec{\tau}$, while the second term is $\vec{\tau}_{\omega\perp}$, the component of $\vec{\tau}_\omega$ that is

perpendicular to $\vec{\tau}$. An illustration of the above principal parameters and their interrelationships is shown vectorially in figure 2.8.

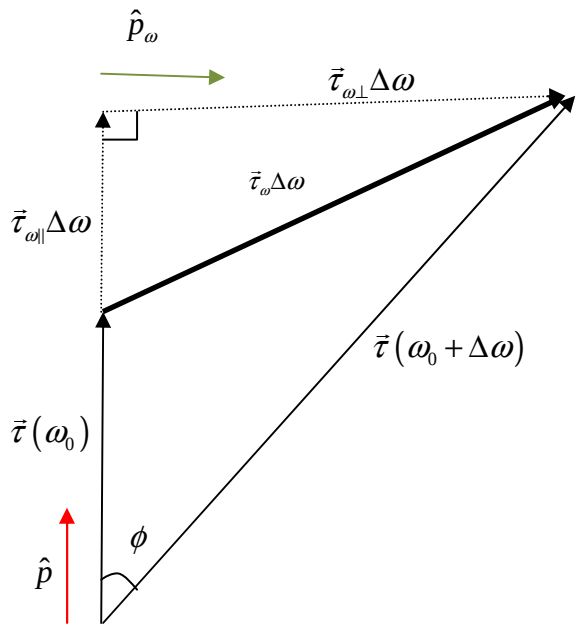

Figure 2.8: Vectorial representation of the PMD vector $\vec{\tau}_\omega$ and the second-order PMD components showing the change of $\vec{\tau}_\omega$ with frequency. The angular rotation rate, $d\phi/d\omega$, of the PMD vector $\vec{\tau}_\omega$ with ω is described by $\left|\hat{p}_\omega\right|$.

The magnitude of the first term, $\Delta\tau_\omega$, is the change of the DGD with frequency/wavelength and this causes polarization-dependent chromatic dispersion (PCD) (Poole and Giles 1988b; Foschini *et al.* 1999; Ireeta *et al.* 2010a). This results into polarization-dependent pulse broadening and compression. It can also be viewed as a polarization-dependent change in chromatic dispersion, DL, of the optical fibre which is described by an effective dispersion (Kogelnik *et al.* 2002),

$$(DL)_{eff} = DL \pm \tau_\lambda . \tag{2.25}$$

The PCD is defined as (equation 2.25), when the customary dispersion measure, DL, is used,

$$\tau_\lambda = -\left(\pi c/\lambda^2\right)\Delta\tau_\omega = \frac{1}{2}\frac{d\Delta\tau}{d\lambda}, \tag{2.26}$$

where λ is the wavelength, c is the speed of light in vacuum, and τ_λ has units, ps/nm. The PCD is proportional to the wavelength derivative of the DGD spectrum. In equation 2.25, the plus and minus signs represent the alignment with the two PSPs.

The second term in equation 2.24, $\Delta\tau\hat{p}_\omega$, describes PSP depolarization, that is the rotation of the PSPs with angular frequency. From figure 2.8, the angular rate of rotation, $d\phi/d\omega = |\hat{p}_\omega|$, of the PMD vector $\vec{\tau}_\omega$ is measured by the magnitude $|\hat{p}_\omega|$, whose units are ps. Pulse distortions caused by PSP depolarization include overshoots and generation of satellite pulses (Kogelnik *et al.* 2002). PSP depolarization is the dominant contributor to SO-PMD as compared to PCD. The ratio of PSP depolarization to SO-PMD is 8/9 (Foschini *et al.* 1999; Ireeta *et al.* 2010a). It should be noted that PSP depolarization can also have major effects on first-order PMD compensators.

It should also be noted that the input and output second-order PMD vectors, $\vec{\tau}_{s\omega}$ and $\vec{\tau}_\omega$ respectively, transform the same way as the first-order PMD vector (Gordon and Kogelnik 2000), i.e.

$$\vec{\tau}_\omega = M\vec{\tau}_{s\omega}, \tag{2.27}$$

where M is the Müller rotation matrix. For the third-order PMD vectors, it can be shown that (Kogelnik *et al.* 2002),

$$\vec{\tau}_{\omega\omega} = M\vec{\tau}_{s\omega\omega} + \vec{\tau}\times\vec{\tau}_\omega. \tag{2.28}$$

Probability density functions for the various second-order PMD components have been obtained (Foschini and Poole 1991; Foschini *et al.* 1999) from the statistical theory of SO-PMD. These components were experimentally confirmed (Foschini *et al.* 2000; Jopson *et al.* 2001) as well as their scaling with mean DGD (Nelson *et al.* 1999). A summary of these results is in Appendix B of this thesis. Higher-order PMD vectors have been described using other formulations (Bruyere 1996; Eyal *et al.* 1999; Shieh 1999) instead of the Taylor series expansion discussed earlier. These formulations attempt to describe better the variations of the PMD vector with optical angular frequency. However, for these formulations, derivation of their statistics has not to date been achieved (Kogelnik *et al.* 2002).

2.6 Random Birefringence Modelling

A deployed single mode optic fibre is modelled as a concatenation of randomly orientated waveplates with each having a certain length and a certain birefringence. A modification in this model was suggested by Suzuki *et al.* (2004) in the way the plates are correlated considering the angle between the segments if totally random or not. Also Bohn *et al.* (2004) suggested a case for the birefringence and the length of each segment being random or

constant. However, the easiest and most straightforward model is to assume a totally random angle for each waveplate with both constant birefringence and length. The simplest way to achieve this is to have the length of each waveplate in the infinitesimal range while keeping their PMDs constant (Madsen *et al.* 2000). Using Müller rotation matrices, the concatenation of the n optical fibre pieces can be written as the matrix product

$$\mathrm{M}^n \equiv \mathrm{M}_n \mathrm{M}_{n-1} \ldots \mathrm{M}_2 \mathrm{M}_1 = \mathrm{M}_n \mathrm{M}^{n-1}. \tag{2.29}$$

Then the PMD vector, $\vec{\tau}^n$, of the n optical fibre pieces can be written in terms of Müller rotation matrices as $\vec{\tau}^n \times = d\mathrm{M}^n \big/ d\omega\left(\mathrm{M}^n\right)^{-1}$, where $\vec{\tau}\times$ is given by

$$\vec{\tau}\times = \begin{pmatrix} 0 & -\tau_3 & \tau_2 \\ \tau_3 & 0 & -\tau_1 \\ -\tau_2 & \tau_1 & 0 \end{pmatrix} \tag{2.30}$$

and is interpreted as the skew symmetric matrix that corresponds to the cross product operator. It can thus be shown that the total PMD vector of such a concatenation is (Madsen *et al.* 2000),

$$\vec{\tau}^n = \vec{\tau}_n + \mathrm{M}_n \vec{\tau}^{n-1}, \tag{2.31}$$

where $\vec{\tau}_n$ is the PMD vector of the nth element. In other words, the total PMD vector of a concatenation of any number of birefringent segments is the vector sum of the individual vectors as long as they are transformed by the appropriate Müller rotation matrices to the same position. Therefore, the total PMD vector, $\vec{\tau}$, is the vector sum of the n PMD vectors that have random direction and also have different lengths, $\delta t_i = \left|\vec{\tau}_i\right|$. This corresponds to a "random walk" when viewed in three dimensions.

For an infinite number of segments ($n \to \infty$), a case for deployed single mode optical fibres modelled as a concatenation of hundreds or thousands of birefringent segments, the three vector components of the PMD vector are independent Gaussian random variables using the central limit theorem. The differential group delay (DGD), which is the modulus of the PMD vector has a Maxwellian distribution (Galtarossa *et al.* 1999; Buchali *et al.* 2000; Galtarossa

et al. 2006b; Djupsjöbacka *et al.* 2009; Li *at al.* 2010a). The probability density function (pdf) of the normalized DGD, $x = \Delta\tau / \langle \Delta\tau \rangle$, is given by

$$f\left(x, \langle \Delta\tau \rangle\right) = \frac{32x^2}{\pi^2 \langle \Delta\tau \rangle^3} \exp\left(-\frac{4x^2}{\pi \langle \Delta\tau \rangle^2} \right). \tag{2.32}$$

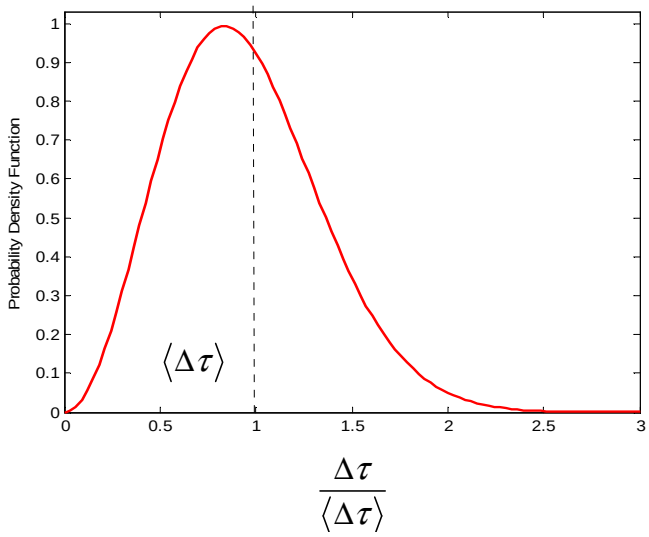

Figure 2.9: The Maxwellian distribution of the normalized differential group delay.

This distribution is illustrated in figure 2.9. This is a broad distribution and so many uncorrelated samples must be considered to get a reliable average. The Maxwellian distribution is a result solely of the assumed statistics of the local optical fibre birefringence. This implies that the pdf depends on the optical fibre modelling. The physical relevance of the statistical distribution function is that it corresponds to the DGD distribution as a function of time, wavelength and the different environmental perturbations. On integration of the Maxwellian pdf, it is found that the probability for the DGD to be larger than $2\langle \Delta\tau \rangle$ is 0.017 and to be larger than $3\langle \Delta\tau \rangle$ is only 4.2×10^{-5}.

In the model considered, it is possible to show that a "random walk" with n steps will take a "walker" on average, a distance proportional to $\sqrt{n}$ from the starting point. Using this analogy, it can be inferred that the average DGD depends on the square root of the optical fibre length $\langle \Delta\tau \rangle = \mathrm{PMD}\sqrt{L}$, where here PMD is the PMD-coefficient. It has units of

$ps/\sqrt{km}$. The latest optical fibres have PMD coefficients of about $0.01\,ps/\sqrt{km}$ while old installed optical fibres have much higher values in the range $0.2-10\,ps/\sqrt{km}$. This can also be described using the beat length, L_B, and the coupling length, L_C, as (Woodward *et al.* 2003; Galtarossa *et al.* 2006a; Galtarossa *et al.* 2006c),

$$\langle \Delta\tau \rangle = \sqrt{\frac{8}{3\pi}} \sqrt{\langle \Delta\tau^2 \rangle} = \sqrt{\frac{8}{3\pi}} \frac{\lambda}{c} \frac{\sqrt{L_C L}}{L_B}. \tag{2.33}$$

The coupling length is the typical length of optical fibre over which the polarization becomes uncorrelated due to polarization mode coupling.

2.7 Concatenation of PMD Vectors

The concatenation of PMD vectors is discussed in more detail in this section. From section 2.6, it was shown that the total PMD vector of a series of two or more segments, whose PMD vectors are known, can be determined using the simple but very powerful concatenation rules (Curti *et al.* 1990; Poole *et al.* 1991; Foschini and Poole 1991; Gisin and Pellaux 1992; Mollenauer and Gordon 1994; Gordon and Kogelnik 2000; Galtarossa and Menyuk 2005). These concatenation rules have been used for the analysis of the growth of the PMD vector with the optical fibre length (Curti *et al.* 1990), for statistical PMD modelling (Foschini and Poole 1991; Nelson *et al.* 2004), in simulation of PMD and in designing multisession PMD compensators (Kogelnik *et al.* 2002). In this study, we shall concentrate on the summation operation for the concatenation rules though other formulations in differential or integral form do exist for both first- and second-order PMD vectors (Gordon and Kogelnik 2000). The concatenation rule for first-order is similar to that for transmission line impedances like we earlier saw in section 2.6. If one is to obtain the PMD vector of an assembly, the PMD vectors of each individual segment are transformed to a common reference point and then the vector sum is taken. This is done in the three dimensional Stokes space. This resultant PMD vector can also be transformed to any other location in the system by use of the known rotation matrices of the different sections. A good example is shown in figure 2.10.

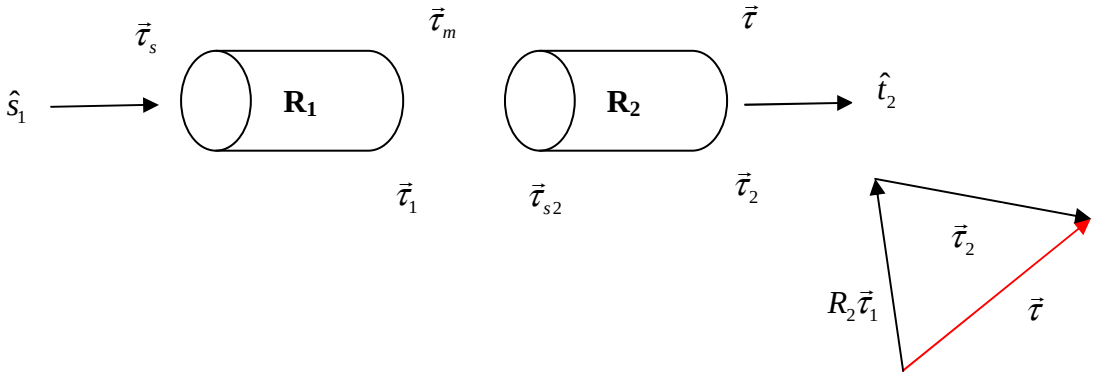

Figure 2.10: Illustration of concatenation of PMD vectors for two segments. The corresponding PMD vector diagram shows the geometrical interpretation of the concatenation (after Kogelnik *et al.* 2002, p. 744).

The PMD vector at the midpoint between the two segments is

$$\vec{\tau}_m = \vec{\tau}_1 + \vec{\tau}_{s2} = \vec{\tau}_1 + R_2^T \vec{\tau}_2 \tag{2.34}$$

with all $\vec{\tau}_i$ and R_i being functions of frequency. The total PMD vector at the output, $\vec{\tau}$, is obtained by transforming it by R_2 to get

$$\vec{\tau} = R_2\vec{\tau}_1 + \vec{\tau}_2 \ , \tag{2.35}$$

knowing that $R_2 R_2^T \vec{\tau}_2 = \vec{\tau}_2$. The corresponding PMD vector diagram is also shown in figure 2.10. This vector diagram provides a simple geometrical interpretation of the concatenation of the two segments. Equation 2.35 is the basic concatenation rule. It can also be used to find the total PMD vector at the input, $\vec{\tau}_S$, by the following transformation

$$\vec{\tau}_S = R_1^T \vec{\tau}_m = R_1^T \left(\vec{\tau}_1 + R_2^T \vec{\tau}_2 \right) \tag{2.36}$$

The rule in equation 2.36 can be generalized to multiple segments and also to differentially small segments.

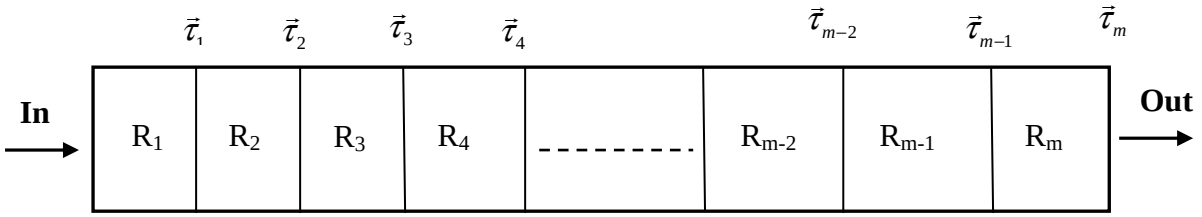

Figure 2.11: Illustration of m segments of PMD. Each of the segments has a known rotation matrix R_n and an output PMD vector $\vec{\tau}_n$ (after Kogelnik *et al.* 2002, p. 744).

The concatenation rule also applies to second-order PMD. When equation 2.35 is differentiated with respect to angular frequency, ω, and after making the proper substitutions, you get

$$\vec{\tau}_\omega = \vec{\tau}_2 \times \vec{\tau} + R_2 \vec{\tau}_{1\omega} + \vec{\tau}_{2\omega}. \tag{2.37}$$

The first- and second-order PMD vectors for many segments can be determined by the repeated use of the two-segment rules in equations 2.35 and 2.37. Considering the illustration of a fibre in figure 2.11 which consists of m segments with each segment having a known rotation matrix R_n and an output PMD vector $\vec{\tau}_n$, the sum rules of the assembly are for first-order PMD

$$\vec{\tau} = \sum_{n=1}^{m} R(m, n+1)\vec{\tau}_n, \tag{2.38}$$

and for second-order PMD

$$\vec{\tau}_\omega = \sum_{n=1}^{m} R(m, n+1)\left\{\vec{\tau}_{n\omega} + \vec{\tau}_n \times \vec{\tau}(n)\right\}, \tag{2.39}$$

In equations 2.38 and 2.39, the rotation matrix of the last $m-n+1$ segments is defined as $R(m,n) = R_m R_{m-1} \ldots R_n$, where $R(m,m) = R_m$ and $R(m, m+1)$ is the identity matrix. Hence, the differential concatenation rule for PMD shows how $\tau(z)$ changes with the differential addition of length Δz (Gordon and Kogelnik 2000) and this is equivalent to equation 2.22, the dynamical PMD equation.

Highlighting these concepts on the polarization of light is necessary to give the reader a good background since they will be applied in chapters 4, 5, 6 and 7, in the analysis of the experimental data obtained from aerial optical fibres on the South African telecommunication network.

CHAPTER 3

MODULATION FORMATS

An optical modulation format is defined as the method which is used to impress information/data onto an optical carrier wave so that it is transmitted over an optical fibre or any other media which could be free space, a nano-photonic optical waveguide or even plastic. Modulation can be realised using two methods: Either by directly varying the laser drive current with the information stream so as to produce a varying optical output power, or by use of an external modulator to modify a steady optical power level emitted by the laser. For high speed systems (> 2.5 Gb/s), *external modulation* is preferred so that undesirable nonlinear effects such as chirping are minimised (Keiser 2000, p.180). In this chapter detailed descriptions of modulation formats are done since they are used to mitigate linear and nonlinear impairments from optical fibre transmission systems.

3.1 Modulation Formats Classification

In single-mode optical fibres, data/information is carried by use of any of the three physical attributes of its optical field, i.e. *intensity*, *phase* (or *frequency*) and *polarization*. Therefore, the classification of modulation formats will depend on which of the above attributes is being used for information transportation.

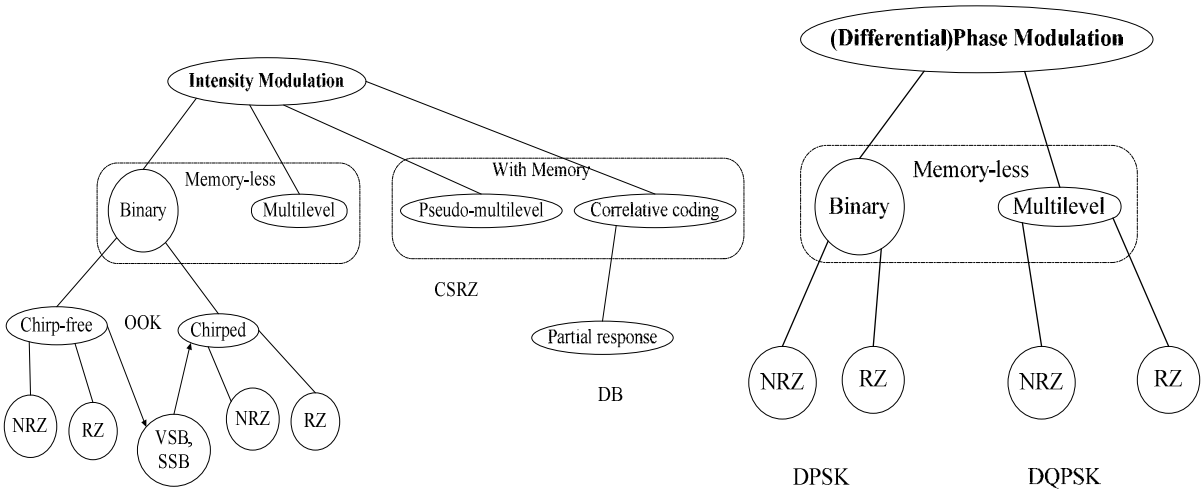

Figure 3.1: Classification of the major intensity and phase modulation formats. (N)RZ: (non-) return to zero; VSB: vestigial sideband; SSB: single sideband; OOK: on/off keying; CSRZ: carrier-suppressed RZ; DB: duobinary; DPSK: differential phase-shift keying; DQPSK: differential quadrature phase-shift keying (after Winzer and Essiambre 2006b).

Figure 3.1 shows some of the most important intensity and phase modulation formats in optical communication systems today.

3.1.1 Data Modulation Formats

Data modulation formats (DMFs) can be described in terms of either intensity, or phase (including frequency) or polarization. It should be noted that this classification does not require for example a phase-modulated optical field to be a constant envelop or an intensity-modulated optical field to have a constant phase. The classification of the modulation format is derived from the physical quantity that is used to transport the data or information.

In high speed optical communications systems, the intensity and phase DMFs have been used widely as compared to impressing information onto the polarization of light (*polarization shift keying*, Pol. SK) (Betti *et al.* 1992; Winzer and Essiambre 2006a; Winzer and Essiambre 2006b). This could mainly be because of the need for active polarization management at the receiver since in the optical fibre the polarization changes randomly (Lepley *et al.* 2000). Another reason could be the fact that Pol. SK does not offer major receiver sensitivity compared to intensity modulation (Betti *et al.* 1992). However, in order to improve the propagation properties of a format by *pseudo-multilevel* or *correlative coding* (Hodzic *et al.* 2003; Xie *et al.* 2004), the polarization degree of freedom are used. This is similar to an auxiliary optical phase modulation we shall discuss in section 3.1.2. Also, in especially research experiments, polarization is used to increase *spectral efficiency* (SE) or *information spectral density* (ISD). Information spectral density (Bigo 2004) or spectral efficiency (Costello *et al.* 1998) is the ratio of the net per channel information data rate to the wavelength-division multiplexed (WDM) channel spacing. This can be achieved in three different ways. Firstly, two different signals at the same wavelength but in two orthogonal polarizations (polarization multiplexing) are transmitted. Secondly, transmitting adjacent wavelength-division multiplexed (WDM) channels in alternating polarizations which reduces coherent WDM crosstalk. Lastly, it can be achieved in nonlinear interactions between the channels (polarization interleaving).

3.1.2 Symbol Alphabet Size

When multilevel signalling is used, $\log_2(M)$ data bits can be encoded onto M symbols and then can be transmitted at a reduced symbol rate of $R/\log_2(M)$ (Winzer and Essiambre

2006b). Here R is the bit rate. Generally, symbol assignment is done irrespective of the symbols assigned before or after it. This is what is known as *memoryless* modulation (Proakis 2001). The major advantage of multilevel signalling is the higher spectral efficiencies at the cost of a reduced tolerance to noise (Proakis 2001; Kramer *et al.* 2003). Also, multilevel signalling allows single-channel data rates to exceed the limits of high speed optoelectronics technology. It also allows for lower symbol rates at a fixed data rate (Winzer and Essiambre 2006b). This is very beneficial in the presence of signal dispersion distortions namely PMD (section 3.6.4), chromatic dispersion (section 3.6.3) and also for the implementation of digital electronic signal processing.

Multilevel phase modulation (Griffin and Carter 2002a; Griffin *et al.* 2002b; Ohm 2004), multilevel intensity modulation (Walklin and Conradi 1999), and the hybrid multilevel phase/intensity modulation (Hayase *et al.* 2003; Ohm and Speidel 2003) have been reviewed in the context of multigigabit/second transmission rates. The *differential quadrature phase-shift keying* (DQPSK), section 3.5.2, is one of the most promising multilevel optical modulation formats.

Correlative coding and Pseudo-multilevel modulation, in the category of modulation formats with more than two symbols, have received considerable attention compared to multilevel formats in optical communications (Winzer and Essiambre 2006b). The case where more than two symbols are used to represent a single bit and where the assignment of redundant symbols to transmitted bits is data independent is called pseudo-multilevel DMFs. If, however, the assignment of symbols depends on the transmitted data information, we then have correlative coding DMFs with the most important subcategory being partial-response DMFs.

3.1.3 Pulsed Modulation RZ Vs NRZ

When information/data is impressed onto the intensity or phase or polarization of optical pulses, the data modulation formats are called pulsed or *return to zero* (RZ). N*on-return to zero* (NRZ) formats are when a constant optical intensity is allowed over several consecutive bits. Detailed discussion of these modulation formats will be presented in sections 3.3.1 and 3.3.2.

3.2 Modulator Technologies

Since the speed of available optoelectronic components has been the main limitation of high data rates in optical communication systems, it becomes important to always consider the practical aspects of modulation and detection hardware when optical modulation formats are being designed. To find the most cost effective modulation technique for a given system application will necessitate knowledge of the aspects of modulation format and the modulator technology. Currently, there are three basic modulator technologies in use i.e. *electro-absorption modulators*, *directly modulated lasers* and the *Mach-Zehnder modulators* (MZMs). For transport systems at 40 Gb/s and above, the MZM technologies are the most used. This is because of their well controllable modulation performance and also there is a possibility to independently modulate intensity and phase of the optical field. The MZM is often fabricated on *Lithium Niobate* ($LiNbO_3$) crystal because of its strong electro-optic coefficient (Wooten *et al.* 2000). Figure 3.2 shows the operation of the MZMs technologies.

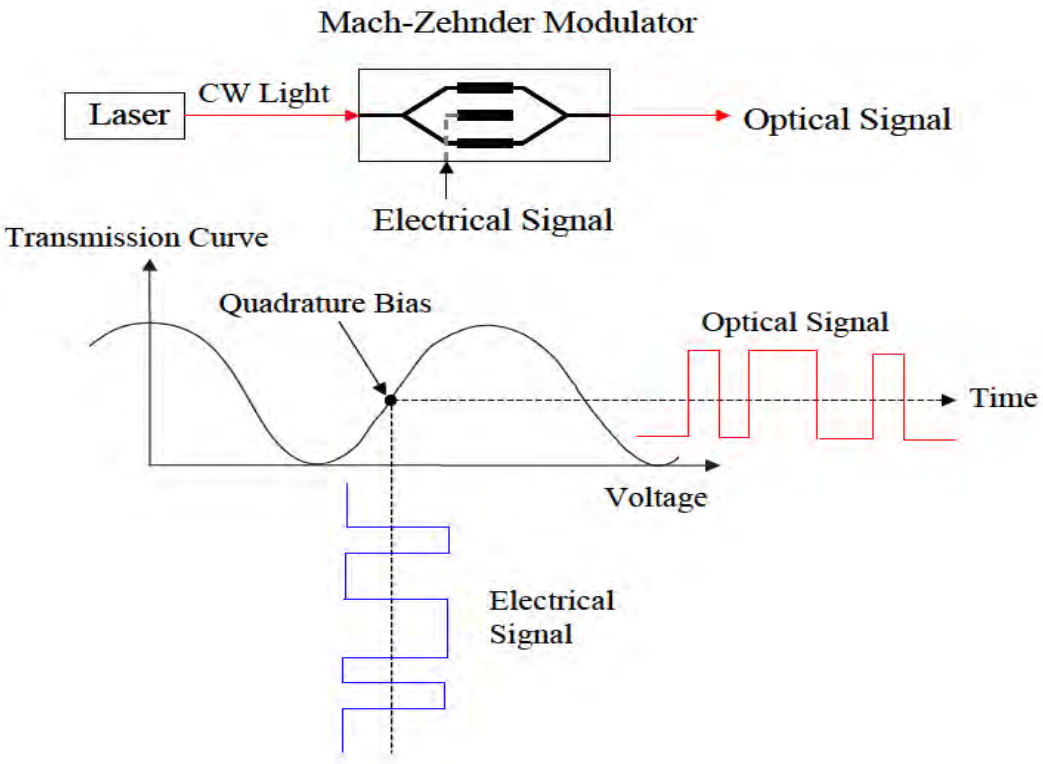

Figure 3.2: Illustrative diagram for a Mach-Zehnder modulator (MZM). The MZM transmission curve forms periodic interference fringes in the output intensity as a function of applied voltage.

The *continuous wave* (CW) light from a laser, which could be a *distributed feedback* (DFB) semiconductor laser light emitting approx. 1550 nm, is coupled into a waveguide in the $LiNbO_3$ crystal. The waveguide splits and follows two separate optical paths. On top of the optical waveguides, metal electrodes are fabricated for propagation of the electrical data signal. This electrical data signal introduces a π phase difference, by means of the electro-optic effect, between the two paths for logic 0, and no phase difference for logic 1. Thereafter, the light waves from the two paths are allowed to interfere at the output such that a π phase difference leads to destructive interference for optical logical 0, and no phase difference leads to constructive interference for optical logic 1. MZMs have a very important parameter V_π which is the voltage swing that is needed to go from null to peak in the MZM transmission curve. For example, to generate NRZ modulation, the *radio frequency* (RF) driver amplifier must provide an output voltage swing of $V_{pp} \sim V_\pi$ i.e. in the range of 5-6 V for a 10 Gb/s $LiNbO_3$ modulator.

3.3 Intensity Modulation Formats

Historically, optical communication systems used a very simple intensity modulation format, simply sending light to signal a “1” and not sending light to signal a “0”. This intensity optical modulation format is known as the *on-off-keying* (OOK). It is still the preferred modulation format for most links due its easy implementation. This optical modulation format has two categories, namely: the *non-return-to-zero* (NRZ) and the *return-to-zero* (RZ).

3.3.1 NRZ-OOK

This is the simplest optical modulation format to generate. It is also just referred to as NRZ. When an MZM is used to generate NRZ, the modulator is biased at 50% transmission and is driven from minimum to maximum transmission. It should be noted that the nonlinear compression of the sinusoidal MZM transfer function at high and low transmissions can suppress overshoots and ripples on the electrical NRZ drive signal upon conversion to optical power (Winzer and Essiambre 2006b). Figure 3.3 shows a schematic diagram for a 10 Gb/s NRZ transmitter and figure 3.4(a) shows the optical spectrum and the optical intensity eye diagram of an idealized NRZ signal.

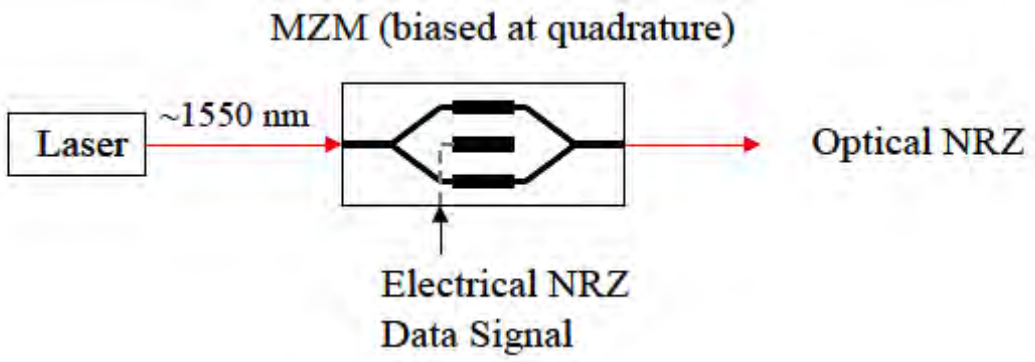

Figure 3.3: Illustrative diagrams for a 10 Gb/s NRZ transmitter

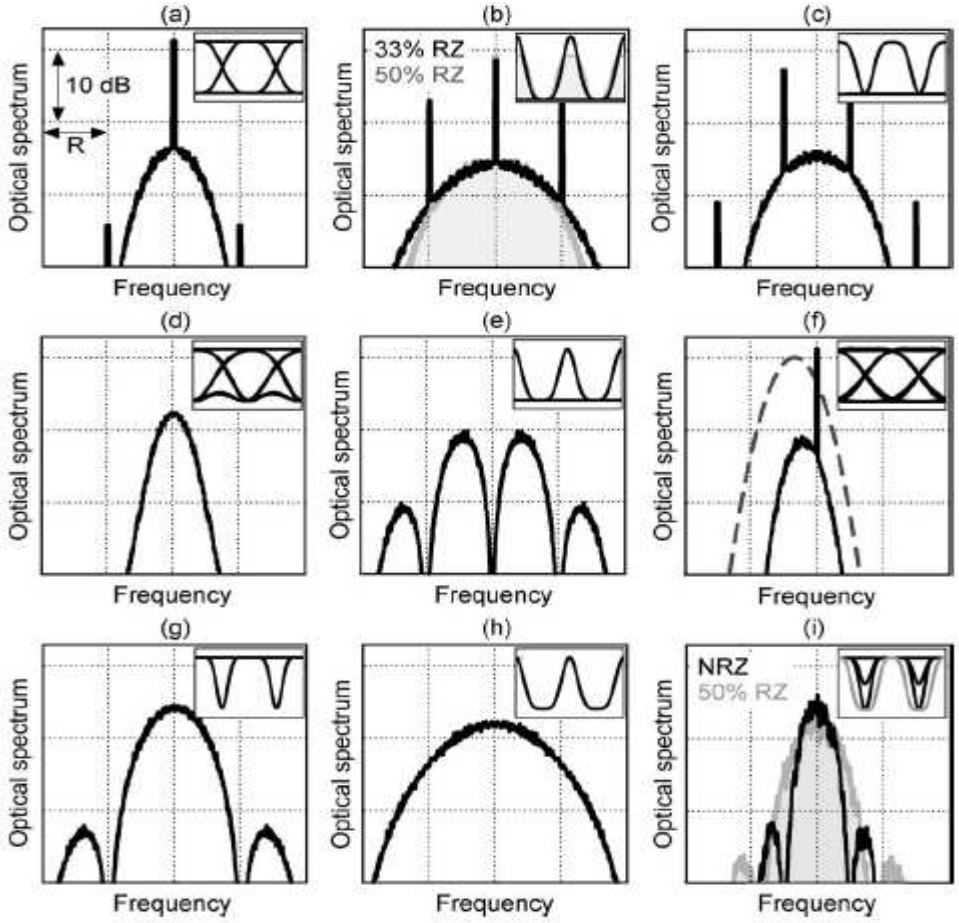

Figure 3.4: Optical spectra and optical intensity eye diagrams of important modulation formats. (a) NRZ-OOK. (b) RZ-OOK. (c) 67% CSRZ-OOK. (d) DB. (e) 33% RZ-AMI. (f) VSB-NRZ-OOK. (g) NRZ-DPSK (MZM). (h) 33% RZ-DPSK (MZM). (i) DQPSK (MZM) [after Winzer and Essiambre 2006b].

3.3.2 RZ-OOK

For transmission speeds at 10 Gb/s and above, the return to zero transmitters just employ a pulse carver in series with the data modulator to convert an optical NRZ format into its RZ equivalent. This is illustrated in figure 3.5.

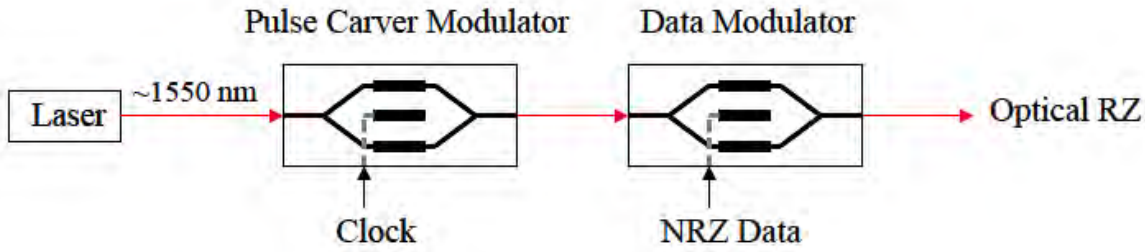

Figure 3.5: Schematic diagram of an optical 10 Gb/s RZ transmitter.

A *pulse carver* can easily be implemented as a sinusoidally driven MZM since multi-gigahertz sinusoidal signals of appreciable drive amplitude are easy to generate. Therefore, in figure 3.5, the first MZM is the pulse carver which produces a periodic RZ pulse train at the bitrate since the drive signal is a pure sine wave with frequency equal to bitrate, i.e. a clock signal. The second MZM is the gating modulator which is used to impress that data on the RZ pulse train. This gating modulator is synchronized with the pulse carver modulator by adjusting the phase of either clock or data signal using a variable delay line. Any one of the three methods below can be used for carving (Winzer and Essiambre 2006b).

a) When an MZM is sinusoidally driven at the data rate between the minimum and maximum transmission, this results in optical pulses with a *full-width at half-maximum* of 50% of the bit duration, i.e. a *duty cycle* of 50%, as shown in figure 3.6 (dashed).

b) When an MZM is sinusoidally driven at half the data rate between its transmission minima, a pulse is produced whenever the drive voltage passes a transmission maximum as shown in figure 3.6 (solid). By this, duty cycles of 33% are realized.

c) When an MZM is sinusoidally driven at half the data rate between its transmission maxima, pulses with 67% duty cycle and with alternating phase are produced. This phase modulation carries no useful data; however, it has the effect of suppressing the

carrier tone in the optical spectrum. The resulting format is called *carrier-suppressed RZ* (CSRZ) which we shall discuss in detail in section 3.3.3.

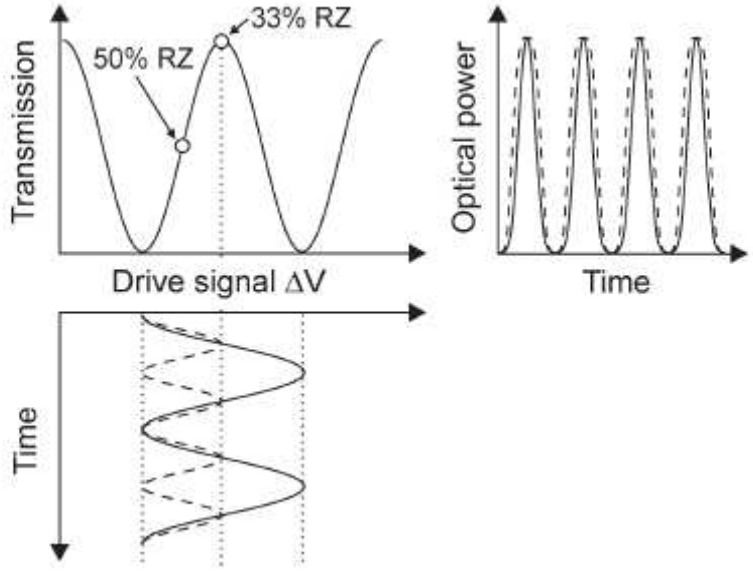

Figure 3.6: MZM sinusoidally driven as pulse carver to produce 33% duty cycle RZ (solid) and 50% duty cycle RZ (dashed). The open circles show the MZM bias points.

Optical spectra and optical intensity eye diagrams of 50% duty cycle RZ (gray) and 33% duty cycle RZ (black) are shown in figure 3.4(b).

It should be noted that the NRZ format requires roughly half the bandwidth of the RZ format. This means that it is easier to implement and also less costly. The receivers for both the NRZ and RZ modulations are based on a *square-law (intensity)* photo-detector. Therefore, NRZ and RZ should obtain the same quantum-limited receiver sensitivity as shown by Bosco *et al.* (2001). However, RZ is found to be less susceptible to *inter-symbol interference* (ISI) compared to NRZ and also achieves a 2 dB better performance than the NRZ (Pfennigbauer *et al.* 2002). Also, the RZ pulse shape benefits from a “soliton-like effect” in an optical fibre making it suffer less distortion due to the optical fibre nonlinearity compared to the NRZ (Hayee and Willner 1999). Therefore, because of the above reasons, RZ is the preferred modulation format for ultra-long haul submarine systems where the use of more costly transmitters and receivers is justified. NRZ modulation is implemented in terrestrial WDM transmission systems where cost is the primary driving factor.

3.3.3 CS-RZ

Carrier-suppressed RZ (CS-RZ) (Hirano *et al.* 1999; Miyamoto *et al.* 1999; Winzer and Essiambre 2006b) is a pseudo-multilevel modulation format with a distinctive characteristic of the sign of the optical field at each bit transition being reversed. The reversing of the sign occurs at every bit transition and is completely independent of the information carrying part of the signal. This distinguishes CS-RZ from correlative coding formats. The most convenient way of realizing CS-RZ is by sinusoidally driving the MZM pulse carver at half the data rate between its transmission maxima as shown in figure 3.7.

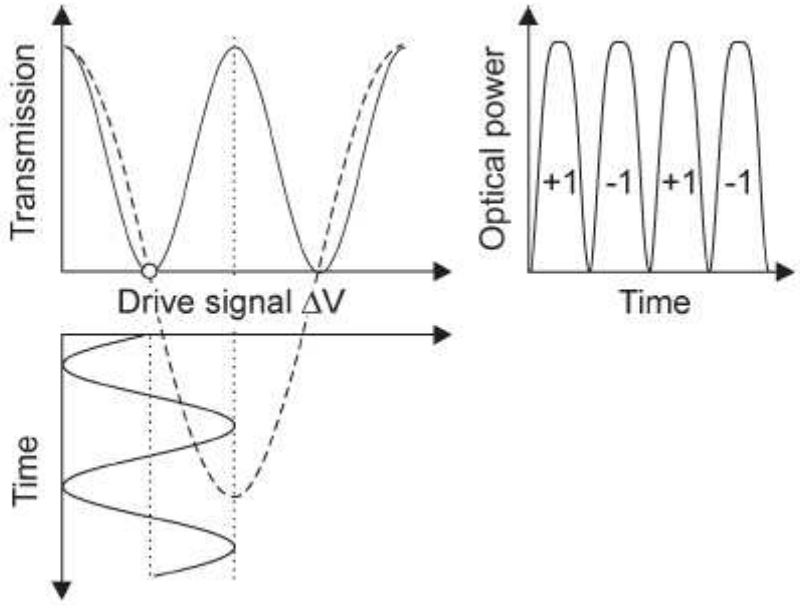

Figure 3.7: MZM driven sinusoidally as pulse carver for 67% duty cycle CSRZ. The solid and dashed transmission curves apply for the optical power and field, respectively. The open circle shows the bias point of the MZM.

Phase inversions between adjacent bits are produced because the optical field transfer function (dashed) of the MZM changes its sign at the transmission minimum. Therefore, on average, the optical field of half of the 1-bits has a negative sign while the other half has a positive sign, which results in a zero-mean optical field envelope. Hence, the carrier at the optical centre frequency is nullified which gives the format its name. The optical spectrum and optical eye diagram of 67% duty cycle CSRZ are shown in figure 3.4 (c).

3.4 Advanced Modulation Formats

When bandwidth is in plenty, the simple NRZ and RZ modulation formats are the natural choices. This is made possible by the immense intrinsic bandwidth of optical fibres, about 25 THz, and has in turn enabled an exponential growth in transmission capacity at a rate that has surpassed *Moore's law* for electronic computers as shown by Hamaide (2002). The possibility of this has been the advancement in technology of transmitting multiple channels on a single strand of optical fibre using WDM. In WDM technology, the crucial element is the *de-multiplexer* (Demux) which is an optical filter that selects a single channel for detection at the receiver. Also, the *erbium doped fibre amplifier* (EDFA) which is an all optical amplifier is another important element in WDM systems. The EDFA allows hundreds of optical channels to be amplified simultaneously without electrical regeneration. Hence, the current state-of-the-art commercial WDM systems are able to carry several hundred 10 Gb/s channels on a single optical fibre.

The exponential growth in optical fibre transmission capacity shows that lightwave systems follow a kind of "optical" Moore's law. But it should also be remembered that optical fibre bandwidth is not infinite. Also, WDM systems are unable to utilize the entire optical fibre bandwidth since even the most advanced optical amplifiers are limited to a bandwidth of approximately 10 THz (Fukuchi 2002). Therefore, employing NRZ or RZ modulation formats becomes questionable when fibre optic transmission systems approach about 10 Tb/s capacities. Hence, as the transmission distances and the per channel bitrates increase, and the channel spacing decrease, more sophisticated *advanced modulation formats* are needed to increase spectral efficiency and also improve on the tolerance to distortion due to fibre nonlinearity.

3.4.1 Correlative Coding and Partial-Response Formats

Within the general class of correlative coding formats, under a subclass referred to as partial-response signalling is the optical *duobinary* (DB) and *alternate-mark inversion* (AMI) (Lender 1963; Kabal and Pasupathy 1975; Proakis 2001). The main distinctive difference of correlative coding formats from CSRZ formats is the correlation between the optical phase and the data information for the former. For the AMI signalling, the phase changes for each 1-bit (even for adjacent 1-bits), independent of the number of 0-bits between them, while in

optical DB, a phase change occurs whenever there is an odd number of 0-bits between two successive 1-bits.

The main advantage of DB signals is their higher tolerance to *chromatic dispersion* (CD) and the narrow band optical filtering compared to binary signalling formats that can be understood both in the frequency domain (Walklin and Conradi 1997; Ono *et al.* 1998) and the time domain (Penninckx *et al.* 1996; Stark *et al.* 1998). Figure 3.4(d) visualizes the optical spectrum and optical intensity eye diagram of the duobinary.

The AMI format, which at times is classified as partial response because of the way it is generated (Kabal and Pasupathy 1975), is not affected by the bandwidth limitation that is characteristic of other partial response formats. In optics, AMI is normally implemented in RZ form (RZ-AMI). The additional phase modulation of AMI helps reduce the effects of some optical fibre nonlinearities (Winzer and Essiambre 2006b). The optical spectrum and intensity eye diagram of 33% duty cycle RZ-AMI are as visualized in figure 3.4(e).

3.4.2 Vestigial Sideband and Single Sideband

Some modulation formats have the capacity to suppress half of their spectral content by appropriate optical filtering in addition to shaping and compressing the optical signal spectrum using correlative coding or pseudo-multilevel signalling. Knowing that the spectrum of real valued basebands signals is symmetric around zero frequency, the redundant half of the spectrum (one of the two spectral sidebands) can be filtered out without losing any information content. This is achieved in *single sideband* (SSB) signalling where one spectral sideband is completely suppressed or in *vestigial sideband* (VSB) signalling where an optical filter with a gradual roll off is offset from the optical carrier frequency so as to suppress major parts of one sideband while also performing filtering action on the other. In practice, it is hard to implement SSB filtering because of the difficulties in realizing the appropriate optical and electrical filter functions (Watts *et al.* 2004) but a demonstration of optical VSB has been achieved on NRZ-OOK (Bigo *et al.* 2001; Idler *et al.* 2001; Bigo 2004), RZ-OOK (Tsuritani *et al*. 2001), and CSRZ-OOK (Mamyshev *et al.* 2002; Agarwal *et al.* 2004). The optical spectrum and intensity eye diagram of VSB-NRZ is shown in figure 3.4(f). In the same figure its VSB counterpart is the dashed line.

3.5 Differential Phase Modulation Formats

To use square-law detection to detect information carried by the optical field's phase, elements which convert phase to intensity have to be fitted into the optical path before the photodiode. Also, the absence of an optical phase reference at such a non-coherent receiver means that the phase reference is provided by the signal itself. In short, each bit will act as a phase reference for another bit and this is the heart of all *differential phase shift keying* (DPSK) formats (Gnauck and Winzer 2005).

3.5.1 Binary DPSK

DPSK encodes information on the binary phase change between adjacent bits. That is, a 1-bit is encoded onto a π phase change, while a 0-bit is shown by the absence of a phase change. The DPSK can be implemented in RZ and NRZ formats as was done for OOK (section 3.3). Advantages of optical DPSK are: (a) the optically pre-amplified quantum limited DPSK receiver gives approximately 3 dB better sensitivity; (b) if the same power is considered, the peak power in DPSK is 3 dB less than in NRZ; (c) the optical power distribution in a DPSK signal is more even compared to NRZ since power is present in every bit slot (Humblet and Azizoglu 1991; Winzer and Essiambre 2006b). The last two advantages imply that DPSK could be more tolerant (resilient) to optical fibre nonlinear effects.

The transmitter in an optical DPSK differentially encodes the transmit data before modulation so that error propagation at the receiver is avoided as shown by Kabal and Pasupathy (1975). Then the pre-coded sequence modulates the phase of the transmit laser between 0 and π. Optical modulation can be achieved either through the use of a straight line *phase modulator* (PM) or an MZM (Chikama *et al.* 1990). The MZM must be biased at a null and the electrical NRZ drive signal amplified to $2V_{\pi}$. From figure 3.2, the MZM transmission curve only shows the output intensity. The output phase varies between 0 and π for successive intensity peaks in the MZM transmission curve. Therefore, when the MZM is biased at null and a high-power RF driver amplifier with $V_{pp} \sim 2V_{\pi}$ is used, one can modulate the output phase between 0 and π to produce an optical *phase-shift keyed* (PSK) signal. DPSK modulation results when the electrical data source is differentially encoded before the MZM driver amplifier. Figure 3.8 shows a 10 Gb/s DPSK transmitter.

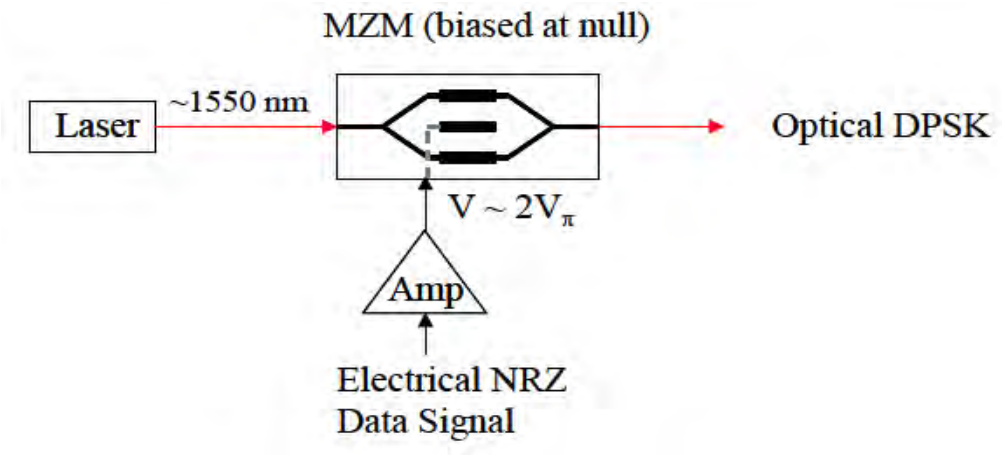

Figure 3.8: 10 Gb/s DPSK transmitter

It should be noted that the DPSK can also be produced with RZ pulses by adding an RZ pulse carver in series with the data modulator, in figure 3.8, to convert the NRZ-DPSK signal to RZ-DPSK. Hence, in this case, the transmitter output is a periodic RZ pulse train with the phase of each pulse modulated between 0 and π according to the data. The optical spectra and intensity eye diagrams for NRZ-DPSK and 33% duty cycle RZ-DPSK are shown in figures 3.4(g) and (h) respectively. The absence of a 0-bit rail in the eye diagrams should be noted, which is a characteristic of phase modulated formats. In the NRZ-DPSK eye diagram, the intensity dips between two bits represent the residual intensity modulation of the MZM caused by the finite NRZ drive signal bandwidth (Winzer and Essiambre 2006b).

3.5.2 DQPSK

The *differential quadrature phase-shift keying* (DQPSK) is the only true multilevel data modulation format (more than 1 bit per symbol) that has received enormous attention in optical communications systems so far (Griffin and Carter 2002a; Griffin *et al.* 2002b; Kim and Essiambre 2003; Cavallari *et al.* 2004; Gnauck *et al.* 2004a; Yoshikane and Morita 2005). Four phase shifts $(0, +\pi/2, -\pi/2, \pi)$ at a symbol rate of half the aggregate bit rate can be transmitted (Winzer and Essiambre 2006b). It also allows data to be encoded into one out of the four different symbols and thus enabling simultaneous transmission of two bits per symbol. The main advantage of DQPSK is the reduced spectral width that is about half that of a binary format at the same bitrate. As early as 2003, DQPSK systems were tested and

demonstrations have shown good performance at bitrates above 10 Gb/s (Cho *et al.* 2003; Wree *et al.* 2003).

The DQPSK is easily implemented by using two nested MZMs as phase modulators. This is illustrated in figure 3.9 for the transmitter setup.

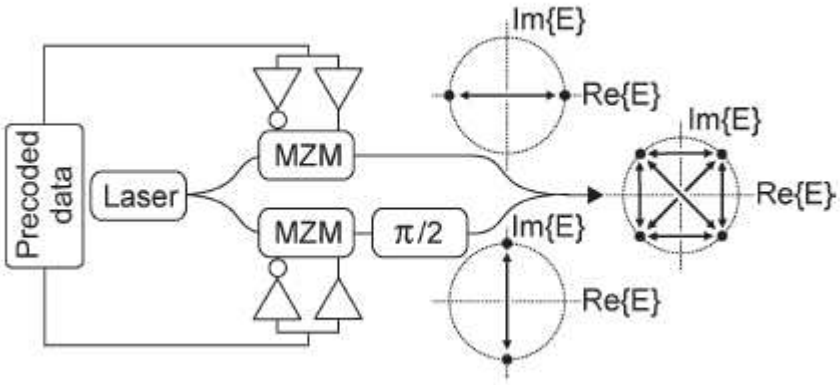

Figure 3.9: DQPSK transmitter illustration. The two MZMs act as phase modulators with the two separately modulated fields being combined with a $\pi/2$ phase shift (Griffin and Carter 2002a; Griffin *et al.* 2002b).

The transmitter setup in figure 3.9 consists of a continuous laser source, a splitter that divides the light into two paths with equal intensity, two MZMs used as phase modulators, an optical $\pi/2$ phase shifter in one of the paths, and a combiner which produces a single output signal. The symbol configurations of the upper and lower paths as well as the output at the modulator are also shown, together with the symbol transitions. When this transmission structure is used, the utilization of the exact π phase shifts produced by the MZMs is first in line. These are independent of the drive signal overshoot and ringing. Then the transmission structure will require only binary electronic drive signals. These are more easily generated at high speeds compared to multilevel drive waveforms. Alternatively, a pulse carver is added to the structure so that RZ-DQPSK is generated.

The optical spectrum and intensity eye diagrams for NRZ-DQPSK (black) and 50% duty cycle RZ-DQPSK (gray) are shown in figure 3.4(i). It should be noted that the shape of the NRZ-DQPSK optical spectrum is similar to that of NRZ-DPSK, but the DQPSK spectrum is compressed in frequency by a factor of 2 due to the halved symbol rate for transmission at fixed bit rate. The benefit of this compressed spectrum is achieving high spectral efficiencies

in WDM systems (Griffin and Carter 2002a; Kramer *et al*. 2003; Gnauck *et al.* 2004a) plus increased tolerance to chromatic dispersion (Griffin and Carter 2002a; Wang and Kahn 2004). DQPSK is also more robust to PMD because of its longer symbol duration compared to binary modulation formats (Griffin and Carter 2002a; Wang and Kahn 2004).

3.6 Advanced Modulation Formats in Optical Networking

In advanced optical networks, densely packed WDM channels are required to propagate over long distances. This includes optical routing using *optical add/drop multiplexers* (OADMs) without optical-to-electrical-to-optical regeneration. In the remaining sections, the tolerances of different advanced modulation formats for impairments found in spectrally efficient optically routed WDM networks are discussed. It should be remembered that generally, all modulation formats need to be resilient to optical amplifier noise, chromatic dispersion, polarization mode dispersion, optical fibre nonlinearity, and repeated optical filtering.

3.6.1 Loss, Amplification and Noise

A single mode optical fibre is an exceptionally transparent medium as highlighted by Winzer and Essiambre (2006b). It has attenuation coefficients < 0.2 db/km across a bandwidth of many terahertz. However, after long propagation distances, in addition to passing through networking elements e.g. *reconfigurable optical add-drop multiplexers* (ROADMs), the power of the signal falls below the threshold for optical receivers to detect. This then necessitates the system to be optically amplified. Some of the optical amplifiers that can be used are; *erbium-doped fibre amplifier* (Desurvire *et al*. 2002), and *distributed Raman amplifiers* (Islam 2003; Headley and Agrawal 2005). In digital communications, *amplified spontaneous emission* (ASE) (Desurvire *et al.* 2002) is generated during optical amplification, which by itself represents an optical source of Gaussian noise. There is also *beat noise* introduced during the conversion of the optical signal into an electrical signal in a square-law detecting optical receiver. The reader is referred to (Olsson 1989; Desurvire *et al.* 2002; Winzer and Essiambre 2006b) for more information. The other noise is *thermal noise* due to the heating of the elements in the fibre optic system.

Generally, the RZ formats require 1-3 dB less *optical signal-to-noise ratio* (OSNR) for the same *bit error ratio* (BER) of their NRZ counterparts (Winzer and Kalmar 1999). OSNR is defined as the average optical signal power divided by the ASE power measured in both polarizations. Thus, it’s a parameter which provides important information for signal quality

estimation, fault localization and automatic system diagnosis (Shen *et al*. 2010). In OOK formats, the RZ-AMI is the best performing modulation format (Winzer *et al.* 2003a). For the spectrally narrow DB format, a 1-2 dB back-to-back penalty is exhibited when compared to OOK formats (Zheng *et al*. 2001; Winzer and Essiambre 2006b).

On using DPSK formats instead of intensity modulation, OSNR requirements are reduced significantly. This gain of balanced detection DPSK over OOK is independent of the target BER and is typically approximately 3 dB. The most sensitive of the modulation formats that is in practice suitable for multigigabit/second transmission is RZ-DPSK (Winzer and Essiambre 2006b). However, DQPSK requires only 1-1.5 dB higher OSNR compared to DPSK at poor BER e.g. 10^{-3}. But the OSNR gap between DPSK and DQPSK increases at good BER e.g. 10^{-12} and the performance of DQPSK approaches that of OOK as shown by Proakis (2001).

3.6.2 WDM Crosstalk and Filter Narrowing

From figure 3.4, the major difference among the modulation formats is their spectral extent variations. As expected, some modulation formats are better suited than others for tight WDM channel packing that is quantified by SE and ISD. In the last couple of years, optical transport systems have been pushed to SEs of 0.8 bits/s/Hz (Kim and Essiambre 2003; Bigo 2004; Gnauck *et al.* 2004a; Raybon *et al.* 2004) and, in some research experiments, even beyond.

Some formats, especially DB, exhibit an OSNR improvement when they are tightly filtered as shown by Winzer and Essiambre (2006b). Also, the narrow-band modulation formats, for example NRZ-OOK, don’t lend themselves well to concatenated filtering at high spectral efficiencies because of their high susceptibility to ISI and , therefore, their low robustness to filter-induced signal distortions. It has been shown experimentally by some researchers that VSB-CSRZ (Agarwal *et al*. 2004) and RZ-DQPSK (Gnauck *et al.* 2004a) show no penalty in 0.8-bit/s/Hz SE WDM networking environment. It has also been confirmed by various researchers (Winzer and Essiambre 2006a) that for optically routed networks at 0.8-bit/s/Hz SE, DB, VSB-CSRZ, and RZ-DQPSK are the best suited modulation formats.

3.6.3 Chromatic Dispersion

Chromatic dispersion (CD) is the spread in the propagation speed of different spectral components contained in a modulated optical signal, which results in signal distortions and indeed pulse broadening in the time domain. The signal quality is degraded by the resulting ISI. In OOK, the peak amplitude of the 1-bits is corrupted and then raises the amplitude within the 0-bits through optical interference of neighbouring 1-bits.

Dispersion tolerances of the order 50 ps/nm are exhibited by most modulation formats except some spectrally narrow formats which generally yield significantly better dispersion tolerance (Walklin and Conradi 1999). This is shown by the high value for DB and DQPSK (Winzer and Essiambre 2006a). It should be noted that the performance of a modulation format to various impairments cannot be taken in isolation but has to be evaluated in the context of the system in which it is operating (Winzer and Essiambre 2006b). This is seen from the format-dependent shrinkage of dispersion tolerance in the presence of fibre nonlinearity, which for this case is more pronounced for DB than for NRZ-OOK (Winzer *et al.* 2004).

3.6.4 Polarization Mode Dispersion

For most modulation formats, a 1-dB penalty occurs at a DGD between 30% and 40% of the symbol duration (Winzer and Essiambre 2006a), with RZ formats being in general more resilient to PMD than NRZ formats (Kogelnik *et al.* 2002; Gené and Winzer 2010). It should be noted that the resilience to PMD also depends to some extent on the waveforms and filters (Winzer *et al.* 2003b) and also on other residual distortions. A good example is the tolerable amount of DGD for DB that is almost doubled when operated at 211 ps/nm residual CD (Winzer and Essiambre 2006b). Also for VSB-NRZ when passed through five OADMs at 0.8-bit/s/Hz SE, a similar effect is observed (Winzer and Essiambre 2006a). The tolerance to first-order PMD scales linearly with symbol duration. Hence, DQPSK has approximately twice the PMD tolerance of binary modulation formats at the same bit rate.

3.6.5 Fibre Kerr Nonlinearity

Inside a single mode optical fibre, very high intensities can be reached because of the high confinement of light within its core. Changes in the optical fibre’s refractive index (Kerr nonlinearity) are induced by such high intensities. Signal distortions over long propagation distances are thus induced by Kerr nonlinearity (Agrawal 2007). Amplitude fluctuations are

converted into phase fluctuations by the Kerr nonlinearity which leads to nonlinear phase noise that is stochastic and can never be completely eliminated (Ip 2010).

Several distinct regimes of transmission exist in systems incorporating dispersion compensation. These regimes are all aimed at minimizing the impact of fibre nonlinearities. In order to improve nonlinear transmission, the dominant nonlinearities in a system often determine the suitability of advanced modulation formats. The reader is referred to Winzer and Essiambre (2006b) for the description of the various regimes.

3.6.6 Nonlinearities and Modulation Formats

A detailed understanding of the limitations from optical fibre nonlinearities for advanced modulation formats is still an active research area. However, some experimental and numerical investigations suggest the types of nonlinear effects that typically limit transmission. Intensity modulated formats are limited by inter-channel and intra-channel nonlinear impairments in WDM systems (Winzer and Essiambre 2006a). The major limitations for phase modulated formats, at 2.5 and 10 Gb/s, on nonlinear transmission in general come from nonlinear phase noise. At 40 Gb/s and above, intra-channel nonlinearities dominate although nonlinear phase noise becomes a limitation at low OSNR (Winzer and Essiambre 2006b). Many system parameters determine optical fibre nonlinearity. Therefore, the comparison of modulation formats with respect to resilience to fibre nonlinearity so much depends on the system design and operating conditions. Hence, one has to specify the characteristics of the system considered when quoting the impact of nonlinearities on an advanced modulation format. The reader is referred to Dahan and Eisenstein (2002), Hodzic *et al.* (2002), and Gnauck *et al.* (2004b) for additional comparisons of various advanced modulation formats for nonlinear transmission.

According to Charlet *et al.* (2002) and Gnauck *et al.* (2004b), at 40 Gb/s, the tolerance of DB to nonlinear transmission does not differ substantially from similar duty cycle OOK. Also CS-RZ has been used in longer reach experiments (Sekiya *et al.* 2003) and achievement of high spectral efficiencies of 0.8 bit/s/Hz using strong optical filtering at the transmitter has been made. At 40 Gb/s, DPSK has a similar tolerance to optical fibre nonlinearity as CS-RZ when operated at an OSNR at the receiver that yields a BER of approximately 10^{-3} (Winzer and Essiambre 2006a). A good comparison of some aspects of transmission performance of

DQPSK relative to other modulation formats can be found in Van den Borne *et al.* (2006a) and Van den Borne *et al.* (2006b).

The background information on data modulation formats presented in this chapter is important because it points out the merits and demerits of the different modulation formats. Three of these modulation formats (i.e. NRZ, RZ and DQPSK) will be considered in chapter 8 when we compare their tolerances in a PMD induced environment for the case of aerial optical fibres.

CHAPTER 4

PMD AND SOP MEASUREMENT TECHNIQUES

Because of the complexity often exhibited by PMD, it is good to see how its measurement can be complicated as well. A variety of techniques for the measurement of PMD are available and each one of them is often associated with many user selectable parameters. In this chapter, we describe the various measurement techniques available and also discuss the "*best practices*" for PMD measurement using these described techniques.

4.1 What it takes to describe PMD

4.1.1 Measurement Parameters

A device's PMD is completely described when the *differential group delay* (DGD) and the *principal states of polarization* (PSP) are both characterized as functions of wavelength. In most literature the terms PMD and DGD are often used interchangeably. For this study, we have used the term PMD to describe the phenomenon and DGD to describe its magnitude. The three-dimensional polarization vector $\vec{\tau}(\lambda)$ contains both the DGD and the PSP information. The magnitude $\Delta\tau = |\vec{\tau}|$ is the DGD while the PSP is given by the direction of $\vec{\tau}$. In most applications, only $\Delta\tau(\lambda)$ is needed and in fact its wavelength dependence is not reported in most cases. The PMD is described by the wavelength-averaged DGD $\langle \Delta\tau \rangle_\lambda$ or the root-mean-square (RMS) average $\langle \Delta\tau^2 \rangle_\lambda^{1/2}$.For description of the various measurement techniques, a discussion of the two general cases of PMD devices with and without polarization-mode coupling will be done. A non-mode coupled device is a simple *birefringent* element, for example a single birefringent crystal. In this crystal, its polarization eigenaxes coincide with the PSPs and are independent of wavelength and $\Delta\tau$ depends only weakly on wavelength, figure 4.1(a).

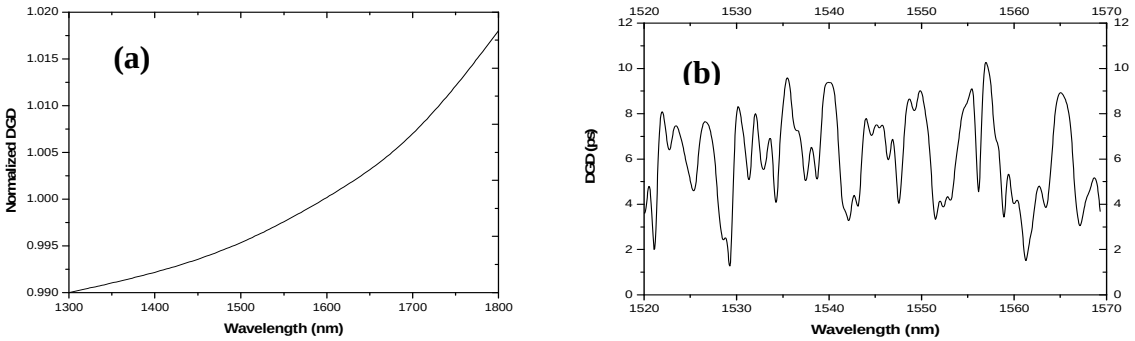

Figure 4.1: (a) Normalized DGD spectrum for a polarization maintaining fibre (PMF). (b) Sample DGD spectrum of a strongly mode-coupled buried optical fibre (measured by author).

In mode coupled devices, such as a telecommunication single mode optical fibre, the eigenaxes do not necessarily coincide with the PSPs. This implies that the PSPs are independent of wavelength only to first order and hence $\Delta\tau$ can be strongly dependent on wavelength, figure 4.1(b).

The degree of mode coupling of the device and what the measurement will be used for determines what exactly must be measured in order to characterize its PMD. In most cases, for non-mode coupled devices, the mean DGD can be approximated by the DGD at some particular wavelength λ_0, $\langle\Delta\tau\rangle \approx \Delta\tau(\lambda_0)$, implying that the DGD need not be resolved as a function of wavelength. However, for mode coupled devices, such as telecommunication single mode optical fibres, $\langle\Delta\tau\rangle$ and $\Delta\tau(\lambda)$ can be very different quantities.

4.1.2 Inherent Uncertainty

The uncertainty should be reported in a useful PMD measurement. This uncertainty comes from both the inaccuracy in the equipment and the environmental instability of the PMD (Galtarossa and Menyuk 2005). For highly mode-coupled optical fibres, such as telecommunication fibres, the DGD can vary greatly with wavelength as well as stress, fibre position, temperature and other environmental parameters such as wind speed and direction. As was shown in section 2.6, very long mode-coupled optical fibres exhibit a *Maxwellian distribution* of its DGD for an optical fibre exposed to these environmental parameters. This implies that, regardless of the measurement technique quality, there exists an inherent

uncertainty associated with DGD measurements. Therefore, this necessitates the report on the uncertainty due to the variance of $\Delta\tau$ to accurately report on the mean DGD of a mode-coupled device. It has been demonstrated by Gisin *et al.* (1996) that the four major classes of PMD measurement techniques are subject to the same level of uncertainty due to this statistical variation of the DGD in mode-coupled devices. This variance applies to all the techniques since they all essentially measure DGD albeit with different spectral resolutions. For an optical fibre with a mean DGD $\langle\Delta\tau\rangle$ measured over a bandwidth of $\Delta\omega_{span}$, the standard deviation σ normalized to $\langle\Delta\tau\rangle$ is (Gisin *et al.* 1996),

$$\frac{\sigma}{\langle\Delta\tau\rangle} \approx \frac{0.9}{\sqrt{\langle\Delta\tau\rangle\Delta\omega_{span}}} \tag{4.1}$$

In the case of a highly mode-coupled optical fibre, $\sigma/\langle\Delta\tau\rangle$ will decrease when the average is made over a wider spectral bandwidth, from equation 4.1, or over more statistically independent samples or if it has a larger mean DGD.

4.2 Measurement Techniques

The measurement techniques can be considered under two major classifications, as either time domain or frequency domain techniques. The major difference between these two techniques is seen in the relationship between the coherence time T_c of the measurement light and $\Delta\tau$ (DGD) being measured. The time domain technique is when $T_c < \Delta\tau$ and the frequency domain is when $T_c > \Delta\tau$. Brief discussions of the different measurement techniques follow but the reader is referred to Derickson (1998) for detailed descriptions.

4.2.1 Time Domain Measurements

The time domain measurement techniques determine the PMD by measuring the differential time delay between the slow and fast orthogonal polarization modes of the propagating light pulse. These methods are: time of flight (Williams 2004), low coherence interferometry (Gisin *et al.* 1991; TIA/EIA 455-124-A (FOTP-124A) 2004), polarization-optical time domain reflectometry (Rogers 1981; Galtarossa and Palmieri 2004a; Galtarossa *et al.* 2008a; Galtarossa *et al.* 2008b) and the modulation phase shift method (Williams 1999).

Other commercially available time domain interferometric techniques which use almost the same principles as the *low coherence interferometry* are: the FTB-5500 (*traditional interferometry technique*, TINTY), FTB-5500B (*generalized interferometry technique*, GINTY) and more recently FTB-5700 (*single-ended dispersion analyzer*). All these instruments are available from EXFO Electro-Optical Engineering Inc., Quebec City, Canada. These measurement techniques are so handy in the field because they facilitate rapid and accurate determination of PMD for even aerial optical fibres which move and vibrate randomly because of the environmental disturbances to which they are exposed.

4.2.1.1 Time of flight technique

This measurement technique is the most intuitive and hence we consider it first.

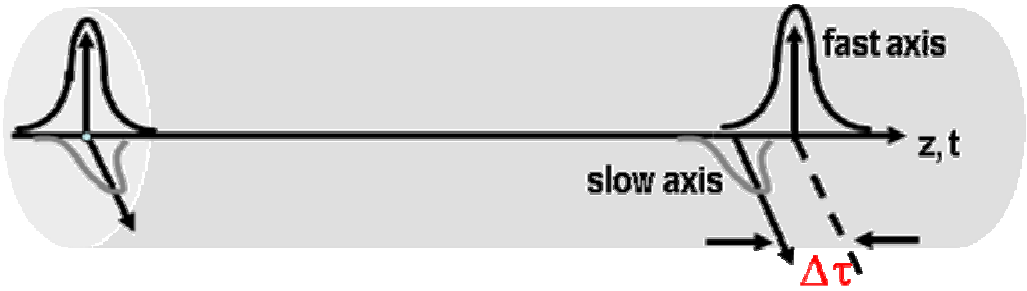

Figure 4.2: Diagram of orthogonal modes of a lightwave pulse launched simultaneously down the fast and slow PSPs of a fibre segment. The output modes emerge at different times which corresponds to the differential group delay $\Delta\tau$.

Figure 4.2 shows a narrow pulse of light transmitted through a non-mode coupled optical fibre segment of DGD $\Delta\tau$. In this measurement technique, short optical pulses are launched into the optical fibre segment and then detected at the output. A fast oscilloscope plots the arrival time of the pulses as the input polarization state is changed. This measurement technique is so common in literature (Poole and Giles 1988b; Namihira and Maeda 1992; Bakhshi *et al.* 1999; Williams 2004) but is very impractical since the pulse width limits the temporal resolution. The requirement is narrow pulse widths of the order of the desired DGD resolution.

4.2.1.2 Low Coherence Interferometry

This is related to the measurement technique described in section 4.2.1.1, however, it is more practical. Figure 4.3 illustrates the low coherence interferometer. A spectrally broad, low

coherence, source sends light through the optical fibre segment and into the interferometer. Interference fringes are observed at the detector when the moveable arm of the interferometer is translated only when the time difference between the two arms matches a delay generated in the optical fibre segment to within the coherence time of the source.

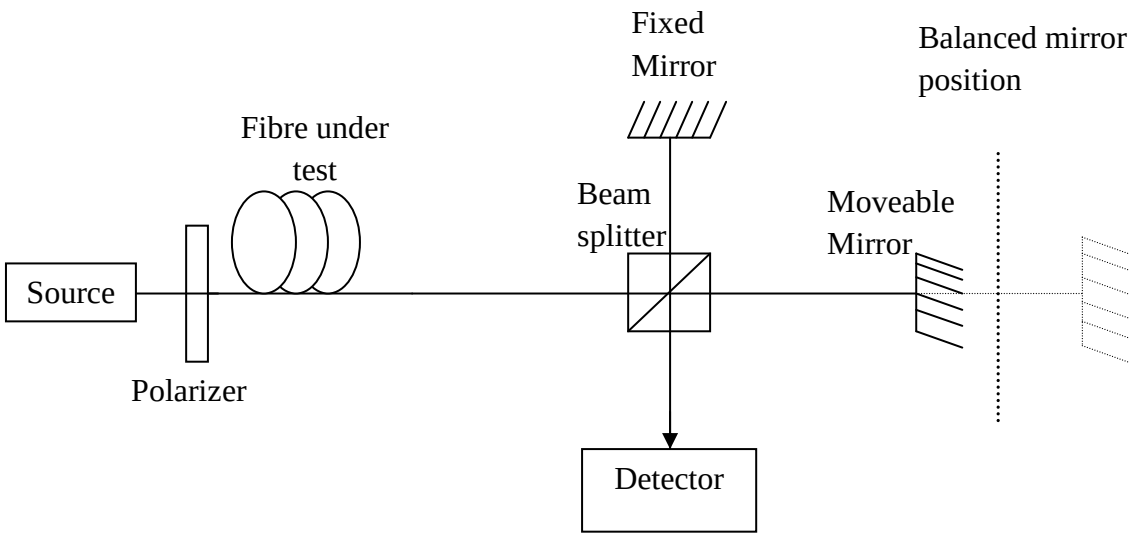

Figure 4.3: Schematic diagram of low-coherence interferometer used to measure PMD.

This condition can be written as equation 4.2 when all possible phase effects are ignored

$$\left|\left(\tau_{arm,1}-\tau_{arm,2}\right)-\left(\tau_i-\tau_j\right)\right|<T_c\,, \tag{4.2}$$

where $\tau_{arm,1}$ and $\tau_{arm,2}$ are the time delays associated with propagation along each arm of the interferometer, and τ_i and τ_j are the two possible propagation times experienced by light travelling along the *i*th and *j*th polarization paths through the optical fibre segment. Equation 4.2 gives an intuitive picture of the interferogram shape.

Plotting the envelope of the interference fringes as the moveable arm of the interferometer is scanned gives a histogram shown in figure 4.4 for a non-mode coupled optical fibre segment and figure 4.5 for a mode coupled optical fibre segment. The reader is referred to Galtarossa and Menyuk (2005) for detailed descriptions.

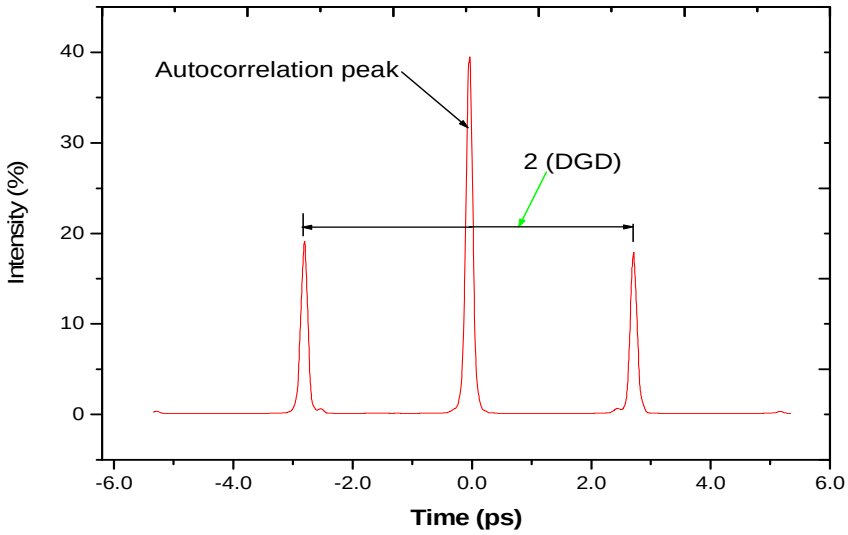

Figure 4.4: Sample interferogram envelope of a polarization maintaining fibre with a PMD of 2.76 ps (measured by the author).

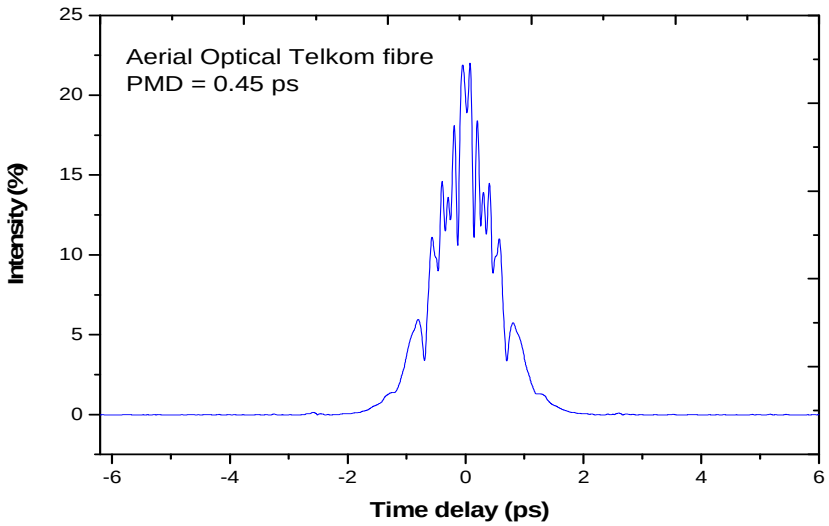

Figure 4.5: Interferogram of a 14.9 km single mode aerial optical fibre (linking St. Albans and Rockland transmission stations in Port Elizabeth) using a GINTY (measured by the author).

Low coherence interferometry has several advantages over other techniques for PMD measurements. The measurements can be done quickly i.e. the required time is essentially the time of travel of the interferometer mirror over the desired scan range. This is normally a few

seconds. Also different from the frequency domain techniques, low coherence interferometry does not require numerical comparison of data sampled at two different points in time. Hence, interferometry is less susceptible to dynamic changes in the measurement path, for example movement of the optical fibre patch cords or even temperature drift. Low coherence interferometry however has a disadvantage of the need to use a spectrally broad light source. This limits the achievable spectral efficiency i.e. the ability to measure with fine temporal resolution in a narrow bandwidth. Fortunately, resolutions as low as 11 fs have been demonstrated using a differential technique (Oberson *et al.* 1996), and long-haul measurements through multiple bandwidth-limiting optical amplifiers have demonstrated good measurement results with a bandwidth of only 20 nm (Cyr *et al.* 2004b). It also has the disadvantage of only measuring the amplitude (i.e. DGD).

4.2.1.3 FTB-5500, FTB-5500B and FTB-5700

The FTB-5500, called “TINTY”, is quite similar to the FTB-5500B, called “GINTY”. The only difference lies in the inclusion of an algorithm that removes the effects of the central autocorrelation peak (ACP), as shown in figure 4.4, for the GINTY. This leaves only the cross correlation peaks (CCP) for use to calculate the PMD of a given optical fibre device. It should be noted that the ACP contains no PMD information and it is known to affect the accuracy of measurements of PMD in TINTY. The reader is referred to Cyr (2004a) and Musara (2009, p.59) for more information about the differences between GINTY and TINTY.

The FTB-5700 is the latest PMD measurement technique to be commercialized by EXFO. Its advantage over GINTY is its ability to make measurements from just one end of the optical fibre link. This makes it a handy instrument because it is normally a challenge to have access to both ends of the optical fibre link since they are normally many kilometers apart and also accessibility to both ends at the same time may be quite demanding in terms of human resource. Of course, some researchers have been able to find a solution to this by putting jumpers at one end of the optical fibre link but this could lead to false results obtained since we are joining two different fibres that have totally different PMDs and properties (though are in the same cable) and the value obtained could be the average of the two. It could also be false if, for example, one of the fibres has higher PMD compared to the other and yet the final value obtained is the overall of the two or three connected together.

The FTB-5700 is able to measure PMD of aerial optical fibre cables subjected to aeolian-induced vibrations and mechanical perturbations because it has a polarization instability filtering method implemented within it. This is achieved since it uses the *state of polarization scrambling analysis* method which is completely immune to polarization instabilities when pairs of optical frequency transmission values are simultaneously sampled (Roberge 2009). In this equipment, this is done by performing serial measurements on the pair of optical frequencies per measurement point. Hence, executing a series of measurements on the optical transmission pair implies that the *state of polarization* (SOP) remains stable during the measurement period.

The single-ended dispersion analyzer (FTB-5700) can perform PMD measurements in two regimes, namely: the stable and unstable polarizations. In the stable regime, it uses the serial optical transmission measurement scheme while in the unstable regime a second measurement for the second optical frequency, due to for example wind, is added. For more detailed information, the reader is referred to Roberge (2009).

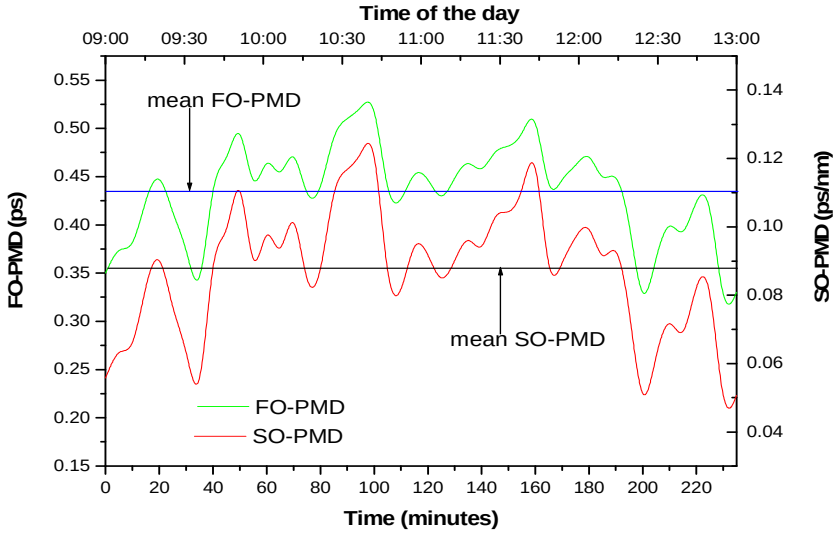

Figure 4.6: The variation of FO-PMD and SO-PMD with time using the FTB-5700 measurement instrument. These PMD measurements were obtained from a 7.46 km aerial optical fibre link in Port Elizabeth, South Africa, owned by Telkom South Africa on 19 August 2010.

We were able to perform both FO-PMD and SO-PMD measurements using the FTB-5700 on a 7.46 km aerial optical fibre linking St. Albans and Rockland transmission stations in Port

Elizabeth, South Africa to ascertain its robustness and accuracy (figure 4.6). From figure 4.6, it can be observed that the deviation from the means for both FO-PMD and SO-PMD is relatively small for measurements taken for a period of four hours.

4.2.2 Frequency Domain Measurements

Measurements of PMD based in the frequency domain measure the same DGD as time domain measurements but from a different perspective. The differential method is the most common approach to DGD measurements in the frequency domain. The propagation delay difference between light travelling on the fast and slow PSPs determines the output state of polarization $\hat{s}_{out}$ of the light. PMD measurements in the frequency domain seek to find out how the output state of polarization changes as a function of angular optical frequency. The polarization dispersion vector $\vec{\tau}$ is related to the change in the output state of polarization (assuming absence of polarization-dependent loss, PDL) as (Poole *et al.* 1988c),

$$\frac{\mathrm{d}\hat{s}_{out}}{\mathrm{d}\omega} = \vec{\tau} \times \hat{s}_{out}, \tag{4.3}$$

where ω is the angular optical frequency of the propagating light. Equation 4.3 has a physical meaning which is: the PMD in an optical device causes the output state of polarization to precess about $\vec{\tau}$ as the angular optical frequency is changed (figure 4.7). From equation 4.3, the precession rate will be equal to the DGD of the optical device:

$$\left|\frac{\mathrm{d}\theta}{\mathrm{d}\omega}\right| = \left|\vec{\tau}\right| = \Delta\tau, \tag{4.4}$$

with θ defined, in figure 4.7, as the angle of rotation of the output state of polarization about the axis of precession $\vec{\tau}$. By measuring $\Delta\theta/\Delta\omega$, which is an approximation of $\mathrm{d}\theta/\mathrm{d}\omega$, the DGD can be obtained. The class of frequency domain techniques which measure $\Delta\theta/\Delta\omega$ will be termed as "*polarimetric techniques*."

The various polarimetric techniques are distinguished from each other by the way they measure $\Delta\theta/\Delta\omega$. In all the techniques, polarized light is launched into the test device and then the output state of polarization as a function of angular optical frequency, $\hat{s}(\omega)$, is measured. However, the change in $\hat{s}$ with optical frequency yields $\left|\Delta\hat{s}/\Delta\omega\right|$ and not $\Delta\theta/\Delta\omega$. This is where the variations in the different approaches arise. We shall discuss three very

similar polarimetric measurements of DGD namely: *Jones Matrix Eigenanalysis* (JME) (Heffner 1992), *Müller Matrix Method* (MMM) (Jopson *et al*. 1999a), and *Poincaré Sphere Analysis* (PSA) (Cyr *et al.* 1999; TIA/EIA FOTP-122 1999). All three can be measured using the same experimental setup shown in figure 4.8.

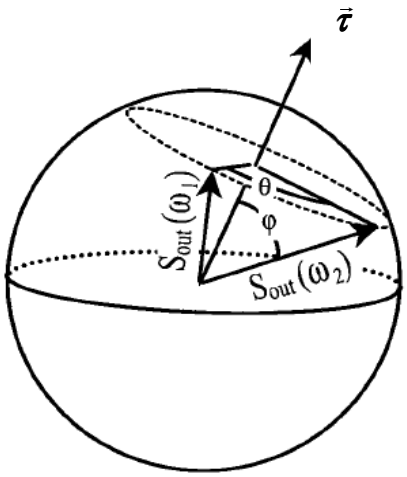

Figure 4.7: Poincaré sphere representation of polarization dispersion vector $\vec{\Omega}$ and the output state of polarization $\hat{s}_{out}$ at angular optical frequencies ω_1 and ω_2.

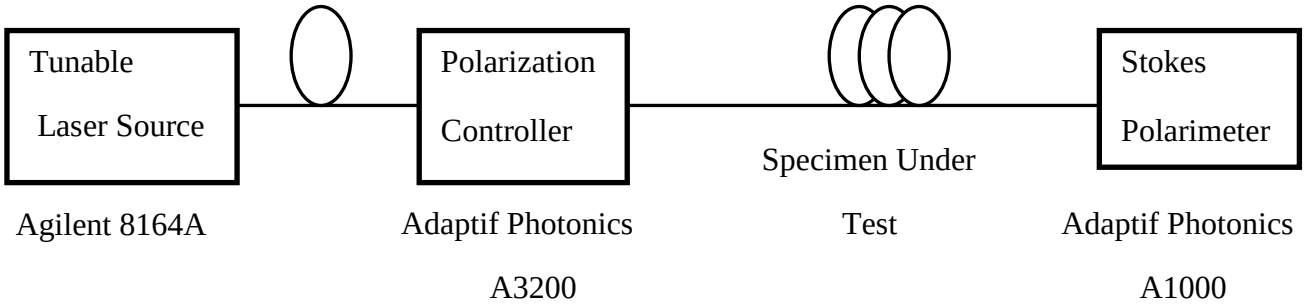

Figure 4.8: General experimental setup for JME, MMM, and PSA measurement techniques.

4.2.2.1 Jones Matrix Eigenanalysis

The JME measurement technique yields $\Delta\theta/\Delta\omega$ and $\vec{\tau}$ by turning the measurement into an eigenvalue problem as shown by Heffner (1992). A 2×2 Jones matrix, the difference matrix Γ, is defined as that matrix which describes the change in the output state of polarization as the angular optical frequency is changed from ω_1 to ω_2,

$$\hat{s}_{out}(\omega_2) = \Gamma(\bar{\omega}, \Delta\omega)\hat{s}_{out}(\omega_1), \tag{4.5}$$

where $\bar{\omega} = (\omega_1 + \omega_2)/2$ is the average frequency while $\Delta\omega = \omega_2 - \omega_1$ is the frequency step size. Note that Γ is not the transfer matrix of the specimen under test i.e. it does not transform an input state to an output state. It however describes the motion of the output state as the wavelength is changed. From equations 4.3 and 4.4, a change in wavelength causes the output state of polarization to precess about the PSP with a rate which is equal to the DGD. Hence, eigenstates of Γ are the PSPs while the DGD is obtained from the eigenvalues.

At an angular optical frequency say ω_1, three noncollinear input states of polarization are input to the specimen under test and the corresponding output states of polarization $\hat{s}_{out}$ are measured. Then the 2×2 Jones transfer matrix $\mathrm{T}(\omega_1)$ can be calculated following Jones (1947) to get:

$$\hat{s}_{out}(\omega_1) = \mathrm{T}(\omega_1)\hat{s}_{in} \tag{4.6}$$

From equation 4.6, $\mathrm{T}(\omega_1)$ is the matrix which describes the transformation of the input state of polarization to the output state of polarization at an angular optical frequency ω_1. The same three states of polarization are again launched at a slightly different optical angular frequency ω_2 so as to calculate $\mathrm{T}(\omega_2)$.

So Γ is obtained as the product $\Gamma(\bar{\omega}, \Delta\omega) = \mathrm{T}(\omega_2)\mathrm{T}^{-1}(\omega_1)$ [1]. Assuming no PDL is present, the output state of polarization will precess about the PSPs. Therefore, the eigenvectors of Γ are the PSPs and the eigenvalues are $\rho_q = \exp(i\tau_{g,q}\Delta\omega)$, where the index q denotes propagation along the fast or slow axis and $\tau_{g,q}$ is the differential group delay. The DGD is then given by (Galtarossa and Menyuk 2005):

$$\Delta\tau(\bar{\omega}) = \left|\tau_{g,s} - \tau_{g,f}\right| = \left|\frac{\mathrm{Arg}(\rho_s/\rho_f)}{\Delta\omega}\right| \tag{4.7}$$

In conclusion, JME allows the full $\vec{\tau}(\omega)$ to be calculated for even the highly mode-coupled telecommunication optical fibres. The matrix Γ is obtained with complete generality and is correct even when PDL is present. But, in the presence of PDL, the eigenstates of Γ will be non-orthogonal and this makes the expression for DGD, equation 4.7, become non exact.

4.2.2.2 Müller Matrix Method

The Müller Matrix Method (MMM) (Jopson *et al.* 1999a) measures PMD in almost the same way the JME measurement technique does except for two slight differences. The first difference is that the calculations are carried out in different vector spaces. MMM uses Müller matrices while the JME uses Jones matrices. Because of this, the algorithm for the MMM is simplified. Secondly, absence of PDL is assumed for the entire MMM measurement technique in contrast to the JME where the absence of PDL is assumed only in the last step i.e. when the DGD is being calculated. Because of this, the MMM determines the difference matrix by launching only two polarization states per wavelength compared to the three for JME and this yields a difference matrix that describes a pure rotation θ of the output state of polarization with wavelength. However, the tradeoff is that the JME difference matrix Γ is exact even when PDL is present but the MMM difference matrix is not. This leads to the JME being less susceptible than the MMM to the presence of PDL. The reader is referred to Jopson *et al.* (1999a) and Williams (2004) for detailed descriptions of MMM.

4.2.2.3 Poincaré Sphere Analysis

This is another measurement technique that is closely related to both JME and MMM. In the Poincaré Sphere Analysis (PSA), the same measurement procedures as for the JME can be used. The only difference is the analysis of the data. Also, like with the MMM, PSA analysis takes place entirely in Stokes space and assumes that PDL is absent throughout the process. The other and major difference of the PSA technique from both JME and MMM is that it works with frequency derivatives of the measured output Stokes vectors rather than derivatives of the polarization transfer matrix. The reader is referred to Williams (2004) and Galtarossa and Menyuk (2005) for the detailed descriptions for the relationship between the output states of polarization and the PMD for the PSA measurement technique.

4.2.2.4 PA, SOP, and PS Techniques

These are some of the other various polarimetric techniques that have similarities with the JME, MMM and PSA. Their names generally come up under the topic “Other measurement techniques.” These techniques, Poincaré Arc (PA), State of Polarization (SOP) and Poincaré Sphere (PS) in general measure the DGD by measuring only $\hat{s}_{out}/\Delta\omega$. This then requires the assumption that

$$\left|\frac{\mathrm{d}\hat{s}_{out}}{\mathrm{d}\omega}\right| = \left|\frac{\mathrm{d}\theta}{\mathrm{d}\omega}\right|. \tag{4.8}$$

This is true when $\hat{s}_{out}(\omega)$ lies on a great circle, and occurs when the input polarization state is launched so that both PSPs are equally illuminated (Gibbon 2007, p.19). However, to maintain this condition in mode coupled devices such as long telecommunication optical fibres is very difficult but it is very possible in non-mode coupled components.

Other measurement techniques are: a) the fixed analyzer technique which offers a simplified approach to a polarimetric measurement (Poole and Favin 1994; Gamatham 2008, p.31). Sometimes it is called *wavelength scanning*. b) the *RF Phase Shift technique* that resembles the time of flight technique (Williams 2004; Galtarossa and Menyuk 2005). c) the *Swept-wavelength Interferometry* which is a new class of measurement technique that has been developed. It determines the PMD from measurement of the full optical transfer function of the device under test (Van Wiggeren *et al.* 2003). d) the *polarization-sensitive optical frequency domain reflectometr*y (P-OFDR) has also recently been developed (Galtarossa *et al*. 2009a; Galtarossa *et al*. 2009b; Palmieri *et al.* 2010a).

After a measurement technique has been chosen, some precautions have to be taken for accurate measurements to be obtained. The patchcords (jumpers) used to connect to the measurement system should have low PMD values and also should be as short as possible. This will help minimize errors from the patchcord birefringence due to asymmetries or stresses from the manufacturing process. Also, care should be taken before the measurement to stabilize both the measurement system and the device under test against temperature changes and movement due to humans, animals, wind etc.

The measurement techniques discussed in this chapter were used in the field and also in the laboratory for measurement of SOPs and PMDs of optical fibres in this study. The analyses of the data obtained by use of some of the instruments described are presented in chapters 5, 6 and 7 in this thesis.

CHAPTER 5

PERTURBATIONS AND ENVIRONMENTAL EFFECTS ON OPTICAL FIBRES

Some precautions need to be taken before measurements are made so as to stabilize the measurement system and also the *fibre under test* (FUT) against perturbations due to humans and also environmental changes due to wind and temperature. This is because PMD in an optical fibre is mainly caused by *birefringence* and complicated by *mode coupling*. These effects are in turn enhanced by the above perturbations resulting in PMD being a statistical phenomenon. In this chapter we highlight the effects of the most common perturbations on aerial optical fibres due to humans and also environmental effects such as wind and temperature.

5.1 Mechanical Perturbations

Even optical fibre leads that have a small amount of PMD can have a profound effect on measurement noise if they are moving during the measurement. This is of particular importance for *polarimetric* measurement techniques that determine PMD by measuring the output state of polarization of the propagating light pulse. A moving optical fibre lead can change the output *state of polarization* significantly which results in a time-dependent output state of polarization. Measuring the state of polarization at different wavelengths, the effect of the optical fibre lead motion will falsely be identified as a change in the polarization state with wavelength (DGD). This DGD error will be proportional to the total DGD that has been measured (not just the DGD of the optical fibre leads). Since the optical fibre lead would have a random motion, this DGD error is also likely to be random but could have an amplitude large enough to obscure the true DGD. In low coherence interferometry, the state of polarization of light is not directly measured and the light propagating down the different states of the FUT is detected simultaneously, so there is much less effect from moving optical fibre leads. In general, PMD measurement accuracy is improved by both stabilizing the measurement and also monitoring PMD over a prolonged time period and using a wide range of wavelength.

5.2 Bend and Twist-Induced PMD

Low PMD optical fibres too can exhibit significant PMD under *bending* and *twisting*, which cause a *stress-induced birefringence*. *Linear birefringence* is induced when the optical fibre is freely bent or bent around the drum. This occurs because the inner part is compressed and the outer part is stretched as shown in figure 5.1.

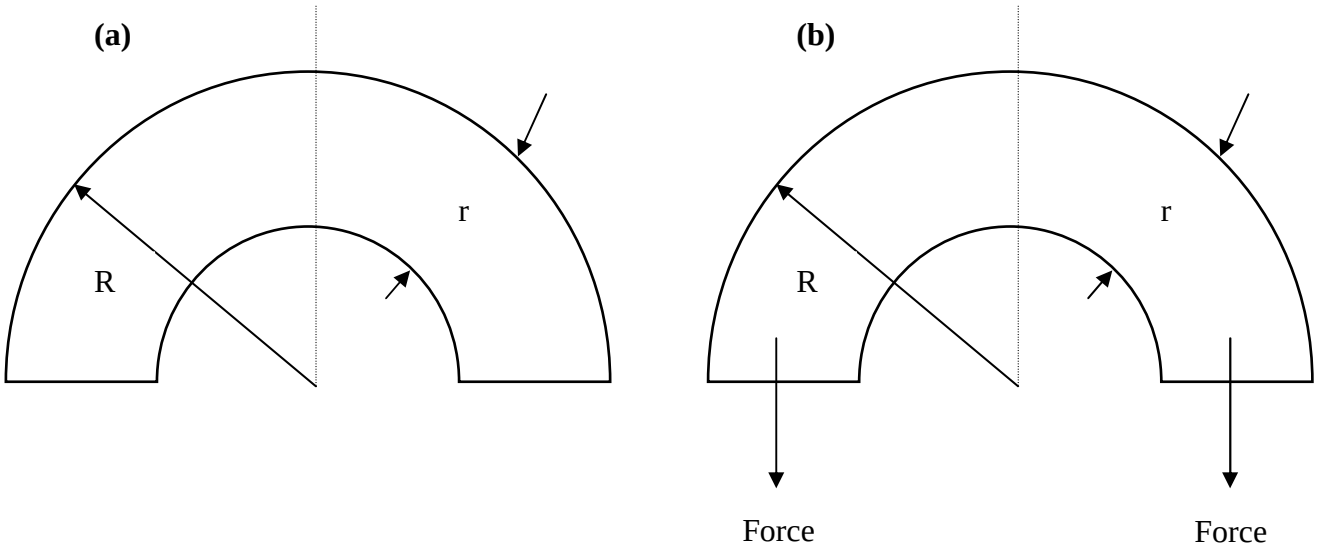

Figure 5.1: An optical fibre that is (a) freely bent and (b) bent by application of a force compressing the inner part and stretching the outer part.

For freely bending fibre, the birefringence, β_B, is given by $\beta_B = 0.5C_s\, r^2/R^2$ where C_s depends on the *strain optical tensor* of the optical fibre and for forced bending, $\beta_B \propto C_s(r/R)f$ where f is the mean axial strain in the optical fibre. Figure 5.2 shows a picture of patchcords that are bent at St. Albans transmission station. The good thing is that such patchcords have very low PMD and so such effects of bending on the overall PMD will be minimal but if one can avoid this it would be better.

Therefore, in general, bending an optical fibre makes its outer layers to exert pressure onto the inner ones and this causes a *linear birefringence* whose fast axis is perpendicular to the bending axis. The modulus of this linear birefringence due to bending, β_B, is inversely proportional to the square of the *bending radius*, R, according to (Jeunhomme 1983; Williams 2004; Galtarossa and Menyuk 2005; Palmieri *et al.* 2010a),

$$\beta_B \simeq 0.276\left(\frac{n^3}{\lambda}\right)\left(\frac{r}{R}\right)^2 \qquad (5.1)$$

where n is the refractive index of the core, λ is the wavelength, r is the optical fibre radius (figure 5.1), and $C_s = 0.552\,n^3/\lambda$. When this is extended to DGD, it is found that the bend induced DGD varies as $1/R$.

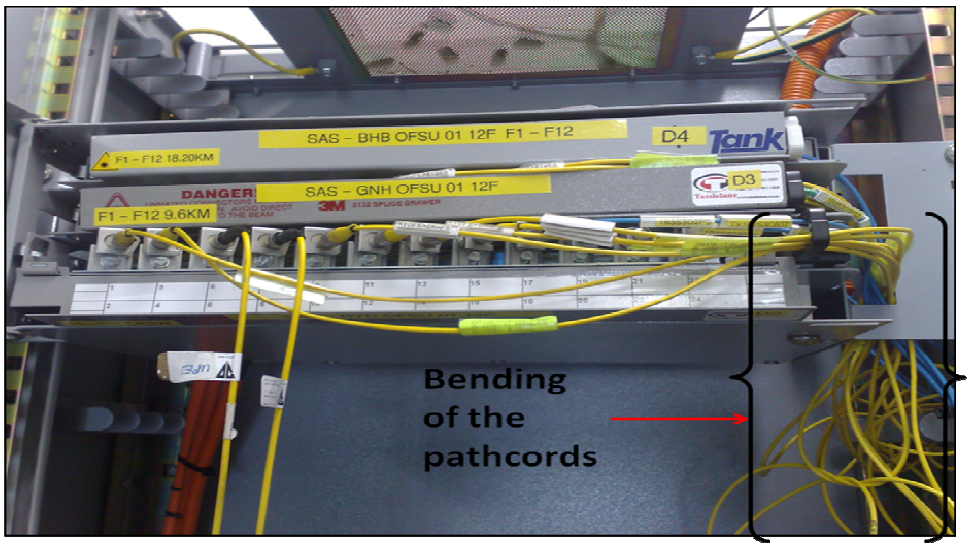

Figure 5.2: Patchcords bent at St. Albans transmission station in Port Elizabeth, South Africa.

When a single-mode optical fibre is *twisted* around its axis (figure 5.3), *optical activity* (i.e. *circular birefringence* is induced (Ulrich and Simon 1979; Mabrouki *et al.* 1998; Galtarossa *et al*. 2009a).

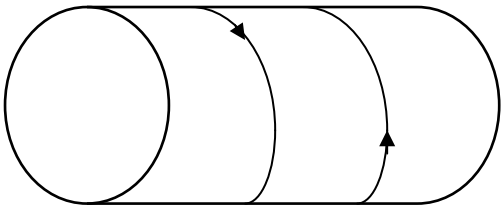

Figure 5.3: A twisted single-mode optical fibre

It has been reported in Rashleigh (1983) and Galtarossa *et al.* (2009a) that the twist-induced circular birefringence is proportional to the twist-rate through the stress-optic rotation coefficient g as shown in equation 5.2.

The circular birefringence, β_C, caused by twist is given as

$$\beta_C(z) = g\frac{\mathrm{d}\delta}{\mathrm{dz}} \qquad (5.2)$$

where $\delta(z)$ is the angle of rotation induced by the twist and g lies between 0.14 and 0.16.

5.3 Interaction of the Aerial Optical Fibre Cable with Wind

In addition to human perturbations, wind too drives mechanical oscillations in aerial optical fibres. The three common excitation mechanisms due to wind are *aeolian* or *vortex-induced* (Wuttke *et al.* 2003), *cable-galloping* (Tomita *et al*. 1988) and *wake-induced* vibrations. Wind is also a major contributor to the bends and twists discussed above in section 5.2. Table 5.1 shows the different excitation mechanisms with the parameter ranges for their occurrence.

Table 5.1: Aerial optical fibre cable vibration mechanisms and the parameter ranges (after Roberge 2009).

Parameter	Vortex-Induced	Galloping	Wake-Induced
Frequency Range	3 to 150 Hz	0.08 to 3 Hz	0.15 to 10 Hz
Peak-to-Peak Amplitude (Expressed in Cable Diameter)	0.01 to 1	5 to 300	0.5 to 80
Wind	Steady	Steady	Steady
Wind Velocity	3 to 30 km/h	25 to 65 km/h	15 to 65 km/h
Cable Surface	Bare or uniformly iced (i.e., hoarfrost)	Asymmetrical ice deposit	Bare, dry

Though not well documented, wind *gusts* too induce optical fibre perturbation. It has been identified as an important parameter to take into account when dealing with optical polarization perturbation for aerial optical fibre cables.

5.3.1 Vortex Induced Vibrations

Vortex induced vibration is the resonant, small amplitude vibration caused by steady, low velocity wind blowing across optical fibre cables under mechanical tension. The optical fibre cable vibration is caused by the periodic aerodynamic force created by vortices in the wake of the air on the leeward side of the optical fibre cable. It is under sustained low velocity winds that vortex induced vibrations occur and they cause the optical fibre cable to resonant at frequencies that reach 150 Hz depending on the installation specifics (see table 5.1). Vortex induced vibrations are very common in long spans of round optical fibre cables installed at

high mechanical tensions. Also from table 5.1, these vibrations occur at wind speeds ranging from 3 km/h to 30 km/h above which an increase in *leeward wake turbulence* is observed until vortex induced vibrations cease. Figure 5.4 shows the variations of the Stokes parameters of an aerial optical fibre link (14.8 km) between St. Albans and Rockland transmission station. The measurements were made on 17 June 2009 from 9:16 to 9:46 am (30 minutes).

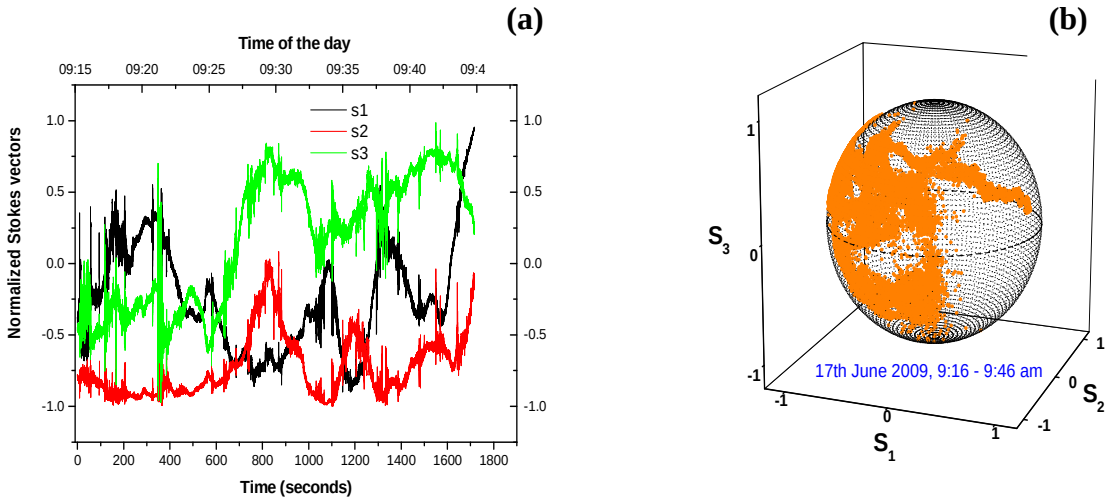

Figure 5.4: (a) Time evolution of normalized Stokes parameters (b) Poincaré representation of the variations of the SOPs collected on 17 June 2009 for 30 minutes on a 14.8 km aerial optical fibre link. The wind speed was 6.5 km/h with mild wind gusts and the temperature was 13.8 ºC.

The average temperature during these 30 minutes was 13.8 ºC and the wind speed was 6.5 km/h, on average, with mild wind gusts. These weather conditions thus fall in the vortex induced vibrations range. A slow shift in the three components of the Stokes vector with relatively little noise is observed (figure 5.4(a)) and figure 5.4(b) shows a relatively smooth random walk-like pattern.

5.3.2 Cable Galloping

Galloping occurs when an optical fibre cable is exposed to a moderate or strong wind in the range 25 to 65 km/h as shown in table 5.1. The shape that results takes that of an elongated ellipse with its major axis predominantly in the vertical direction (Tomita *et al.* 1988; Roberge 2009). Figure 5.5 shows an illustration of optical fibre cable galloping vibrations on the St. Albans to Rockland transmission stations in Port Elizabeth, South Africa.

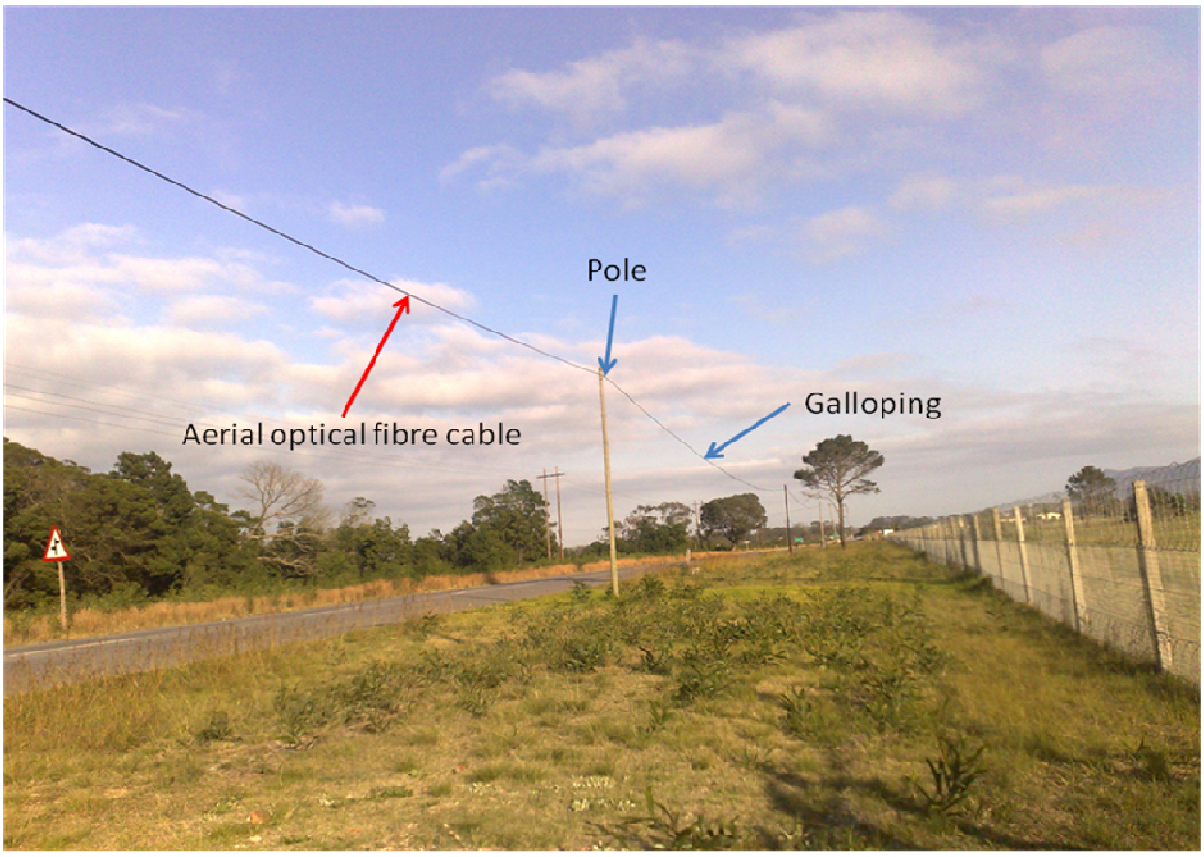

Figure 5.5: A photograph showing the aerial optical fibre cable that links St. Albans and Rockland transmission stations in Port Elizabeth, South Africa. Also shown is the cable galloping due to strong winds.

This wind induced cycle cable loading mechanism is characterized by large amplitude and low frequency movement of a non-concentric designed cable or even a round cable whose shape has been distorted due to tensions from the poles supporting it. In figure 5.6 (section 5.3.4), we present the variations of the SOPs on a Poincaré sphere as well as the variations of the components of the Stokes vectors for an aerial optical fibre cable exposed to wind speeds of 37 km/h with wind gusts of 58 km/h measured for 30 minutes.

5.3.3 Wake Induced Vibrations

This type of vibration occurs when two cable lines hang side by side and are separated by a spacer. The *wake* from the windward cable induces lower drag and creates lift forces on the leeward line. Cables that share a spacer or a support yoke influence one another's motion by coupling through the spacer. The motion that results could be in the vertical or the horizontal plane. However, on the optical fibre transmission network in South Africa, we don't have such cables with spacers and hence these vibrations are not experienced.

5.3.4 Wind Gusts

Wind *gusts* are defined as sudden, brief increase in the speed of the wind. Wind gusts are observed when the peak wind speed reaches at least 30 km/h and the variation in wind speed between the peaks and the lulls is at least 17 km/h (Roberge 2009). The time duration of a wind gust is approximately less than 20 seconds. Wind gusts affect the whole system i.e. pole-cable combination, by feeding natural resonance frequency and by moving the center of mass of the whole structure.

Figure 5.6 shows the variations of the Stokes parameters of an aerial optical fibre link (14.8 km) between St. Albans and Rockland transmission station. The measurements were made on 23 June 2009 from 10:26 to 10:30 am (4 minutes). In figures 5.6 (b), (c), (d) and (e), we present per minute population on the Poincaré sphere with time. As can be visualized from these figures, the population growth increases with time.

The average temperature during these 4 minutes was 18.5 ºC and the wind speed was 37 km/h, on average, with wind gusts up to 58 km/h. These weather conditions thus fall in the galloping vibrations range. From figure 5.6(a) it is clear that the instantaneous noise on the Stokes unit vector components increased by a significant amount when compared to figure 5.4(a). This large white noise like behaviour of the Stokes vector components indicates a major increase in the stress induced by the wind on the aerial optical fibre cable. It should be noted that this white noise-like structure comes from very small but numerous changes in the mode coupling of the aerial optical fibre. Also, with constant wind, a rapid white noise like rotation of the Stokes vector is observed (figure 5.4(a)) while wind gusts generate slow rotations of large amplitude of the Stokes vector (figure 5.6(a)).

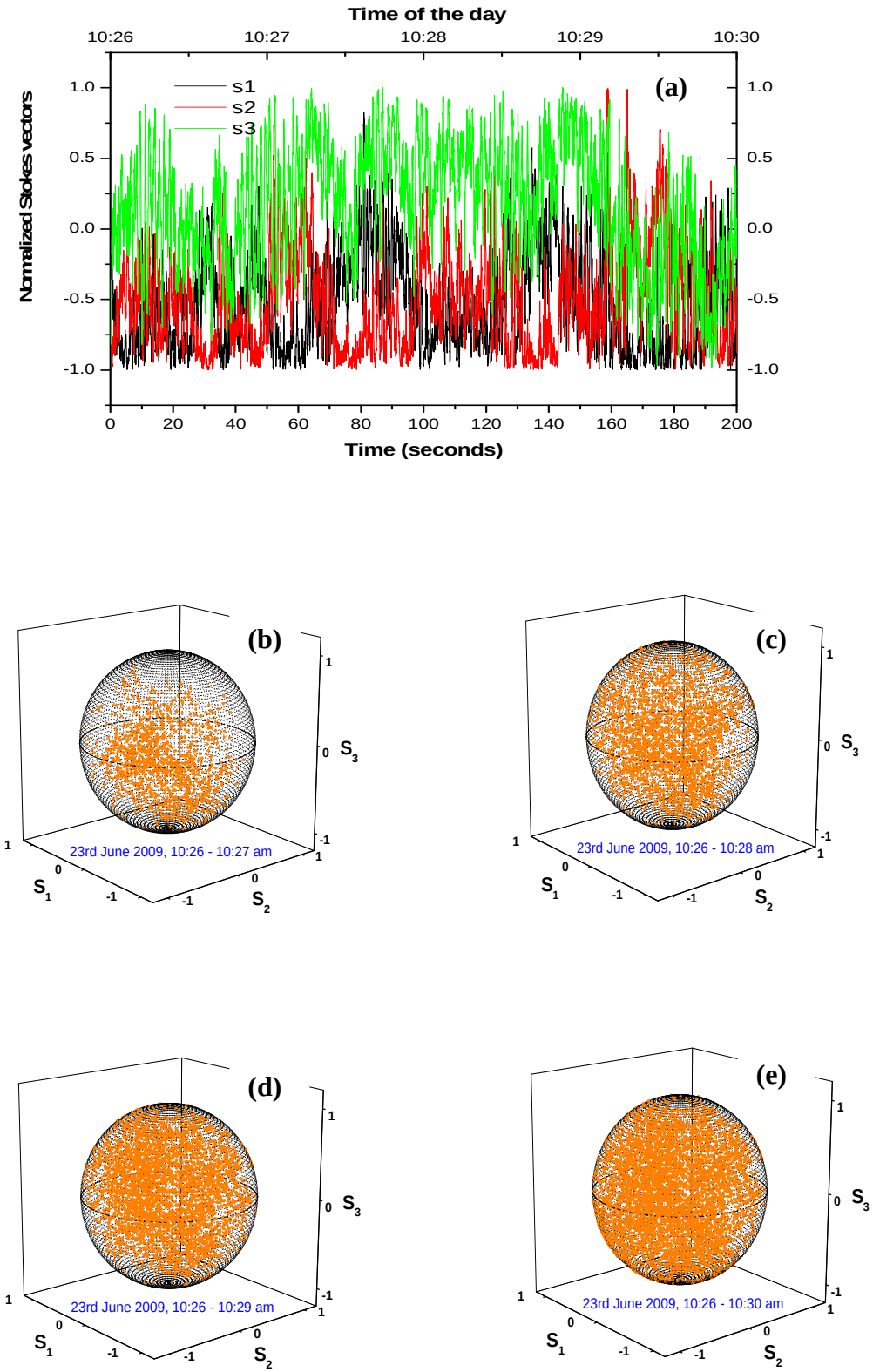

Figure 5.6: (a) Time evolution of normalized Stokes parameters; (b), (c), (d) and (e) Poincaré sphere representation of the variations of the SOPs collected on 23 June 2009 per minute for 4 minutes on a 14.8 km aerial optical fibre link. The wind speed was 37 km/h with wind gusts of up to 58 km/h and the temperature was 18.5 ºC.

Therefore, bends, twists and strain on an optical fibre affect its birefringence while the movement or oscillations of the optical fibre affects the SOP of the propagating light pulse. For an optical fibre movement from its original plane, a significant change in the SOP is observed due to either the geometric phase effect or the birefringence of the fibre or both (Tomita and Chiao 1986; Schinn 2003). The change in the *Berry phase* also commonly known as the *geometric phase effect* occurs when the elliptical SOP of light rotates without a change in the geometry of the fibre and on the degree of polarization (DOP) of the light (Schinn 2003; Musara 2009, p.7). This is also confirmed by our results shown in figure 5.6 above.

5.4 Effects of Temperature

Temperature also induces changes in birefringence of an optical fibre (Hakki 1996; Cameron *et al.* 1998a; Willner *et al*. 2004). Hence, temperature needs to also be kept stable during a measurement even for devices with relatively low temperature dependence of their PMD in a laboratory environment (De Lignie 1994). Changing the temperature of a device will change the birefringence slightly and this will cause a change in the state of polarization with time. This produces a DGD error proportional to the total DGD of the measurement. Hence, temperature drift is of great concern because as the temperature increases, the output state of polarization will precess about the eigenaxes of the fibre under test (FUT). This implies that the drifting temperature will systematically bias the measured DGD as opposed to the random error due to the optical fibre in motion.

Figure 5.7 illustrates the effect of change in temperature which causes a change in the optical fibre birefringence that in turn causes a change in the output state of polarization of the light pulse. These SOPs were collected on 10 June 2009 for 30 minutes on an aerial optical fibre cable (14.8 km) linking St. Albans and Rockland transmission stations. The temperature changed from 15.5 ºC to 19 ºC and the wind speed was low (6.9 km/h) with very mild wind gusts. Therefore, fluctuation in the temperature of the exposed aerial optical fibre leads to a random fluctuation of the Stokes unit vector parameters (figure 5.7(a)) and well as random population of the Poincaré sphere (figure 5.7(b)). This is in agreement with other researchers such as Poole *et al.* (1991) and Cameron *et al*. (1998a).

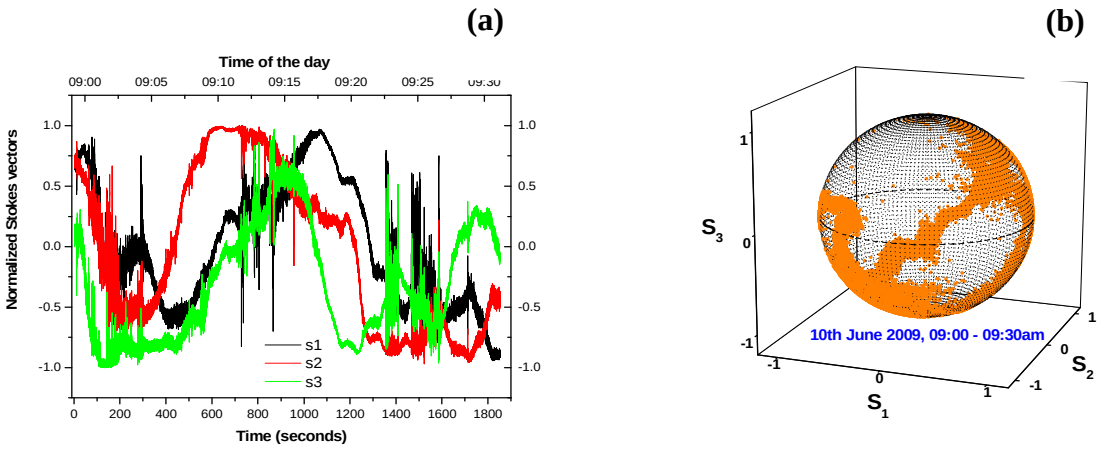

Figure 5.7: (a) Time evolution of normalized Stokes parameters (b) Poincaré representation of the variations of the SOPs collected on 10 June 2009 for 30 minutes on a 14.8 km aerial optical fibre link. The wind speed was 6.9 km/h with mild wind gusts and the temperature changed from 15.5 ºC to 19 ºC in this time period.

It has also been shown that greater PMD variations occurred during the sunset and sunrise when the temperature changes are high (Poole *et al.* 1991; Cameron *et al.* 1998a). The variations of PMD during the night are also much less compared to day time. Figure 5.8 confirms these findings. It shows the spread of SOPs on Poincaré spheres for day time (from 12 noon to 12:30 pm) and night time (from mid night to 00:30 am). The average temperatures and average wind speeds are 25.3ºC and 10.2 km/h for the former and 13.6ºC and 8.7 km/h for the latter respectively.

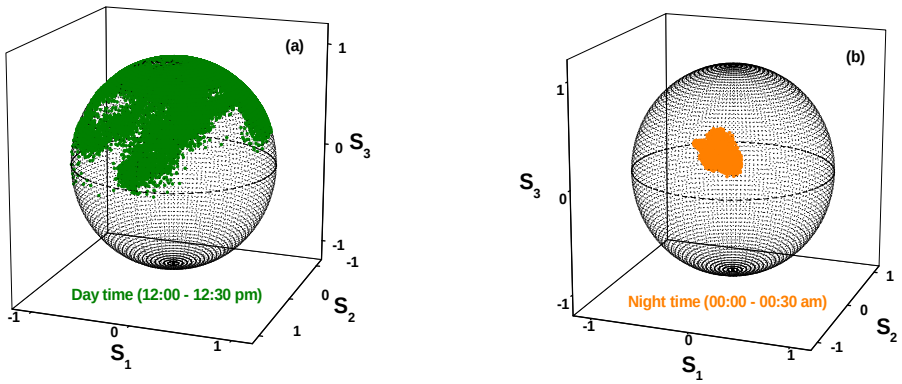

Figure 5.8: Illustration of the spread of the SOPs on the Poincaré sphere for 30 minutes on 10 June 2009 for an aerial optical fibre cable linking St. Albans and Rockland transmission stations, (a) during day time (temperature is 25.3ºC and wind speed is 10.2 km/h) and (b) during the night (temperature is 13.6ºC and wind speed is 8.7 km/h).

The spread of SOPs during day time (figure 5.8(a)) is much more random compared to that at night (figure 5.8(b)). This is mainly because at night the temperatures are relatively low and the wind is also calm as compared to day time (for this case noon) where the temperatures are normally at their highest and wind speeds as well. Also shown by Cameron *et al*. (1998a) is the impact temperature has on aerial optical fibres compared to the secured buried fibres (Allen *et al.* 2003). In aerial optical fibres, the SOP fluctuations are more random than for a buried optical fibre.

In this chapter, all the weather information was provided by the South African Weather Service in Port Elizabeth, South Africa. However, we were also able to acquire a *pocket weather tracker* (figure 5.9) that we placed at St. Albans transmission station so as to measure the environmental parameters more accurately since it was nearer our aerial optical fibre cable.

In the next chapters, some of the weather information will be from this pocket weather tracker for measurements collected in August 2010, while those made earlier (June 2009) will be from the South African Weather Service.

Figure 5.9: Kestrel 4500 pocket weather tracker at St. Albans transmission station.

5.5 Summary of Results

In section 5.3, a slow drift of the normalized Stokes vectors with little noise and a smooth random walk pattern for the population on the Poincaré sphere was observed in the vortex-induced vibrations for wind speeds in the range 3 to 30 km/h. However, rapid white noise-like rotation of the Stokes parameters as well as random population of the Poincaré sphere was obtained in the presence of wind gusts in the cable galloping region.

In section 5.4, an investigation of the influence of temperature on the SOP spread was done. It was found that the SOP spread is much more random during the day compared to the evenings and night times because of the higher temperatures for the former. The average temperature was 25.3ºC during the 30 minutes from noon and it was 13.6ºC during the 30 minutes from mid night on 10 June 2010.

Acknowledgements

The author extends his sincere thanks to Prof. Ernest van Dyk and Dr. Freddie Vorster of the Center of Energy Research, Department of Physics, Nelson Mandela Metropolitan University for the loan of the Kestrel 4500 pocket weather tracker used for the measurement of the environmental parameters in August 2010 at St. Albans transmission station in Port Elizabeth, South Africa. The author is also grateful to Ms. Varsha Nagar of the Port Elizabeth office of the South African Weather Service for providing weather information for the month of June 2009.

CHAPTER 6

PMD MEASUREMENTS AND COMPENSATION

State of polarization (SOP) and polarization mode dispersion (PMD) are stochastic in nature due to changes in the properties of the optical fibres and its positions because of both intrinsic and extrinsic perturbations. In this chapter, we investigate PMD and SOP changes in aerial fibres. This is of particular relevance in South Africa, as part of the backbone of the national grid includes long distances of aerial optical fibre between exchange stations. Statistical distributions for first order polarization mode dispersion (FO-PMD) and second order polarization mode dispersion (SO-PMD) are experimentally confirmed when measured using the FTB-5700 Single-Ended Dispersion Analyzer[1] instrument for aerial optical fibres. With only 184 PMD values obtained by use of the FTB-5700 Single-Ended Dispersion Analyzer (measured during August 2010), the predicted theoretical Gaussian fit was obtained with a mean of 0.47 ps and standard deviation of 0.08 ps. This small standard deviation was justification for its robustness and accuracy. The determination of the time scale over which to compensate FO-PMD in aerial fibres using the directional time drift autocorrelation function method is also discussed. It is found to be slightly higher than 390 s for SOP measurements made on a particular windy and hot day (Ireeta *et al.* 2010b). This is due to the fact that the changes of the PMD vector are known to be slower than the state of polarization (SOP) changes.

Available techniques to mitigate or compensate for PMD mainly target buried, ducted and submarine fibres (Waddy *et al.* 2005). This is because the PMD changes in such optical fibres are slow since the strain remains relatively constant and temperature fluctuations are minimal. The direct exposure of aerial optical fibres to the fluctuating environment makes the mitigation or compensation of PMD challenging because of their rapid changes in PMD. Most results in this chapter have been presented/published at/in peer reviewed conferences and journals respectively (Ireeta *et al*. 2010a; Ireeta *et al*. 2010b).

6.1 Statistical Distributions of PMD

To develop effective PMD compensation techniques, it is important to measure and also characterize the probability density functions (pdfs) of random quantities such as the DGD. In

[1] We would like to acknowledge EXFO (EXPERTISE REACHING OUT) company for the loan of this instrument.

this section, the PMD of the aerial optical fibre (ITU-T G.652) was measured during the month of June 2009 (winter season) and August 2010 (spring season) using the FTB-5700 single-ended dispersion analyzer. The aerial optical fibre cable links two local Telkom exchange transmission stations in Port Elizabeth, South Africa, and is exposed to dynamic environmental changes. Wind caused the optical fibre cable to gallop and oscillate mainly due to its direction and speed. This, together with temperature fluctuations, lead to the change in birefringence of the optical fibre. Since the aerial optical fibre was in a dynamic state, its PMD and SOP changed on short time scales.

The experimental set up was such that at one end of the looped fibre was the FTB-5700 and the other end was the open optical fibre (figure 6.9, section 6.4). This is a single-ended measurement technique that uses the same principle as the polarization optical time-domain reflectometer (P-OTDR) that is based on measurement of the degree of polarization of the back scattered light as a function of distance in the fibre (Corsi *et al.* 1999; Galtarossa *et al.* 2000a) as earlier discussed in chapter 4.

The aerial optical fibres were exposed to severe vortex-induced oscillations. Vortex-induced oscillations are aerial optic fibre cable vibrations that are due to steady winds with a velocity range between 3 and 30 km/h and have a frequency range from 3 to 150 Hz (Roberge 2009) as earlier discussed in chapter 5. During the month of June 2009 (winter season), the winds were fairly steady with low speeds (mean speed of 18.7 km/h). In total, 224 PMD measurements were made at 30 minute intervals in this period using the FTB-5700 instrument. Then in the month of August 2010 (spring season), the winds were mild with an average of about 9.1 km/h (period during which measurements were made). In this period, 249 PMD values were made on an unlooped fibre (7.4 km long) and 184 PMD values on two fibres that had been looped (14.8 km long) using the FTB-5700. For comparison purposes we also made PMD measurements using the GINTY instrument. It should be noted that during the month of June 2009, the weather information was provided by the South African Weather Service which is some few kilometers from the transmission stations. However, for the August 2010 measurements, we used the Kestrel 4500 pocket weather tracker that was placed at one of the transmission stations. This was helpful since the weather measurements were for the conditions where our aerial optical fibre cable is located.

6.1.1 FO-PMD Statistical Distributions

Figure 6.1(a) shows a histogram of the PMD values measured during the month of June 2009 in the winter season. During this period, extremes of both temperature and wind speeds were

observed. The instrument with its measurement techniques gave us accurate results despite the rapid changes in environmental conditions. These measurements were carried out at random times during this period. The average PMD of the optical fibre was 0.46 ps with a standard deviation of 0.09 ps. Hence we were able to quantify the PMD changes in the aerial fibre exposed to the dynamic environment. Both the Maxwellian and Gaussian probability density functions (pdf) were fitted onto the data and from figure 6.1(a), it clearly shows that the Gaussian is a better fit to the distribution as would be expected theoretically (Gisin *et al*. 1996; Shtaif and Mecozzi 2000).

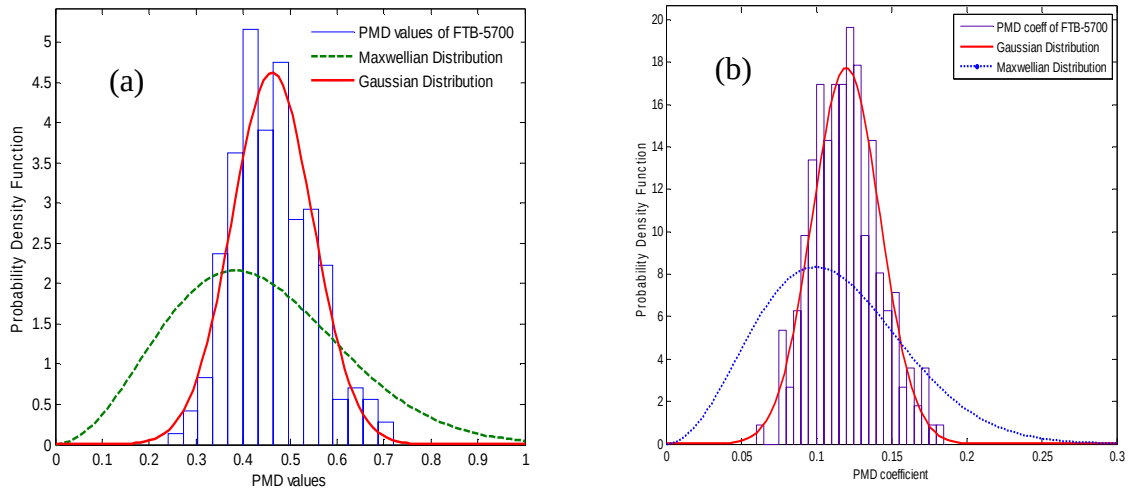

Figure 6.1: (a) the histogram of the PMD values (ps); (b) the histogram of the FO-PMD coefficient values (ps/√km) obtained on measuring the aerial optical fibre (ITU-T G.652) from 8 to 23 June 2009 using the FTB-5700. The bin size is 25. Also shown are the Gaussian and Maxwellian distributions fittings.

Figure 6.1(b) shows a histogram of the FO-PMD coefficient values measured. These measurements were also carried out at random times during this period. The average FO-PMD coefficient of the optical fibre was 0.12 ps/√km with a standard deviation of 0.02 ps/√km. Both the Maxwellian and Gaussian probability density functions (pdfs) were fitted onto the histogram and clearly from figure 6.1(b), it indicates that the Gaussian is a better fit to the distribution as expected from theory (Gisin *et al*. 1996; Galtarossa and Palmieri 1998; Shtaif and Mecozzi 2000; Lee *et al.* 2003).

In order to test the accuracy and robustness of the FTB-5700 instrument, we made measurements on the same optical fibres of our aerial cable after more than one year (August 2010) as well as during a different season (spring). Figures 6.2 (a) and (b) show histograms

for the PMD and FO-PMD coefficient values respectively obtained during this period. Again both the Maxwellian and Gaussian probability density functions (pdfs) were fitted onto the histogram and clearly from figures 6.2 (a) and (b), the Gaussian is a better fit to the distributions. The average PMD of the optical fibre was 0.47 ps with a standard deviation of 0.06 ps while the average FO-PMD coefficient of the optical fibre was 0.16 ps/√km with a standard deviation of 0.02 ps/√km. The slight differences between these values of the two different measurement periods could be because of the environmental conditions.

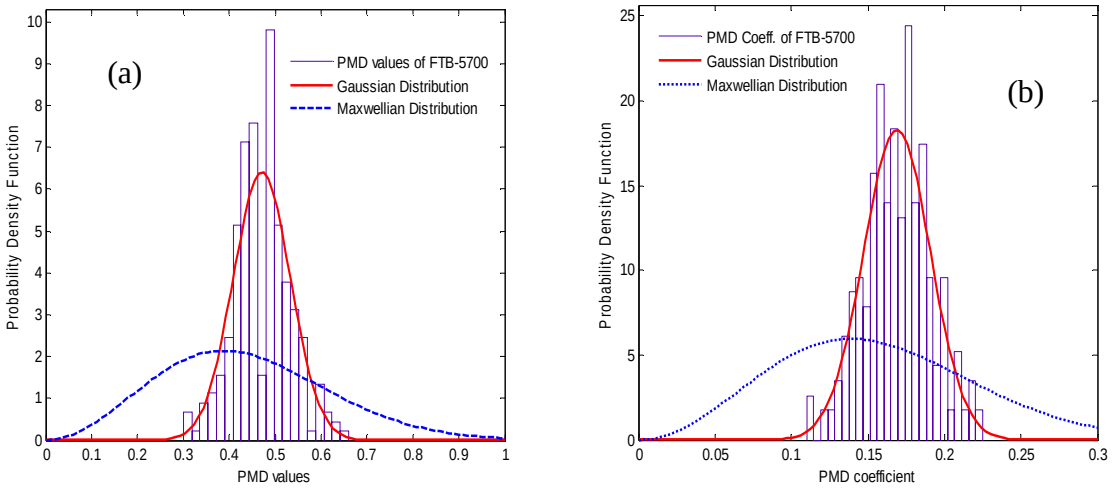

Figure 6.2: (a) the histogram of the PMD values (ps) (b) the histogram of the FO-PMD coefficient values (ps/√km) obtained on measuring the aerial optical fibre (ITU-T G.652) from 17 to 24 August 2010 using the FTB-5700. The bin size is 25. Also shown are the Gaussian and Maxwellian distributions fittings.

During June 2009, the average wind speed was 18.7 km/h and the average temperature was 15.1ºC while in August 2010, the wind speed was less than half (9.1 km/h) and the temperature was 12.4 ºC.

Some researchers have used the traditional interferometric methods for PMD measurements (Brodsky *et al.* 2003; Mudau 2008, p.82). Brodsky *et al.* (2003) made 950 and Mudau (2008), of our research group, made 150 000 PMD measurements for them to be able to get a Gaussian fit for the PMD statistics. However, in this study, we were able to get the Gaussian fit with only 224 PMD measurements (during the month of June 2009) and 184 PMD measurements (during the month of August 2010) using the FTB-5700 instrument under different weather conditions. This justifies its robustness in accurately measuring the PMD of aerial fibres. The reason being this instrument has SOP scrambling analysis (SSA) implemented in it to be able to measure an aerial optic fibre cable under aeolian perturbations.

6.1.2 SO-PMD Statistical Distributions

Figure 6.3 shows histograms for the SO-PMD values measured using the FTB-5700. The measurements were also carried out at random times during the winter month of June 2009 (figure 6.3(a)) and spring month of August 2010 (figure 6.3(b)). The average SO-PMD of the optical fibre was 0.10 ps/nm with a standard deviation of 0.04 ps/nm for the June 2009 period and 0.10 ps/nm with a standard deviation of 0.03 ps/nm for the August 2010 period.

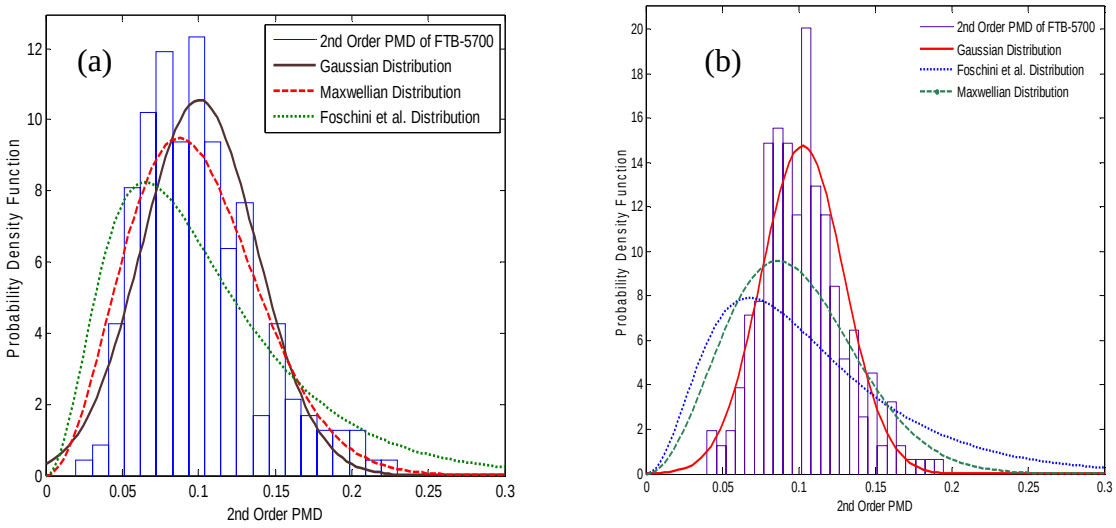

Figure 6.3: The histograms of SO-PMD values (ps/nm) obtained on measuring the aerial optical fibre (ITU-T G.652) (a) from 8 to 23 June 2009, (b) from 17 to 24 August 2010 using the FTB-5700. The bin size is 25. Also shown are the Gaussian, Maxwellian and Foschini *et al.* (2000) distributions.

The zero difference in these values implies that for this particular aerial optical fibre used, environmental conditions did not affect the SO-PMD as much as they did for FO-PMD (section 6.1.1). The SO-PMD statistics we obtained (figure 6.3) are similar to those obtained by many researchers (Foschini *et al*. 1999; Nelson *et al*. 1999; Phua and Haus 2002; Zalevsky and Eckhouse 2004; Musara *et al*. 2009c).

The Gaussian, Maxwellian and Foschini *et al.* (2000) pdfs were fitted onto the histograms and to a good approximation it is seen that the Gaussian distribution is the best fit to the distributions followed by the Maxwellian and then the Foschini *et al.* (2000) distributions. This is in agreement to the findings made by Foschini *et al*. (1999), Foschini *et al*. (2000), Foschini *et al*. (2001), Forestieri 2003, Musara *et al*. (2009b), and Musara *et al*. (2009c). This was true notwithstanding the fact that we considered few SO-PMD values i.e. 224 values during the June 2009 period and 249 values during the August 2010 period.

6.2 FTB-5700 Versus GINTY

This section provides a comparison of the PMD values obtained when measured using the FTB-5700 and GINTY instruments. The aerial optical fibre used was the same for both instruments. It was looped at the Rockland transmission station to give a total length of 14.8 km. All the measurement instruments were placed at St. Albans transmission station. The GINTY experimental setup was such that at one end of the FUT was the EXFO FLS 5800 CD/PMD polarized broadband source that covers the C- and L- bands (1530 – 1625 nm) and the other end was the GINTY. The measurements were all done during the spring season (from 17 to 24 August 2010). The data presented in the proceeding subsections was obtained at random times during this measurement period.

6.2.1 First-Order PMD (FO-PMD)

In figure 6.4, statistics for the first-order PMD values obtained using the single-ended dispersion analyzer with FTB-5700 and the general interferometric method (GINTY) with FTB-5500B are presented.

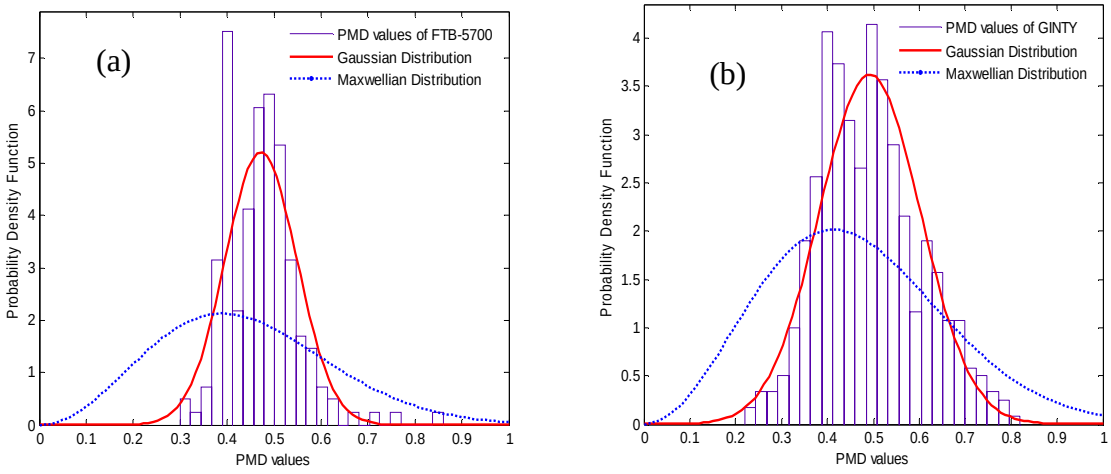

Figure 6.4: Statistics of First-Order PMD (FO-PMD) for (a) FTB-5700 single-ended dispersion analyzer and (b) the General interferometric method (GINTY) with FTB-5500B for a 14.8 km long aerial optical fibre linking Rockland and St. Albans transmission stations. The bin size is 25. Also shown are the Gaussian and Maxwellian distributions fittings.

The total number of measurement values obtained using the FTB-5700 instrument were 184 while those for the GINTY were 503. It should be noted that during measurements with GINTY, it was set to average 5 PMD measurements and on average it would take us about 4 hours to obtain 100 measurements. Then for the FTB-5700, it would take approximately 6

minutes, on average, to record a PMD reading. The average PMD of the aerial optical fibre was 0.47 ps with a standard deviation of 0.08 ps for the FTB-5700 (statistics of figure 6.4(a)). When the GINTY was used, the average PMD value of the aerial optical fibre was 0.49 ps with a standard deviation of 0.11 ps (statistics of figure 6.4(b)). These two values show that the two instruments are accurate in determining the aerial optical fibre PMD since the difference between them is small. The PMD value of this aerial optical fibre is known to be 0.46 ps. Both the Maxwellian and Gaussian probability density functions (pdfs) were fitted onto the histograms and clearly from figure 6.4, it indicates that the Gaussian is a better fit to the distributions compared to the Maxwellian. The Gisin *et al.* (1996) PMD uncertainty principle was applied to the two distributions above and we obtained 11% and 12% for the FTB-5700 and GINTY statistics respectively. These two percentages fall within the range proposed by Gisin *et al.* i.e. for a PMD of 1 ps, the measurement uncertainty due to the statistical nature of the DGD was found to be about 9 % and for a PMD of 0.1 ps, the uncertainty was 28%. Therefore, these results clearly demonstrate that the FTB-5700 can detect unstable polarization conditions and can provide accurate PMD measurement values though it is a single-ended measurement instrument.

6.2.2 First-Order PMD Coefficient

In this subsection, first-order PMD (FO-PMD) coefficient values are presented. Figure 6.5(a) shows the statistics of PMD coefficient values obtained from the FTB-5700 instrument while figure 6.5(b) for those obtained using the GINTY.

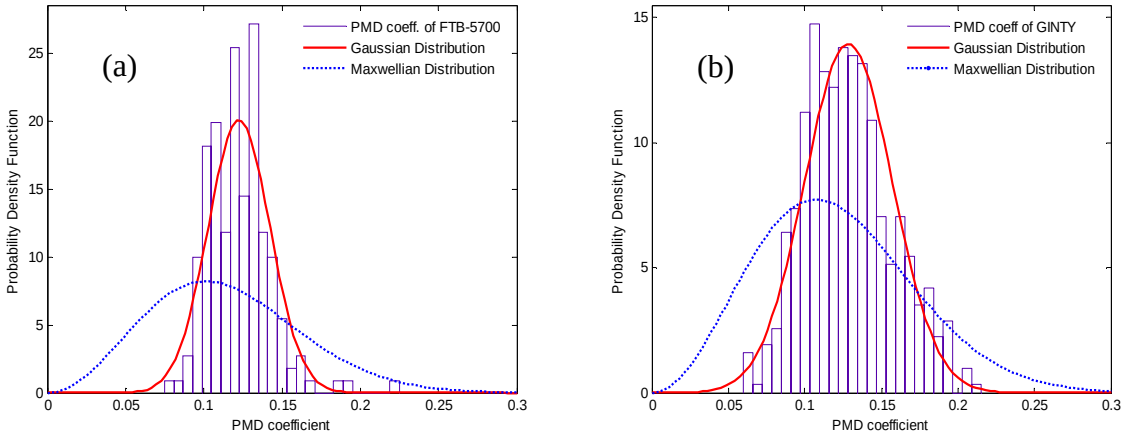

Figure 6.5: Statistics of First-Order PMD (FO-PMD) coefficients (ps/√km) for (a) FTB-5700 single-ended dispersion analyzer and (b) the General interferometric method (GINTY) with FTB-5500B for a 14.8 km long aerial optical fibre linking Rockland and St. Albans transmission stations. The bin size is 25. Also shown are the Gaussian and Maxwellian distributions fittings.

The same numbers of measurement values for both the FTB-5700 and GINTY as described in section 6.2.1 above were considered here. The average FO-PMD coefficient of the aerial optical fibre was 0.12 ps/√km with a standard deviation of 0.02 ps for the FTB-5700 (statistics of figure 6.5(a)). For the GINTY, the average FO-PMD coefficient value of the aerial optical fibre was also 0.12 ps/√km with a standard deviation of 0.03 ps/√km (statistics of figure 6.5(b)). The two FO-PMD coefficient values obtained for both instruments are equal. This implies that both the FTB-5700 and the GINTY accurately determined the actual FO-PMD coefficient value of this aerial optical fibre. Both the Maxwellian and Gaussian probability density functions (pdfs) were fitted onto the histograms and clearly from figure 6.5, it indicates that the Gaussian is a better fit to the distributions compared to the Maxwellian.

6.2.3 Second-Order PMD (SO-PMD)

Figure 6.6 shows histograms for the SO-PMD values measured using the FTB-5700 and GINTY. The statistics obtained for SO-PMD values from the FTB-5700 are shown in figure 6.6(a) while those for GINTY are shown in figure 6.6(b). The average SO-PMD of the optical fibre was 0.10 ps/nm with a standard deviation of 0.04 ps/nm for the FTB-5700 and 0.12 ps/nm with a standard deviation of 0.05 ps/nm for the GINTY.

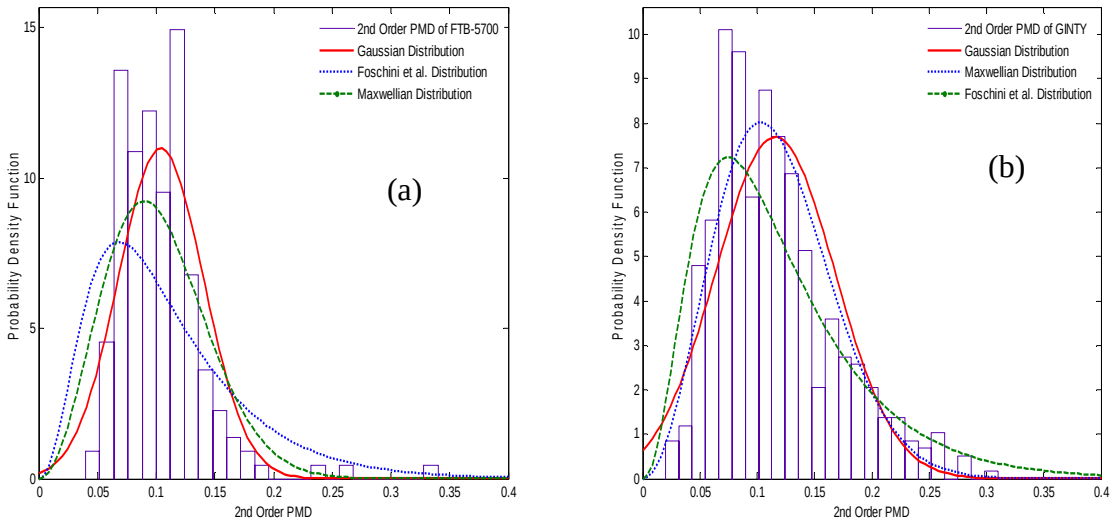

Figure 6.6: Statistics of Second-order PMD (SO-PMD) (ps/nm) for (a) FTB-5700 single-ended dispersion analyzer and (b) the General interferometric method (GINTY) with FTB-5500B for a 14.8 km long aerial optical fibre linking Rockland and St. Albans transmission stations. The bin size is 25. Also shown are the Gaussian, Maxwellian and Foschini *et al.* (2000) distributions fittings.

The two SO-PMD values obtained using the two instruments indicate a slight difference that is minimal and can be ignored. Then the theoretical equation for the mean of the SO-PMD distribution, $(2G/\pi)\tau^2$ see Appendix B, was applied to these statistics to determine the accuracy. This equation was first proved by Foschini *et al.* (2000) and has also been applied to determine the mean for the rate of change of SOPs by Ireeta *et al.* (2010b) as will be discussed in chapter 7. With the PMD of the aerial optical fibre being 0.46 ps, the theoretical mean is 0.12 ps/nm which is approximately the same as the experimentally measured SO-PMD means using the FTB-5700 and the GINTY. This theoretical mean proof together with the SO-PMD statistics obtained (figure 6.6), that are similar to those obtained by many researchers (Foschini *et al*. 1999; Nelson *et al*. 1999; Phua and Haus 2002; Zalevsky and Eckhouse 2004; Musara *et al*. 2009c), shows again that the FTB-5700 can accurately measure SO-PMD of an aerial optical fibre.

The Gaussian, Maxwellian and Foschini *et al.* (2000) pdfs were fitted onto the histograms and to a good approximation it is seen that the Gaussian distribution is the best fit to the distribution of the FTB-5700 statistics followed by the Maxwellian and then the Foschini *et al.* (2000) distributions (figure 6.6(a)). However, to a good approximation, the Maxwellian pdf is the best fit for the statistics of the GINTY followed by the Gaussian pdf and lastly the Foschini *et al.* (2000) pdf (figure 6.6(b)). The reason for this could be because of the difference in the number of measurement values used in the two instances. For the GINTY, 503 values were used while for the FTB-5700, 184 values were used. Confirmation for this is shown in figure 6.3(a) where the number of SO-PMD measurement values was 224 for the FTB-5700 and the statistics approximately tends to fit the Maxwellian distribution. In future more extensive SO-PMD measurements should be done using the FTB-5700 to prove this.

6.3 PMD Variations

In this section, the fluctuations of the FO-PMD, FO-PMD coefficients, and SO-PMD are monitored over time and also with respect to the environmental conditions. Long term measurements of FO-PMD have been done before by Mudau (2008) of our research laboratory using the GINTY only. However, in this current study, the FO-PMD coefficients and SO-PMD fluctuations were also monitored in addition to making a comparison between the measurements obtained using the FTB-5700 and the GINTY. This is the first time to our knowledge that such a comparison has been done. These measurements were made on a 14.8

km long deployed aerial optical fibre that links St. Albans to Rockland transmission stations. The weather information was obtained from the Kestrel 4500 pocket weather tracker that was set up at St. Albans transmission station.

6.3.1 Fluctuation with Time

Figure 6.7 visualizes the fluctuations of the above parameters with respect to time. These measurements were carried out during the month of August 2010 (spring season) but the results presented here are for 24 August 2010 from 09:00 am to 14:00 pm. During this measurement period the mean temperature was 15.5ºC and the mean wind speed was 22.7 km/h. The parameter fluctuations when the FTB-5700 instrument was used are shown in figure 6.7(a) while those when the GINTY was used are shown in figure 6.7(b). From both these graphs, it is clear that generally the parameter fluctuations for both instruments follow the same trend. That is, the peaks and troughs for both instruments happen at almost the same time. A case in point is that the maximum FO-PMD, FO-PMD coefficient, and SO-PMD values for both instruments are obtained at approximately 10:55 am. Another observation from the graphs is the smaller fluctuation of the FO-PMD values for the FTB-5700 instrument as compared to the GINTY. The former's values fluctuate between 0.35 ps and 0.52 ps yet those for the latter fluctuate between 0.35 ps and 0.78 ps.

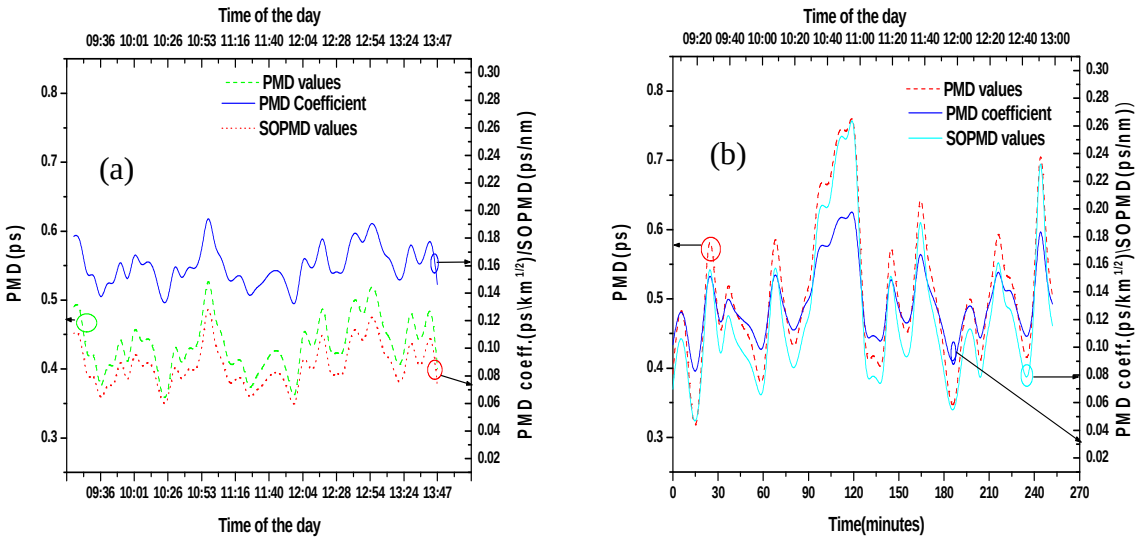

Figure 6.7: The fluctuation of FO-PMD, FO-PMD coefficients and SO-PMD measured on a deployed aerial optical fibre that links St. Albans and Rockland transmission stations in Port Elizabeth. These measurements were made on 24 August 2010 from 09:00 am to 14:00 pm using (a) FTB-5700 and (b) GINTY.

For this reason, the robustness of the FTB-5700 single-ended dispersion analyzer instrument is tested for its ability to accurately measure PMD of an aerial optical fibre. This is because the PMD of the aerial optical fibre in use is about 0.46 ps so the deviation from it is more pronounced with GINTY compared to the FTB-5700. The same pattern is also observed for the FO-PMD coefficient values as well as the SO-PMD values.

It should be noted that these random fluctuations of these PMD parameters are due to environmental changes especially temperature and wind speed since they are known to change the birefringence and mode coupling of an optical fibre. More discussions on this are presented in section 6.3.2 that follows.

6.3.2 FO-PMD Fluctuation with Environmental Effects

Figure 6.8 shows the variations of FO-PMD with respect to time for the GINTY and the FTB-5700 as well as the temperature and wind speed variations. The measurements presented in this section were taken on 23 August 2010 from 08:45 am to 14:00 pm. It should however be noted that more measurements were done during August 2010 though not shown. During this measurement period, the mean temperature was 14.9ºC with maximum temperature of 17.1ºC and minimum temperature of 12.1ºC. As indicated in figure 6.8(c), the temperature fluctuations are small but gradually increased with time until it was approximately constant from 12:00 noon. The wind speeds were however fluctuating randomly with a mean of 18 km/h, a minimum of 7.2 km/h and a maximum of 32 km/h. This still lies in the vortex-induced oscillations' range (section 5.3). The collection of the weather data was done every minute so that the FO-PMD variations are monitored more accurately with time.

The FO-PMD fluctuations when the GINTY was used are shown in figure 6.8(a) while those when the FTB-5700 instrument was used are shown in figure 6.8(b). Generally, the FO-PMD variations for both instruments are in a random pattern. This is due to the rapid variations in the wind speeds and small variations in the temperature as shown in figure 6.8(c). It should be noted that the FO-PMD fluctuation is due to the change in the state of polarization (SOP) of the laser pulse resulting from the combined effect of the change in birefringence and the mode coupling as well as the Berry phase effect on the aerial optical fibre cable. However, a particular trend can be observed from figures 6.8(a) and 6.8(b). An increase in FO-PMD is observed from about 10:15 am to about 11:00 am when a peak is achieved for both instruments. A close look, in this time period, on the temperature graph (figure 6.8(c)), a gradual increase in temperature is observed.

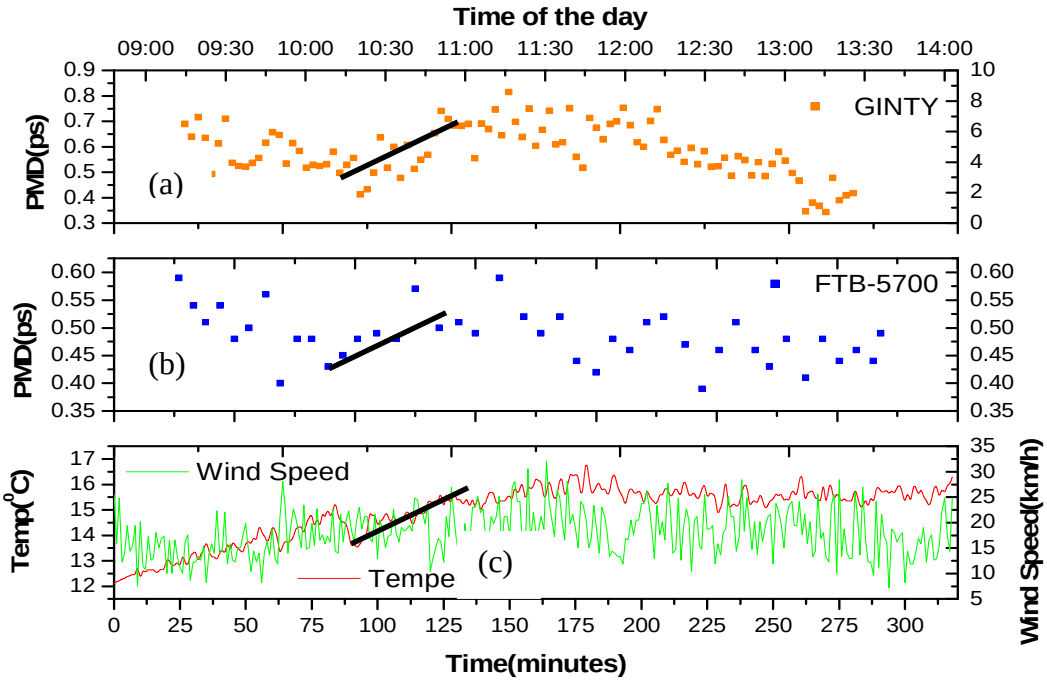

Figure 6.8: Fluctuation of FO-PMD measured on a deployed aerial optical fibre that links St. Albans and Rockland transmission stations in Port Elizabeth. These measurements were made on 23 August 2010 from 08:45 am to 14:00 pm using (a) GINTY and (b) FTB-5700. (c) Temperature and wind speed as a function of time (the line represents the increase in PMD with temperature).

This implies that the increase in FO-PMD was due to the increase of the temperature of the aerial optical fibre. However, after 12:00 noon, the temperature variations became quite small. This implies that the random fluctuations of the FO-PMD in both instruments are mainly due to the rapid fluctuations in the wind speeds. This is in agreement with Mudau (2008) of our research laboratory, Karlsson *et al.* (2000) and Zhang *et al.* (2007) who made long-term FO-PMD measurements only that they did not make a comparison of the GINTY with the FTB-5700 during their measurements and also did not show FO-PMD variations for short time (in this particular case a 5.3 hour period is considered).

6.4 States of Polarization Monitoring

The aerial fibre cable links two local Telkom Exchange transmission stations in Port Elizabeth, South Africa, and is exposed to dynamic environmental changes. Wind caused the optical fibre cable to gallop and oscillate depending on its direction and speed. This together with temperature fluctuations lead to the change in birefringence of the optical fibre (section

6.3.2). Since the aerial optical fibre is in a dynamic state, its PMD and SOP can both change on short time scales.

Research on aerial fibres has been done by many groups but has however been focusing on cable installation, stresses and the optical fibre life span (Waddy *et al*. 2005). A few of these groups have studied polarization effects in aerial fibres and it helped in determining the possible causes of system degradation (Waddy *et al*. 2005). Findings in these studies have also shown that SOPs in aerial fibres follow a stochastic random walk (Waddy *et al*. 2002; Wuttke *et al.* 2003). It has also been shown that PMD and SOPs in aerial fibres on a high voltage transmission system are correlated to the fluctuations in current and wind (Wuttke *et al*. 2003). Interferometric measuring techniques have been used to measure PMD with change in temperature in aerial fibres (Cameron *et al*. 1998b; Waddy *et al*. 2001). These interferometric techniques have been found to be more accurate compared to the polarimetric techniques for aerial fibre cables especially in the presence of sudden changes in their environments (De Angelis *et al.* 1992).

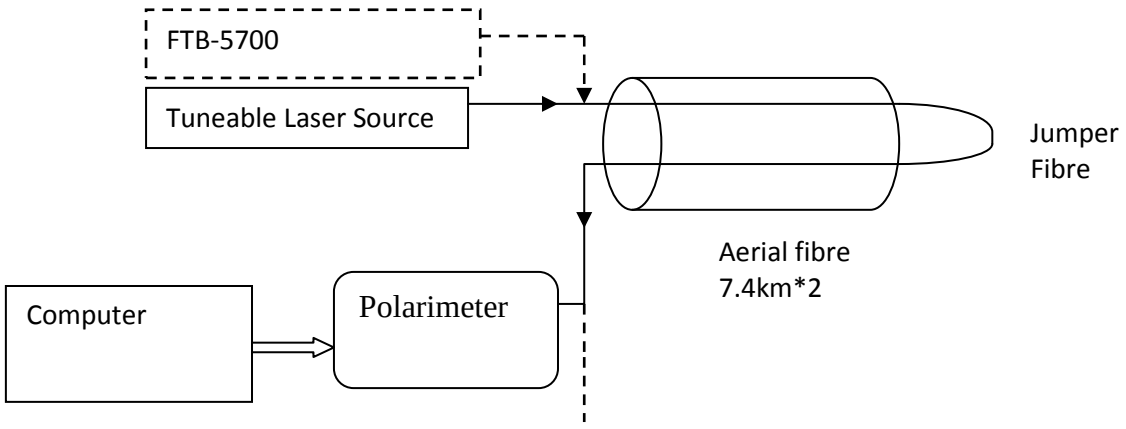

Figure 6.9: Experimental setup for the field aerial fibre SOP measurement and PMD measurement using the FTB-5700 Single-Ended Dispersion Analyzer.

The experimental setup (figure 6.9) used during the field measurements consisted of the looped fibre under test (FUT) which was 14.8 km long. This FUT was secured in a deployed loose-tube that contains 12 optical fibres. The Agilent 8164A narrow band tunable laser source (TLS) provided a continuous wave of a light beam that was launched into the FUT at a wavelength of λ=1550 nm. The propagating laser light in the FUT undergoes relative SOP changes and was measured using a polarimeter. All patchcords used at the transmission

station where our equipment was stationed, were securely taped on the walls to ensure that the relative SOP changes were only due to the dynamic environmental changes of the FUT.

For analysis, we used the equation (Waddy *et al*. 2002; Waddy *et al*. 2005),

$$\gamma = \arccos(\vec{S}_{t_o} \cdot \vec{S}_{t_o+t}) \tag{6.1}$$

where $\vec{S}_{t_o}$ and $\vec{S}_{t_o+t}$ are the normalized Stokes vectors at times t_o and $t_o + t$ respectively from the experimental SOP data. The rate of change of the SOP in degrees per second was obtained from equation (6.1).

6.4.1 SOP variations for the Patchcords excluding the FUT

First, for 30 minutes, at intervals of 30 ms, an SOP measurement run was carried out after joining together the taped patchcords excluding the FUT to ascertain the impact of the temperature and vibrations inside the transmission exchange station container. It was found that they had no major effects since the normalized Stokes parameters are approximately independent of each other as shown in Figure 6.10(a). The mapping of the Stokes parameters illustrated in Figure 6.10(b) on the Poincaré sphere was not as random like would have been expected for an aerial optical fibre cable.

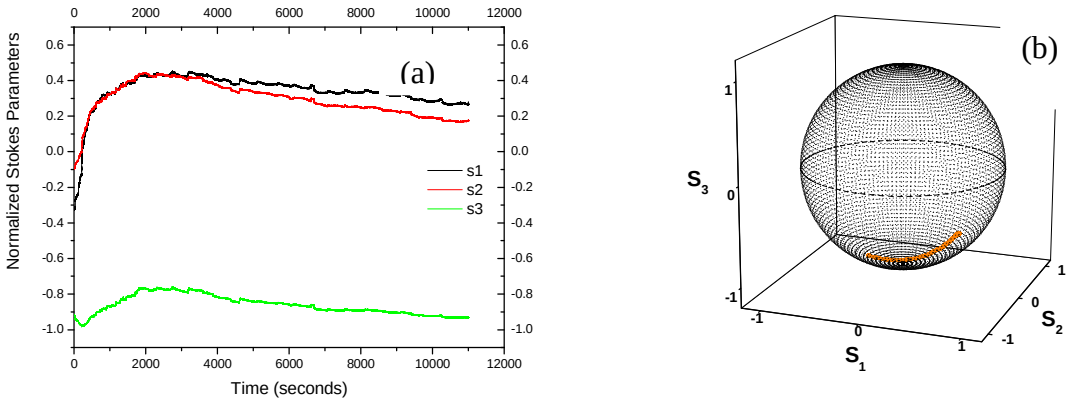

Figure 6.10: Time evolution of the normalized Stokes parameters of the taped patchcords excluding the 14.8 km long looped fibre under test (FUT) optical fibre monitored for 30 minutes, at 30 ms intervals, during the winter month of June 2009.

6.4.2 SOP variations for the complete FUT

With the FUT included, SOP data collection was made lasting 30 minutes in steps of 30 ms for every measurement. The experimental directional time drift autocorrelation function (ACF) was used to determine the decorrelation of the laser light propagating in the aerial fibre (Waddy *et al*. 2005).

$$R(\Delta t) = \frac{1}{N} \sum_{t=0}^{N-1} \vec{S}(t) \cdot \vec{S}(t + \Delta t) \qquad (6.2)$$

where $\vec{S}(t)$ and $\vec{S}(t + \Delta t)$ are the normalized Stokes vectors at times t and $t + \Delta t$ respectively from the experimental SOP data and N is the total number of points used. The ACF describes how correlated the normalized Stokes vectors are in the time domain.

The results shown in this subsection show the variations of SOPs and the calculated ACFs of the SOP measurements made during the month of June 2009 (winter season). During this period, it was observed that the wind speed was fluctuating randomly with an average of 18.7 km/h. The temperature variations were more stable compared to those of wind speed with an average of 15.1^{o}C, a highest of 27.4^{o}C and a lowest of 14.3^{o}C.

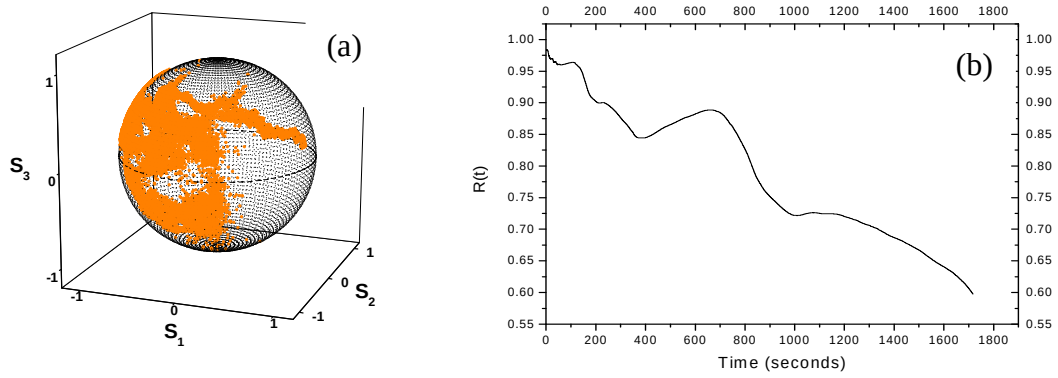

Figure 6.11: (a) Variation of SOPs, (b) the ACF for the aerial deployed optical fibre. The SOP measurements used for the mapping on the Poincaré sphere and also for calculation of the ACF, R(t), were collected on 17 June 2009 from 09:15 am - 09:45 am. Equation 6.2 was used to calculate the ACF.

For SOP monitoring analyses, we used measurement data collected on 17, 22 and 23 June 2009. On 17 June, the wind speed fluctuations were relatively uniform (average wind speed was 9 km/h) and the temperature increased gradually from about 6.9^{o}C to 18.6^{o}C. The average temperature on this day was 12.8^{o}C. Then on 22 June, the wind speed fluctuations increased compared to those on 17 June (average wind speed was 17.6 km/h with a highest of 37.4 km/h). The accompanying average temperature on this day was 16.9^{o}C with a highest of 20.3^{o}C and lowest of 13.5^{o}C. On 23 June, the temperature also increased gradually with a minimum of 15^{o}C, a maximum of 20^{o}C and an average of 17.4^{o}C while the random wind speed and wind gusts fluctuations were significant. The average wind speed was 27 km/h and a highest of 78.5 km/h.

Figure 6.11(a) shows the population of the Poincaré sphere on 17 June 2009 from 09:15 am to 09:45 am for the normalized Stokes vectors collected for 30 minutes at 30 ms intervals. The SOP coverage on the Poincaré sphere is sparsely populated because on this particular day the environmental parameters were not fluctuating so fast. Figure 6.11(b) shows the ACF of these SOP measurements. As can be seen, over a 1600 seconds time span, 50% decorrelation is not observed but after some more additional time it would be observed.

Figures 6.12(a), (b) and (c) show variations of SOPs on 17, 22 and 23 June 2009 from 12:20 to 12:50 pm respectively. The random changes in birefringence and mode coupling along the aerial optical fibre length resulted in fast SOP fluctuations. The population of the Poincaré spheres increased on these days because of the changing environmental conditions experienced by the optical fibre cable. On 23 June 2009 the Poincaré sphere surface was almost completely populated because of the rapid fluctuations of the environmental parameters; wind speed, wind gusts and temperature (figure 6.12(c)). Population of the Poincaré sphere is close to and on its surface because the light source (tuneable laser) used was highly polarized with a degree of polarization (DOP) > 0.9. Figures 6.12(a$'$), (b$'$) and (c$'$) show the ACFs for the deployed aerial optical fibre. The SOP measurements used for calculation of the ACFs, R(Δt), were collected on 17, 22 and 23 June 2009 from 12:20 pm – 12:50 pm respectively for 30 minutes in steps of 30 ms. Equation 6.2 was used to calculate the ACF. It is observed that as the population of the Poincaré spheres increased, the 50% decorrelation times reduced. On 17 June in figure 6.12(a$'$) the decorrelation time was 520 s, on 22 June in figure 6.12(b$'$) it was 410 s and on 23 June as shown in figure 6.12(c$'$) it was 390 s. This is in line with findings by Karlsson *et al.* (2000).

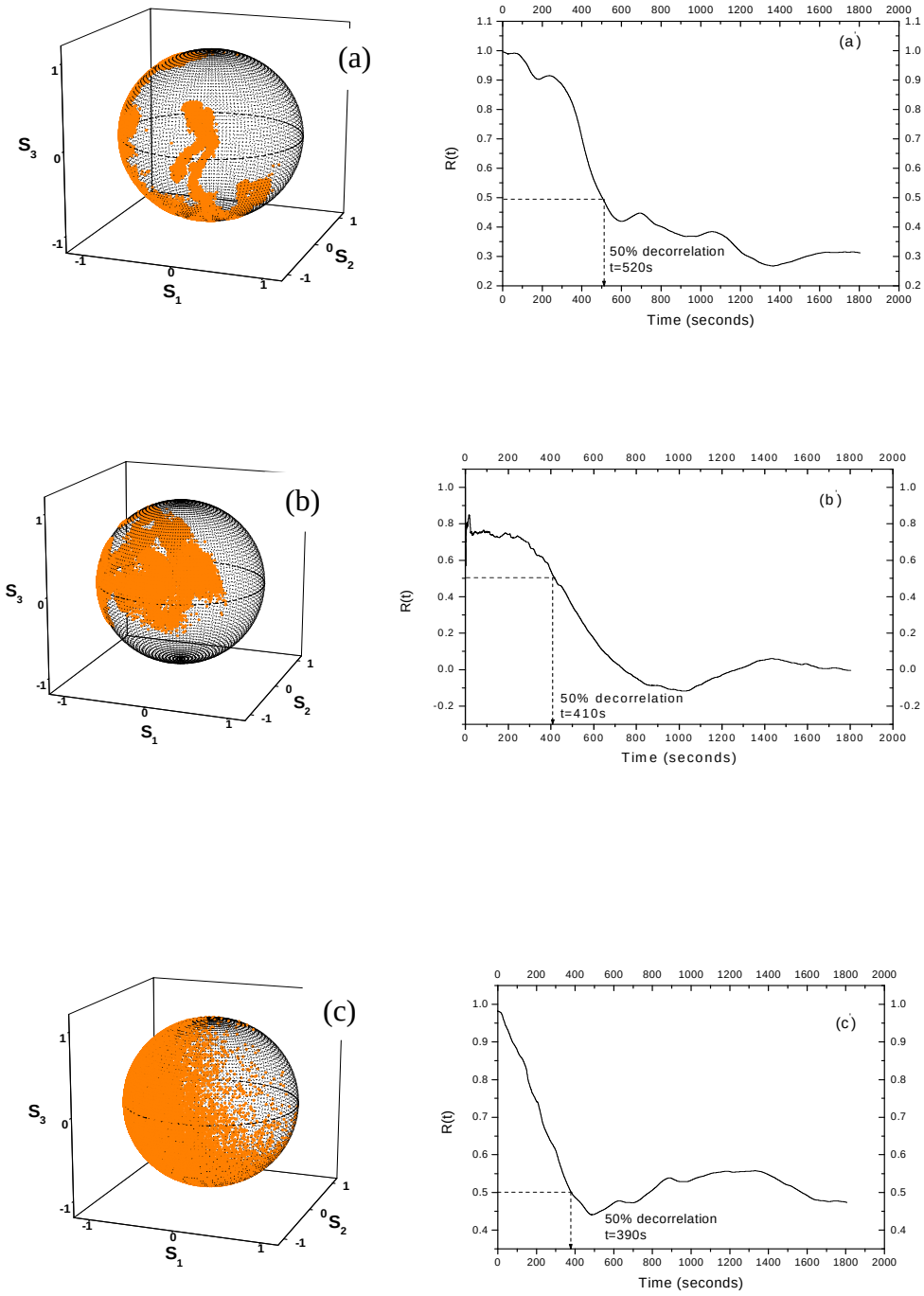

Figure 6.12: ((a), (b) and (c)) Variation of SOPs on 17, 22 and 23 June 2009 from 12:20 pm – 12:50 pm respectively. ((a'), (b') and (c')) The ACFs for the deployed aerial optical fibre. Equation 6.2 was used to calculate the ACF.

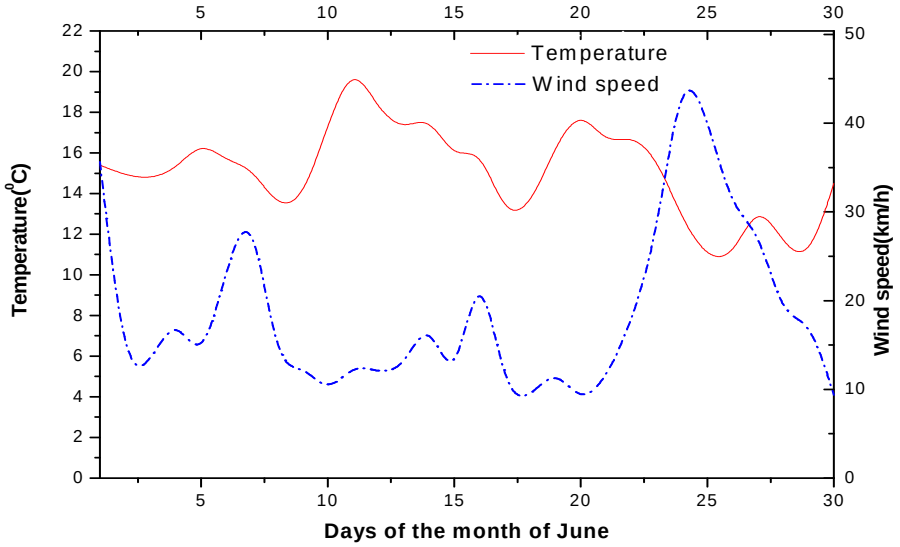

Figure 6.13: The temperature and wind speed fluctuations during the month of June 2009 in Port Elizabeth, South Africa.

Figure 6.13 shows the variations of temperature and wind speed in Port Elizabeth, South Africa in the month of June 2009 during the winter season. It is observed that the wind speed was fluctuating randomly with an average of 44.6 km/h during this period with dominant peaks on 6, 16 and 25 June. The temperature variations were more stable compared to those of wind speed; dominant peaks were on 11 and 20 June 2009.

In the next analysis, a specific look at the variation of the SOPs on two separate days and at different times of that particular day is made. This was done to confirm the generalized trend we have described above. The measurement data collected on 17 and 23 June is used. The variations in temperature, wind speeds and wind gusts for these two days are shown in figures 6.14(a) and 6.14(b). It is observed that the temperature variations were not as random as the wind speeds and the wind gusts on both days. Figures 6.14(c) and 6.14(d) show the population of the Poincaré spheres on 23 June 2009 from 08:30 to 09:00 am and from 11:00 to 11:30 am for the normalized Stokes vectors collected for 30 minutes at 30 ms intervals respectively.

23 June from 08:00 am to 15:00 pm

17 June from 09:00 am to 13:00 pm

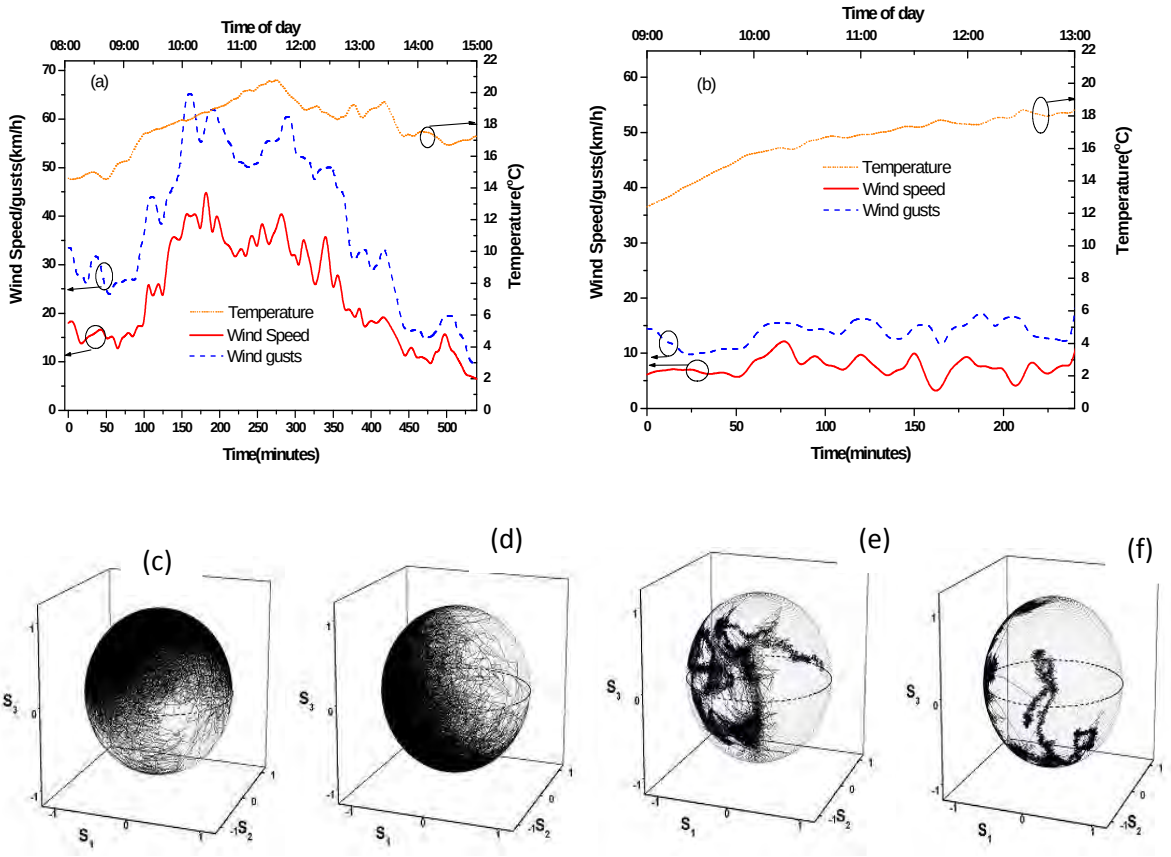

Figure 6.14: Temperature, wind speed and wind gusts variations on the (a) 23 and (b) 17 June 2009 in Port Elizabeth. Figures (c), (d), (e) and (f) show the SOP coverage on the Poincaré sphere at different times. (c) and (d) are from 08:30 to 09:00 am and from 11:00 to 11:30 am on 23 June while (e) and (f) are from 9:15 to 09:45 am and from 12:10 to 12:40 pm on 17 June 2009.

It is observed from both these figures that the Poincaré sphere surfaces are almost completely populated because of the rapid fluctuations of the environmental parameters; wind speed, wind gusts and temperature (figure 6.14(a)). Figures 6.14(e) and 6.14(f) represent normalized Stokes vectors collected on 17 June 2009 for 30 minutes in steps of 30 ms from 09:15 to 09:45 am and from 12:10 to 12:40 pm. The SOP coverage on the Poincaré spheres is not as populated as those for figures 6.14(c) and 6.14(d) because on this particular day the environmental parameters were not fluctuating as fast. The wind gusts and speeds have slight fluctuations and the temperature had a gradual increment with a small gradient (figure 6.14(b)). The random changes in birefringence and mode coupling along the aerial optical fibre length result in fast SOP fluctuations as depicted in figures 6.14(c) and 6.14(d) and the

reverse for figures 6.14(e) and 6.14(f).

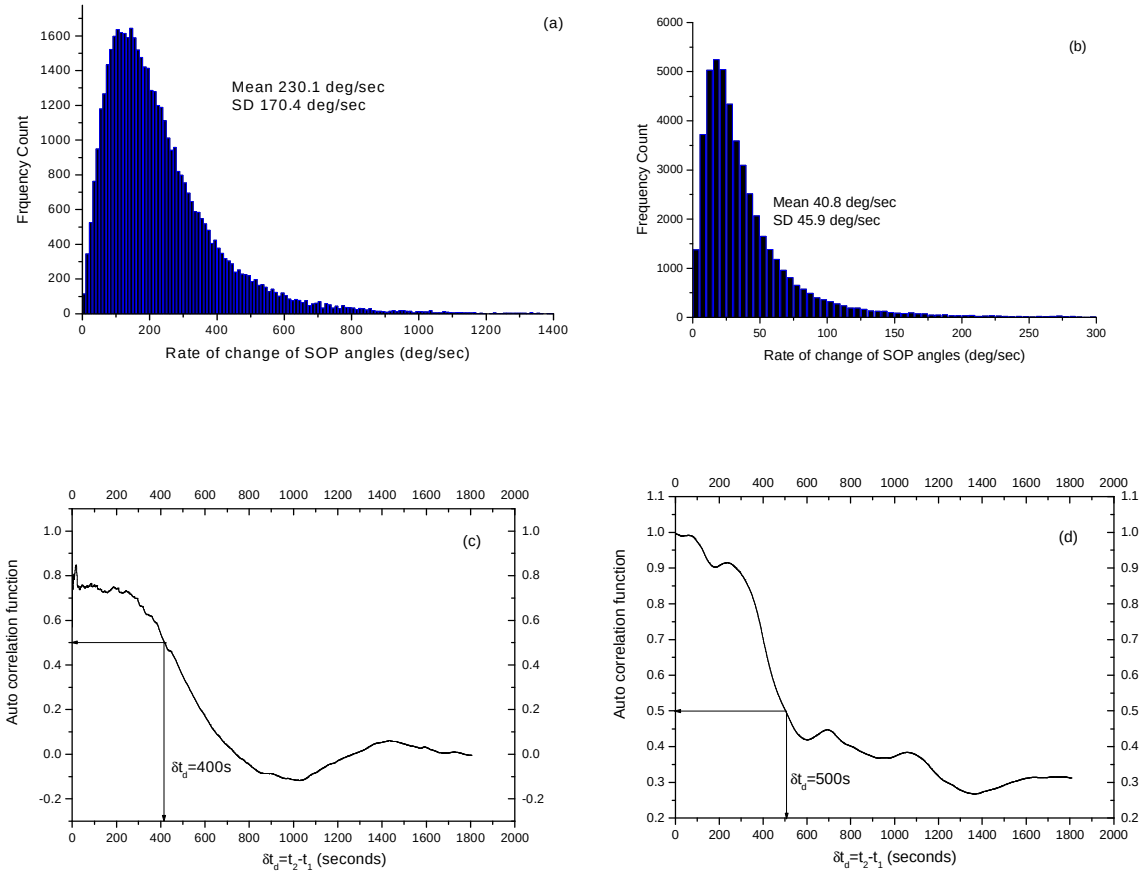

Figure 6.15: Histograms for the rates of change of SOP angles for 23 and 17 June 2009 and the corresponding autocorrelations for the times 11:00 to 11:30 am and 12:10 to 12:40 pm respectively.

Figures 6.15(a) and 6.15(b) show the histograms for the relative changes in SOP angles per unit time for the output SOPs collected on 23 and 17 June 2009 respectively. Detailed descriptions on this will be discussed in chapter 7. Both histograms are skewed towards low SOP angles. The mean rates of the change of SOP angles are 230.1 deg/sec and 40.8 deg/sec for figures 6.15(a) and 6.15(b) respectively. This shows that the fluctuations in figure 6.15(a) were more random compared to those in figure 6.15(b) and this is confirmed in figures 6.14(a) and 6.14(b) respectively for the particular environmental conditions on those days.

6.5 PMD Compensation

In PMD compensation, the compensator has to track the changing PMD vector. This is the same as tracking the changing SOPs though the PMD vector fluctuations are normally slower (Gibbon 2007, p.58). Therefore, the PMD vector must be changing slower than the 230.1 deg/sec and 40.8 deg/sec for the SOPs on the different days.

Figures 6.15(c) and 6.15(d) show the corresponding decorrelation times of the laser light in the aerial optical fibre on the two days. They are approximately 400 s and 500 s which means that the laser light in the aerial optical fibre decorrelates faster on a day with rapid fluctuations (figure 6.14(a)) compared to the one with slower fluctuations (figure 6.14(b)). This is in line with findings by Karlsson *et al.* (2000). Determination of the decorrelation times helps in knowing the time scale over which the polarization effects occur for PMD compensation to be made accurately. This PMD compensation time should be slightly higher than the decorrelation time since SOP changes are always faster than PMD vector changes.

From our results in section 6.4, it is observed that the different weather parameters lead to different decorrelation times of the laser light in the aerial optical fibre. Therefore, PMD compensation in aerial optical fibres is a greater challenge than it is for a buried optical fibre because the response of the compensator is always several orders of magnitude faster. From our measurements it would be slightly higher than 390 s. This is the fastest 50% decorrelation time for the laser pulse in this particular aerial optical fibre and the environmental parameters were at their highest in terms of their rapid fluctuations.

6.6 Summary of results

In section 6.1, we were able to fit a Gaussian pdf to the FO-PMDs, FO-PMD coefficient values and the SO-PMDs for an aerial optical fibre exposed to severe vortex-induced oscillations on the South African telecommunication network measured using an FTB-5700 single-ended dispersion analyzer. The PMD values obtained confirmed its accuracy and robustness in unstable polarization conditions.

In section 6.2, the statistics of the FO-PMD values obtained from both the FTB-5700 and the GINTY were compared and also the Gaussian pdf fitted. We obtained 11% and 12% PMD uncertainty for the FTB-5700 and GINTY respectively. These two values perfectly fall within

the range that was proposed by Gisin *et al.* (1996). However, histograms of the SO-PMD values from both these instruments better fitted the Maxwellian distribution compared to the Gaussian and the Foschini *et al.* (2000) distributions. The measured mean SO-PMD values obtained were approximately equal to the theoretical mean equation proposed by Foschini *et al.* (2000).

We were also able to investigate the variations of FO-PMD, FO-PMD coefficients and SO-PMD with the environmental parameters in section 6.3. This was done for both the GINTY and FTB-5700 measurement instruments. Environmental changes, especially temperature and wind speed, change the birefringence and mode coupling of the aerial optical fibre and this in turn leads to the fluctuation in the measured PMDs.

In sections 6.4 and 6.5, we investigated the rate at which PMD compensation can be achieved in aerial optical fibres. The compensator has to track the changing PMD vector. This is the same as tracking the changing SOPs though the PMD vector fluctuations are normally slower. Determination of the decorrelation time helps in knowing the time scale over which the polarization effects occur for PMD compensation to be made accurately. The time for PMD compensation should be slightly higher than the decorrelation time since SOP changes are always faster than PMD vector changes. Response times for accurate PMD compensation for the aerial fibre were determined and the maximum would be slightly higher than 390 s on a windy and hot day.

Acknowledgements

The author extends his sincere thanks to Alex du Toit, Deon Flynn and Neil Calder of Telkom SA for their assistance with the measurements presented in this chapter. They obtained for us permission to use the network and were always available to receive us at the St. Albans transmission exchange station. The author is also grateful to Dr. Vitalis Musara, a Postdoctoral student at Nelson Mandela Metropolitan University for the fruitful discussions that helped in the analysis of results in this chapter.

CHAPTER 7

STATISTICAL CHARACTERIZATION OF THE OUTPUT SOP

Changes in the optical fibre properties due to both intrinsic and extrinsic variations result in polarization mode dispersion (PMD) and state of polarization (SOP) becoming stochastic in nature. The statistics for first-order PMD (FO-PMD) and second-order PMD (SO-PMD) with wavelength approach the Maxwellian (Foschini and Poole 1991; Zhang *et al.* 2007) and Foschini *et al.* (2000) distributions respectively when measured using the Jones matrix eigenanalysis (JME) as described in chapter 4. This is different from what was discussed in chapter 6 since we were measuring these parameters with respect to time at a fixed wavelength λ=1550 nm. In this case a wavelength sweep is done with a small step size using the Agilent 8164A narrow band tunable laser source (TLS) using the experimental setup shown in figure 4.8. In this chapter we investigate a theoretical statistical distribution that corresponds to output SOP variations. Though it has been shown that the statistical distributions are skewed to the low relative SOP angles side (Waddy *et al.* 2005), to our knowledge, there have been no reports on their theoretical statistical distribution. The SOP variations can either be with wavelength (for buried fibre) or with time (for aerial fibre). Results show that the statistics of the relative SOP changes approach the distribution first proposed by Foschini *et al.* (2000). Knowing this statistical distribution and behaviour of the relative changes in SOP angles helps one to determine the rate of PMD compensation. Results in this chapter have already appeared in a peer reviewed international journal (Ireeta *et al.* 2010a).

7.1 PMD Statistics

In this section, FO-PMD and SO-PMD measurements presented were obtained from ITU-T G.652 deployed buried optical fibres that are each 14.2 km long in the same cable. The fibres are owned by Telkom South Africa and are deployed in Port Elizabeth. For our measurements, we made two different links with the use of patchcords to enable us obtain an end to end access. In the first link, we joined four optical fibres together to obtain a 56.8 km long optical fibre. For the second link we considered only two of these four optical fibres to obtain a link which was 28.4 km long. It should be noted that the patchcords (single mode

fibre) which we used to connect the optical fibres had negligible PMD. The JME method was used for the PMD measurements and the wavelength range was from 1520 to 1570 nm in steps of 0.05 nm so as to get rid of noisy spectra. In the following subsections, FO-PMD and SO-PMD measurements acquired over wavelength are statistically analyzed.

7.1.1 FO-PMD Statistics

Figure 7.1 shows the statistical distributions for FO-PMD obtained from optical fibre link 1, which is 56.8 km long after connecting four optical fibres together, and optical fibre link 2, that is 28.4 km long after connecting just two of these four optical fibres. These two links give the general picture of the FO-PMD statistical behaviour obtained for all the optical fibres that were tested. The mean FO-PMD of link 1 was 9.5 ps while that of link 2 was 8.0 ps. The increase in FO-PMD of link 1 is due to the fact that we joined more optical fibres (which also have their own FO-PMD) to link 2. It should be noted that the same measurement procedures were followed in both cases and there were no optical fibre movements during the measurement period.

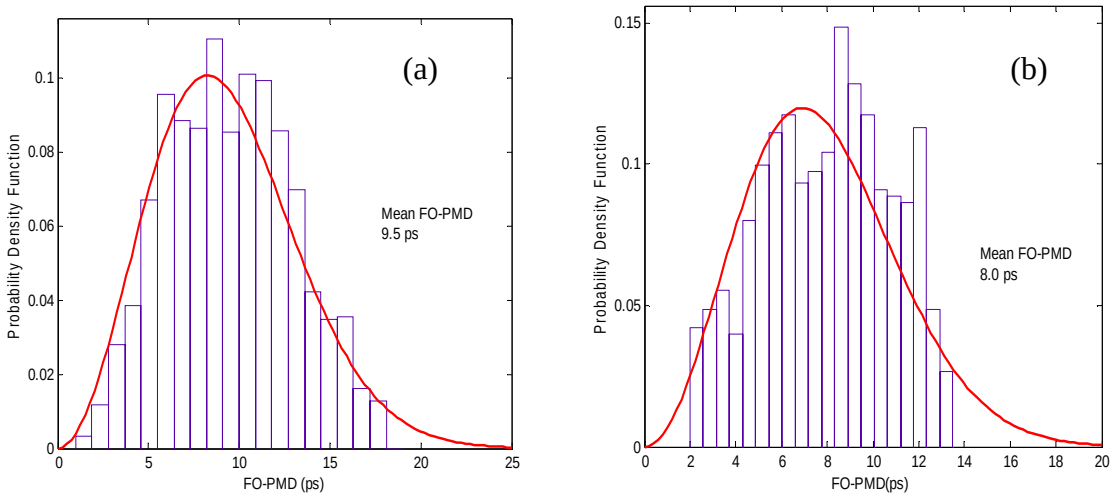

Figure 7.1: The FO-PMD statistical distributions for (a) Link 1, 56.8 km long (with mean PMD of 9.5 ps) and (b) Link 2, 28.4 km long (with mean PMD of 8.0 ps) deployed buried optical fibre in Port Elizabeth, South Africa owned by Telkom SA. The solid line mapped onto the histograms is the theoretical Maxwellian distribution.

From figure 7.1(a), it is clear that the FO-PMD or DGD statistical distribution of link 1 approaches the theoretical Maxwellian distribution. However, from figure 7.1(b), the statistical distribution of link 2 does not approach the Maxwellian distribution as it did in

figure 7.1(a). The reason for this is because in link 2 there is limited random mode coupling as compared to link 1 which is double the length. It should be remembered that random coupling is responsible for the significant variations of FO-PMD and PSPs as a function of wavelength. This is because according to Foschini and Poole (1991), FO-PMD follows a Maxwellian distribution if and only if there exists infinite random mode coupling.

7.1.2 SO-PMD Statistics

In this subsection, statistical distributions for SO-PMD for links 1 and 2 are also presented. Figure 7.2(a) shows a better fit for the theoretical Foschini *et al.* (2000) distribution compared to figure 7.2(b) for links 1 and 2 respectively. This is again because of the presence of high random mode coupling in link 1 (56.8 km long) compared to link 2 (28.4 km long) that leads to an increase in the variations of the FO-PMD and PSPs with wavelength.

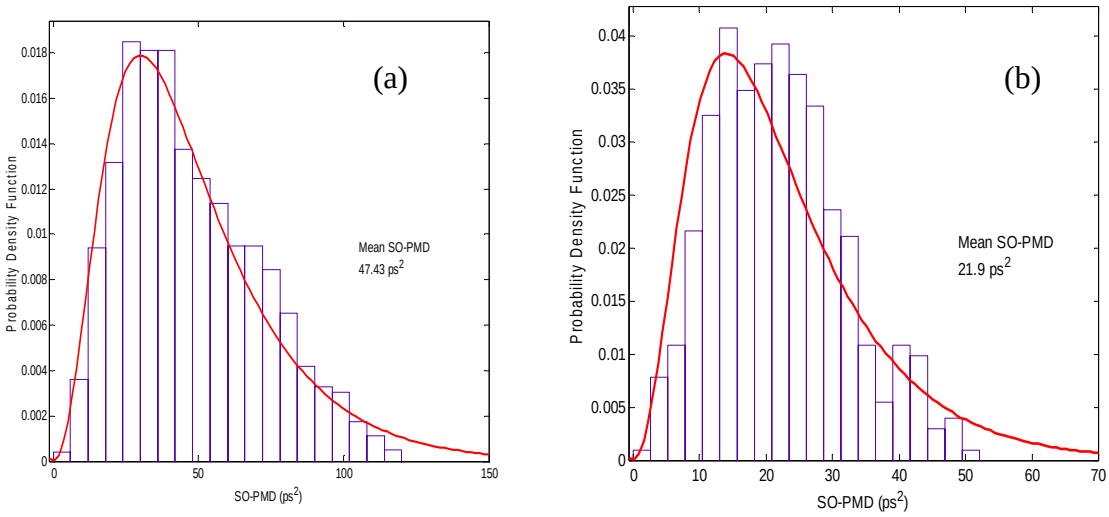

Figure 7.2: The SO-PMD statistical distributions for (a) Link 1, 56.8 km long and (b) Link 2, 28.4 km long deployed buried optical fibre in Port Elizabeth, South Africa owned by Telkom SA. The solid line mapped onto the histograms is the theoretical Foschini *et al.* (2000) distribution.

During SO-PMD measurements and analyses, it was observed that links which had high SO-PMD approached the Foschini *et al.* (2000) distribution compared to those with low SO-PMD. In these results presented, the mean SO-PMD of link 1 was 47.43 ps^2 while that of link 2 was 21.9 ps^2. The FO-PMD variation with wavelength is equivalent to polarization-dependent chromatic dispersion (PCD) and PSPs with wavelength is equivalent to PSP depolarization. This was discussed in section 2.5 and will again be looked at in detail in section 7.2.

7.2 Statistical Theory of SOP

The statistical distribution of the relative changes in SOP angles per unit wavelength, as shown in figure 7.3, is skewed to the low value side like for the theoretical SO-PMD (Foschini *et al.* (2000) distribution) and the Maxwellian distributions for FO-PMD as discussed in section 7.1.

The relative changes in SOP angles per unit time/wavelength were obtained using the following equation (Waddy *et al*. 2002),

$$\psi = \arccos(\vec{s}_1.\vec{s}_2)\,. \tag{7.1}$$

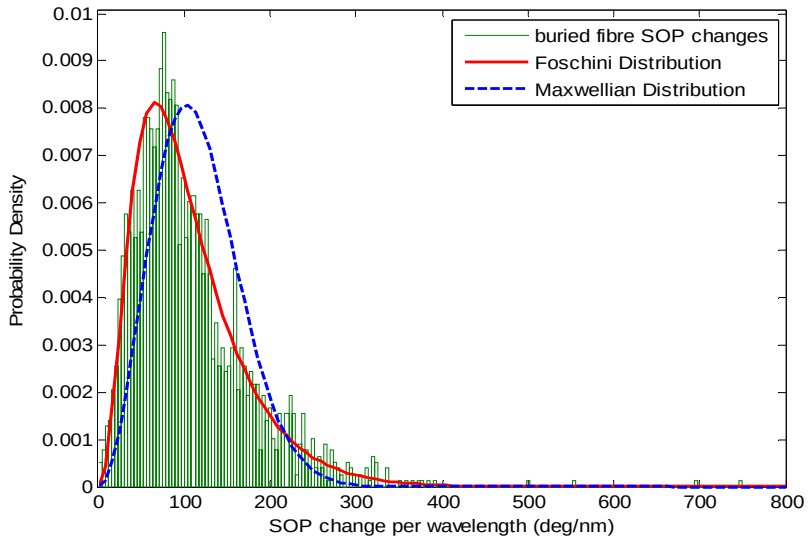

Figure 7.3: Probability density function of the change in SOP angles in degrees per unit wavelength for a buried fibre at a local exchange station in Port Elizabeth, South Africa, 28.4 km long, and with wavelength range 1520 to 1570 nm in steps of 0.05 nm.

In this equation, $\vec{s}_1$ and $\vec{s}_2$ are the normalized Stokes vectors at times t_1 and t_2 respectively for experimental SOP data at a given wavelength (for this particular case λ=1550 nm) for a deployed aerial optical fibre. They are also the normalized Stokes vectors at wavelengths λ_1 and λ_2, respectively for deployed buried optical fibre experimental SOP data. The rates of SOP change and SOP changes per wavelength were obtained by dividing ψ with sampling time (30 ms) and wavelength difference (0.05 nm) respectively.

The SO-PMD is obtained by taking the derivative of equation (2.18) with respect to angular frequency to obtained equation 2.24 as was shown in chapter 2 (Foschini *et al*. 2000). It was

also indicated in section 2.5 that the subscript ω stands for differentiation with respect to angular frequency. Equation (2.24) has two important terms on the right hand side; the magnitude of the first term, $\Delta\tau_\omega$, is the change of the DGD with wavelength and this causes polarization-dependent chromatic dispersion (PCD) while the second term, $\Delta\tau\vec{p}_\omega$, describes PSP depolarization, that is the rotation of the PSPs with angular frequency. Once again, PSP depolarization is the dominant contributor to SO-PMD as compared to PCD. The ratio of PSP depolarization to SOPMD is 8/9 (Foschini *et al.* 1999), thus equation (2.24) approximately reduces to

$$\left|\vec{\tau}_\omega\right| \approx \Delta\tau\left|\vec{p}_\omega\right|. \tag{7.2}$$

The polarization dependent properties of a single mode fibre, at position l, can be expressed by a real 3×3 rotation matrix $R(l,\omega)$ according to equation (7.3) below.

$$\vec{s} = R(l,\omega)\vec{s}_{in} \tag{7.3}$$

This implies that the rotation of the Stokes vector is used to determine the birefringence of the fibre (Foschini and Poole 1991). Therefore, the angular frequency dependence of the rotation matrix $R(l,\omega)$ leads to polarization dispersion. The manifestation of angular frequency dependence, for a given fixed input state, is the angular frequency dependent output state of polarization $\vec{s}$ (Foschini and Poole 1991).

Therefore, the output SOP, $\vec{s}$, like the approximate SO-PMD in equation (7.2), is dependent on angular frequency, as discussed in section 2.5, according to the following equation

$$\vec{s}_\omega = \vec{\tau}\times\vec{s}\ . \tag{7.4}$$

This means that for a fixed input SOP, the output SOP, $\vec{s}$, will precess around $\vec{\tau}$ as the angular frequency is changed. The angle of precession is determined by the direction of $\vec{s}$ relative to $\vec{\tau}$ while the rate at which $\vec{s}$ precesses around $\vec{\tau}$ is determined by the magnitude, $\Delta\tau$.

Because of the angular frequency dependence of both the approximate SO-PMD and the output SOP as shown in equations 7.2 and 7.4 respectively, we used the pdf for SO-PMD as provided in Foschini *et al.* (2000) to fit on the histogram of relative changes in SOP angles with both time and wavelength.

This pdf is derived from the 6-D vector characteristic function when normalized. The pdf of the SO-PMD magnitude $\left|\vec{\tau}_{\omega}\right|$ is obtained as (Foschini *et al.* 2000),

$$P_{\left|\vec{\tau}_{\omega}\right|} = \left(\frac{32x}{9.24\langle x\rangle^2}\right)\tanh\left(\frac{4x}{1.71\langle x\rangle}\right)\operatorname{sech}\left(\frac{4x}{1.71\langle x\rangle}\right), \text{ for } x \geq 0$$

$$\text{and } P_{\left|\vec{\tau}_{\omega}\right|} = 0, \text{ for } x < 0 \tag{7.5}$$

where x is the magnitude of the SO-PMD at a particular frequency and $\langle x\rangle$ is the mean SO-PMD. We substituted $\langle x\rangle = 2G\tau^2/\pi$, where Catalan's constant G = 0.915965…, into equation 7 of Foschini *et al.* (2000) to obtain equation 7.5. This equation is also shown in Appendix B in this thesis. For this section, equation 7.5 is applied to the statistical distributions for the change in SOP angles per unit time and per unit wavelength. Therefore, variable x will be the rate of change of SOP as well as the change in SOP per wavelength (Ireeta *et al.* 2010a).

In Figure 7.3, a histogram of the changes in SOP angles per unit wavelength for a buried deployed optical fibre is shown and also the fitting of the two probability density functions (pdfs), Maxwellian and Foschini *et al.*, equation 7.5, to the data. From this point on in this chapter we shall refer to equation 7.5 as the Foschini distribution. From Figure 7.3, it is quite clear that the Foschini distribution approximates the histogram better than the Maxwellian distribution. Other distributions for example Rayleigh and Weibull were also fitted as shown in figure 7.4 but were found to deviate significantly as compared to the Maxwellian and Foschini distributions.

Figure 7.4 visualizes a histogram for the SOP changes with wavelength for a deployed buried optical fibre link in Port Elizabeth, South Africa. The link was 28.4 km long and the tunable laser source was set to sweep between 1520 and 1570 nm wavelength range with a resolution of 0.05 nm. The Rayleigh, Weibull and Foschini distributions are also mapped onto the histogram.

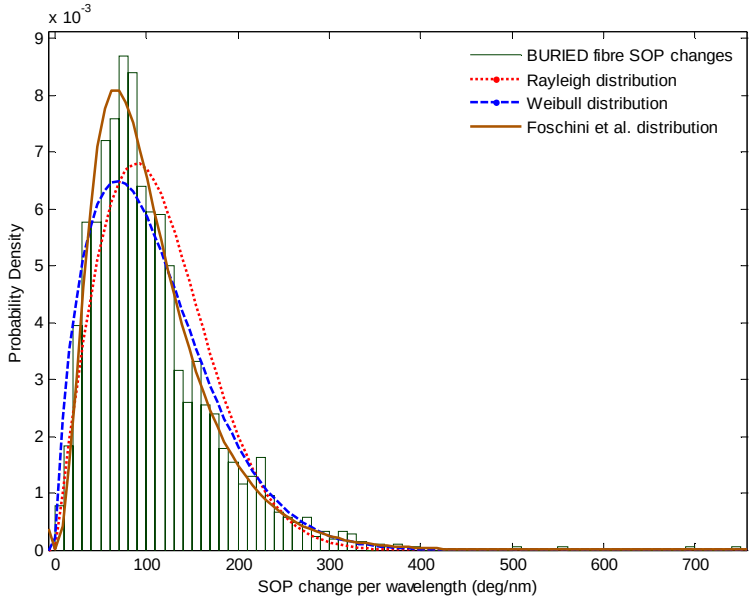

Figure 7.4: Probability density function of the change in SOP angles in degrees per unit wavelength for a buried fibre in Port Elizabeth, South Africa, 28.4 km long, and with wavelength range 1520 to 1570 nm in steps of 0.05 nm. The Rayleigh, Weibull and Foschini *et al.* (2000) distributions are mapped onto the histogram (experimental data for this figure is the same as that used in figure 7.3).

As observed in figure 7.4, the Foschini distribution is a better fit compared to both the Rayleigh and Weibull distributions. Similar trends were observed for different links of deployed buried optical fibres in the same cable. These links differed both in length as well as the optical fibres from the cable that were used. In section 7.3, the statistical investigations of the SOP changes were done for a deployed aerial optical fibre link to ascertain whether this Foschini distribution also holds for it.

7.3 SOP Monitoring Experimental Setup

In this section, the statistical investigations were extended to the time varying output SOP fluctuations at a fixed wavelength (λ=1550 nm) from a deployed aerial optical fibre cable to find out whether the Foschini distribution still applies for the relative change in SOP angles per unit time. This is because, unlike in a buried fibre where PMD changes are slow since the strain remains relatively constant and the temperature fluctuations underground are minimal, SOP changes in an aerial fibre are fast due to rapid changes in PMD and fibre movement (i.e. Berry's topological phase effect).

The experimental set up included an Agilent 8164A tunable laser source (TLS), the ITU-T G.652 fibre under test (FUT) and the Adaptif A1000 polarimeter in sequence. The experimental set up is shown in figure 4.8 (chapter 4). The input SOP was fixed during aerial optical fibre measurements over time but varied with wavelength for buried fibre measurements. The Adaptif A1000 polarimeter was used to measure the three normalized Stokes parameters (s_1, s_2, s_3). It has a sampling rate in the range 500 Hz to 1 MHz. However, the shortest time possible for our SOP data collection was 30 ms because the Labview program we were using needed about 30 ms to synchronize with the equipment. We were able to catch the fastest SOP fluctuations with this time increment. The FUT was secured in a deployed loose-tube aerial cable that links two transmission exchange containers in Port Elizabeth, South Africa. The two exchange transmission stations are St. Albans and Rockland. The fibres in the cable were looped at one end leading to a total length of 14.8 km. In the FUT, laser light traveling through it undergoes relative SOP changes due to changes in the environment. We collected SOP data on this aerial fibre for a month during the winter season, i.e. from 1 to 30 June 2009. The mean DGD of the FUT was 0.46 ps. Each set of SOP data collection took approximately 30 minutes at intervals of 30 ms.

7.4 Rate of SOP Change Histograms

The results shown in this section are for a particular day that had a fairly rapid change in the wind speeds, wind gusts, and temperature. This day had a minimum temperature of about 15ºC and a maximum of 20.5ºC, wind speeds of 12.6 km/h and 45 km/h as minimum and maximum, respectively, and wind gusts with a minimum of 23.4 km/h and maximum of 64.8 km/h . The lowest values for all the environmental parameters were during the morning hours, i.e., before 09:00 a.m. and in the evening hours, i.e., after 15:00 p.m., while the highest values for all the environmental parameters were obtained between 10:00 a.m. and 13:00 p.m.

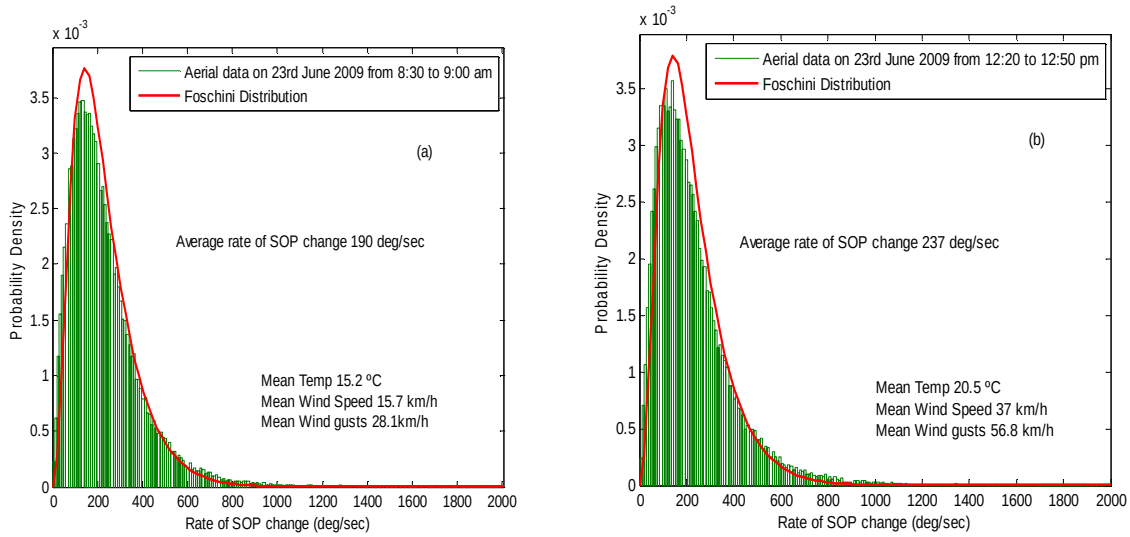

Figure 7.5: The rates of SOP changes in degrees per second taken for 30 minutes in June 2009 during the winter season in Port Elizabeth, South Africa: (a) aerial data taken from 08:30 to 09:00 a.m. (b) aerial data taken from 12:20 to 12:50 p.m.

Figures 7.5(a) and 7.5(b) show the histograms of the rates of SOP change for periods of low and high environmental activity, respectively. Figure 7.5(a) is for the SOP data collected for 30 minutes from 08:30 a.m. to 09:00 a.m. and figure 7.5(b) for the SOP data collected also for 30 minutes, from 12:20 to 12:50 p.m. on the same day.

These two sets of data illustrate the extremes of the rates of SOP changes; they are, on average 190 deg/sec and 237 deg/sec respectively. Similar trends were observed on other data analyzed, as shown in figure 7.6, and it was found that during the nights and early mornings, the SOP fluctuations are minimal when compared to those collected during the day. Figure 7.6 shows histograms for the rate of SOP change at two different time periods on 17 June 2009. Both SOP data collections were collected for 30 minutes at resolutions of 30 ms. Figure 7.6(a) is for SOP data collected from 12:00 (noon) to 12:30 p.m., day time, while figure 7.6(b) is for SOP data collected from 00:00 (mid night) to 00:30 a.m., night time. From figure 7.6, it is observed that the spread of the rate of SOP change data is far more pronounced in figure 7.6(a) compared to figure 7.6 (b).

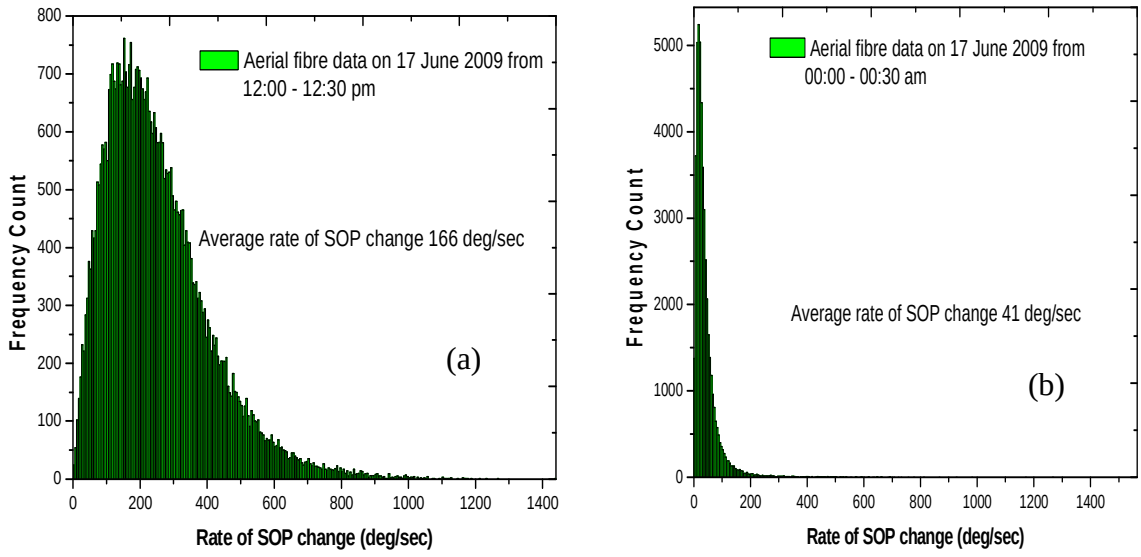

Figure 7.6: Histograms for the rate of change of SOPs (a) during the day from 12:00 to 12:30 p.m. (b) during the night from 00:00 to 00:30 a.m. on 17 June 2009 for a deployed aerial optical fibre in Port Elizabeth, South Africa.

Also the average rate of SOP change in figure 7.6(a) was 166 deg/sec while that for figure 7.6(b) was 41 deg/sec. This confirms that the rate of fluctuation of SOPs is higher during the day as compared to night time.

The Foschini distribution in equation 7.5 fitted well to both histograms as shown in figures 7.5(a) and 7.5(b) for the relative changes in SOP angles. We used the Pearson chi-square test for the goodness of fit. The significance probabilities (p-values) for our fittings were about 0.14, a value that is close to zero. This validates our findings because histograms approach theoretical distributions as the p-value approaches zero (Musara *et al*. 2009d). This approximate fitting could be due to PMD being the major contributing factor to SOP changes in the aerial fibres, like it is for the buried fibres. The PMD will change due to the changing birefringence because of varying temperatures of the exposed aerial optical fibre and this will be complicated by the increased mode-coupling sites created due to fibre movements from the wind.

7.5 Summary of results

In section 7.1, the Jones matrix eigenanalysis method was used to measure the FO-PMD and SO-PMD of deployed buried optical fibre links. From the histograms obtained, it was observed that the FO-PMD statistics could be fitted with the Maxwellian distribution while the SO-PMD statistics could be fitted with the Foschini distribution very well. This was found to hold if and only if the optical fibre link in consideration was long enough to posses numerous random mode-coupled sites since random coupling is responsible for the significant variations of FO-PMD and PSPs as a function of wavelength.

We have presented relative changes in SOP angles per unit time on deployed aerial optic fibres. It was observed that fast SOP fluctuations occurred during the daytime (around noon) and the slow SOP changes were experienced in the morning and in the evening. The SOP variations in aerial fibres are due to environmental fluctuations, while SOP variations in buried fibres are due to random mode coupling and the distribution of birefringence along the fibre. The statistical distributions of the rate of change of SOP angles approached the statistical distribution derived by Foschini *et al*. (2000). Having a statistical distribution of the rates of change of SOP angles helps one know the time scale over which the polarization effects occur to enable accurate PMD compensation.

Future work will involve more rigorous mathematical proofs showing why SOP variations follow the Foschini distribution and not the Maxwellian distribution.

Acknowledgement

The author is grateful for the encouragement and discussions he had with Dr. Vitalis Musara, a Postdoctoral student, at Nelson Mandela Metropolitan University, for results presented in this chapter.

CHAPTER 8

TOLERANCE OF DIFFERENT MODULATION FORMATS

The current focus is to determine the data modulation format that is best suited for systems limited by PMD (Marcuse and Menyuk 1998; Taga *et al.* 1998; Jopson *et al.* 1999b; Bülow 2000; Khosravani and Willner 2000; Lee *et al.* 2000; Winzer and Essiambre 2006b; Wree *et al.* 2007). Most researchers seem to be in agreement that the return-to-zero (RZ) format is more robust to PMD than the ordinary and simple to implement non-return-to-zero (NRZ) format. However, one should take caution when comparing the two formats as there are different boundary conditions that may favour different formats. A good example is keeping the average power constant which gives the RZ format an advantage since RZ is accompanied by a better baseline sensitivity. Alternatively, if the peak power is kept constant, it gives the NRZ format an advantage since it provides more photons per bit. However, both RZ and NRZ have a PMD-induced system limitation with the increase in transmission speeds. In order to mitigate nonlinear transmission impairments because of increasing the distances and per channel bit rates and also decreasing channel spacing, more advanced modulation formats have been proposed and one of these is the DQPSK format.

To make the fairest comparison amongst the different modulation formats in regard to which format is most degraded by PMD, the power margin should be kept constant. Also, since PMD is a random process that drifts with time, attention should be paid to the statistical characteristics by for example estimating the outage probability (Bülow 1998). In this study we considered two intensity modulation formats namely; *non-return-to-zero* (NRZ) and *return-to-zero* (RZ), and one differential phase modulation format; *differential quadrature phase-shift keying* (DQPSK) to investigate which of them is more tolerant in a PMD-induced aerial optical fibre. Results in this chapter have been presented at a peer reviewed conference (Ireeta *et al*. 2010c)

8.1 Transmitted Optical Spectra

The optical spectra of the modulation formats; DQPSK, RZ and NRZ are compared when the transmission speeds are all set to 10 Gb/s for a 50 km single-mode aerial optical fibre with a DGD of 1 ps. This comparison is shown in figure 8.1.

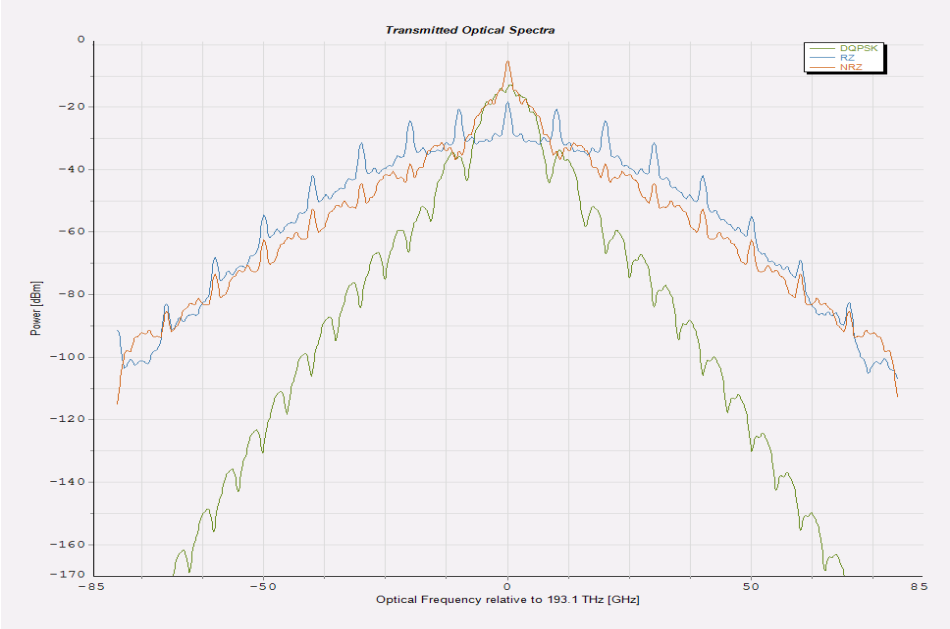

Figure 8.1: 10 Gb/s optical spectra for DQPSK (green), NRZ (red) and RZ (blue). A 50 km long single-mode aerial optical fibre with a DGD of 1 ps was used.

From figure 8.1, it is clear that the RZ and NRZ modulation formats have broader spectra compared to the DQPSK modulation format. This is in agreement with what was shown in figure 3.4 in chapter 3 as well as in Winzer and Essiambre (2006b). The implication of this is that the DQPSK modulation format has the highest spectral efficiency and hence the possibility of tight packing of DWDM channels on a single mode optical aerial fibre.

It is also observed that the RZ modulation format has the lowest peak power compared to NRZ and DQPSK modulation formats. This therefore means that nonlinear effects in DWDM channels are reduced when RZ modulation format is used. This leads to a trade off between a modulation format with a high spectral efficiency or one which allows a lowered launch power in the DWDM channels.

8.2 Simulation Model

The Virtual Photonic Inc. (VPI) simulation software, version 8.3, is used to investigate the tolerance of the three modulation formats over a mimicked aerial optical fibre.

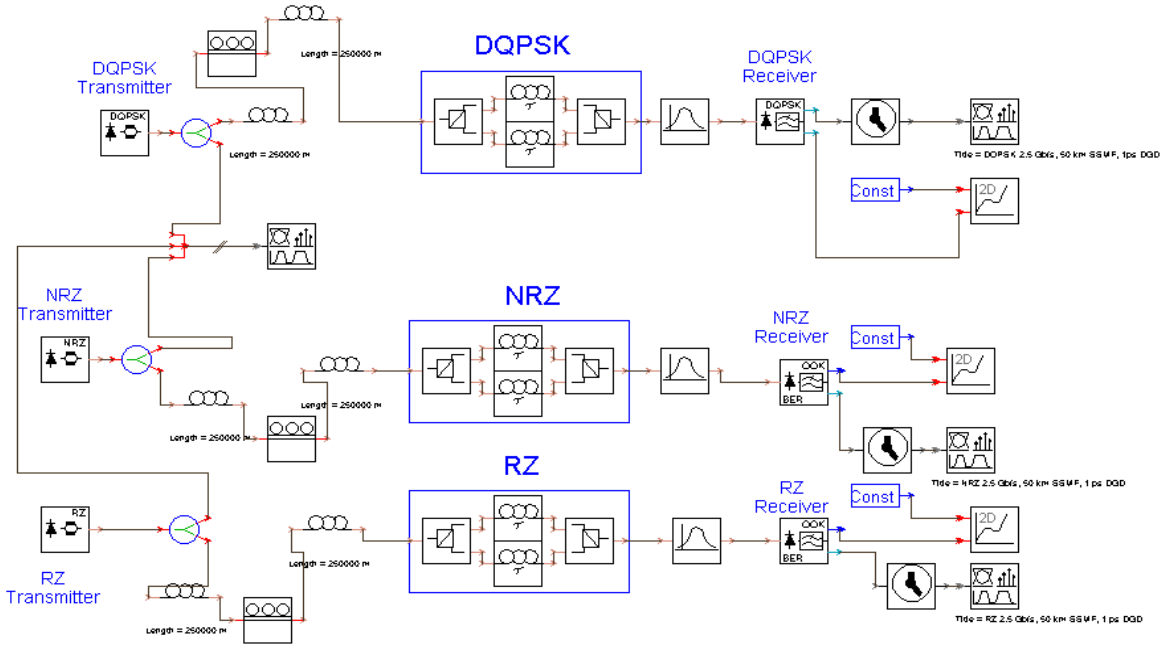

Figure 8.2: Schematic layout used to investigate the tolerance of DQPSK, NRZ and RZ modulation formats over an aerial optical fibre.

The setup used for the simulation is shown in figure 8.2. It includes the three transmitters for DQPSK, NRZ and RZ modulation formats. Next is the mimicked aerial optical fibre which has a polarization controller between two optical fibre lengths. The polarization controller is used to control the coupling angle between the two aerial optical fibres. The coupling angle of the polarization controller can be varied between 0º and 180º. After the aerial optical fibre is the block which is used to change the DGD of the transmission setup. The last part of the setup is for analysis which consists of a *bit-error rate* (BER) tester.

8.3 Performance Metrics for Analysis of Tolerance to PMD

To analyze the output at the receiver of the transmission system, we used three parameters namely; the eye diagram, the bit-error rate (BER) and the Q factor. All three were used so that we could obtain an accurate picture and information of the tolerance of the modulation

formats. It should be noted that all three methods have their own pros and cons over each other as will be discussed in the subsections that follow.

8.3.1 Eye Diagram

The eye diagram is a useful tool for the qualitative analysis of the signal used in digital transmission systems. In addition, it is used to measure the repeatability of the pulses reaching the receiver of an optical fibre transmission system. It provides an at-a-glance evaluation of system performance and it can offer insight into the nature of channel imperfection. It can also be used to examine signal integrity. When the visual display is carefully analyzed, a first-order approximation of signal-to-noise ratio can be obtained.

In an optical transmission system, the point of measurement could be prior to the modulator in a transmitter or after the demodulator in a receiver depending on which part of the system requires examination. When the quality of the transmitted signal is better and the received signal is more uniform, then it is expected that the eye will appear to be more open. On the other hand, when the eye starts to close, it means that transmission errors are more likely since successive bits are interfering with each other (Hecht 1999, p.356; Ireeta *et al.* 2010c). Figure 8.3 shows results of eye diagrams obtained in our laboratory using the RZ/NRZ/DB 10 Gb/s modulation unit for transmission. Figure 8.3(a) was obtained for transmission through a polarization maintaining fibre (PMF), 2 m long, while figure 8.3(b) was obtained for a 6 km optical fibre within a loose cable wound on a 1.8 m diameter drum.

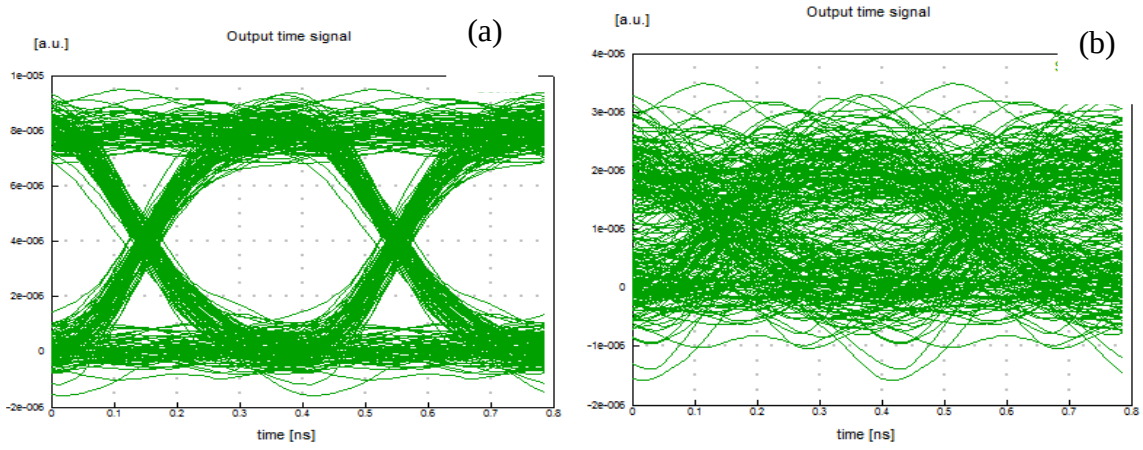

Figure 8.3: Eye diagrams of a 10 Gb/s transmission speed through (a) 2 m polarization maintaining fibre (b) 6 km optical fibre[2].

[2] The author extends his sincere thanks to Romeo R.G. Gamatham, a PhD student at NMMU, for assisting him to learn how to use the Modulation unit, BER tester and the Optical Sampling Oscilloscope (PSO) that have been recently acquired in our OFRU Laboratory.

It is observed that the eye opening of the PMF is bigger compared to the closed eye of the 6 km optical fibre. This is because of the higher PMD of the latter (PMD of 10.3 ps) compared to that of the former (PMD of 2.5 ps).

8.3.2 Bit-Error Rate

By determining the bit-error rate (BER), one is able to make an analysis of an optical communication system. This helps to predict its performance like the eye diagram in section 8.3.1. The BER in simple terms is defined as the ratio of the number of errors to the total number of bits. The BER becomes very significant when one wishes to maintain a sufficient signal-to-noise ratio in the presence of imperfect transmission due to optical fibre dispersion, losses due to components and noise (Vacondio *et al.* 2009; Gavioli *et al.* 2010; Gené and Winzer 2010; Li *et al.* 2010b; Pan and Yao 2010). Figure 8.4 illustrates the variation of BER with the received power at the output of a transmission system. As the power reaching the system receiver increases, the BER becomes small. The most important factor is the 10^{-9} BER equivalent to approximately -24.8 dBm of power. This is the maximum bit-error rate acceptable in telecommunications though lower rates such as 10^{-12} are needed for computer data transmission.

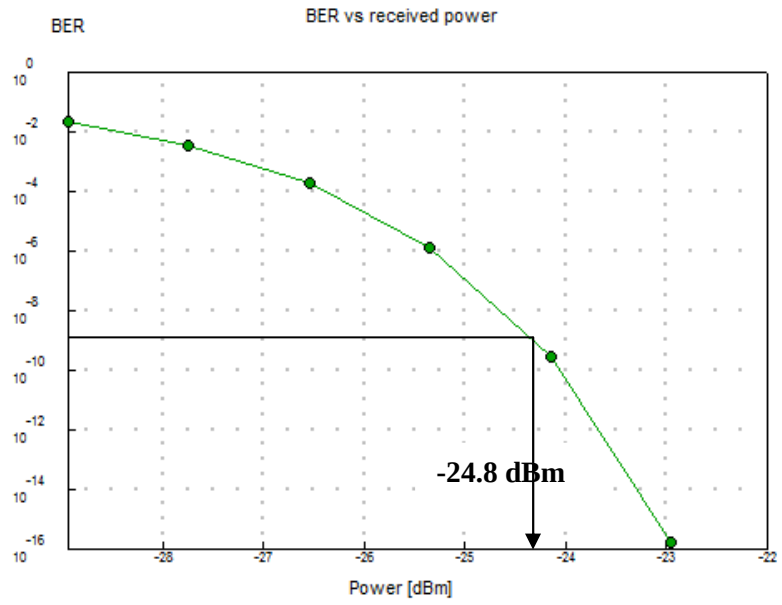

Figure 8.4: The variation of bit-error rate (BER) with the received power.

The BER is also defined in terms of the probability of error (PE) as (Keiser 2000, p.282),

$$PE = \frac{M-1}{M \times \log_2(M)} erfc \sqrt{\frac{3 \times \log_2(M)}{M^2 - 1} \times \frac{E_b}{N_0}} \tag{8.1}$$

where $erfc$ is the error function, E_b is the energy in one bit, N_0 is the noise power spectral density, i.e. noise power in a 1 Hz bandwidth, and M represents the cardinal of the symbol alphabet and is equal to 2^{N_b}. It is important to note that PE is proportional to E_b/N_0 which is a form of signal-to-noise ratio. The practical measurement limit is approximately 10^{-13} which implies that for sensitivities smaller than this, other more accurate measurement methods have to be employed rather than the BER method.

8.3.3 Q-factor

The Q-factor is also widely used to specify receiver performance since it is related to the signal-to-noise ratio required to achieve a specific bit-error rate (BER). Figure 8.5 shows the variation of BER with the Q-factor.

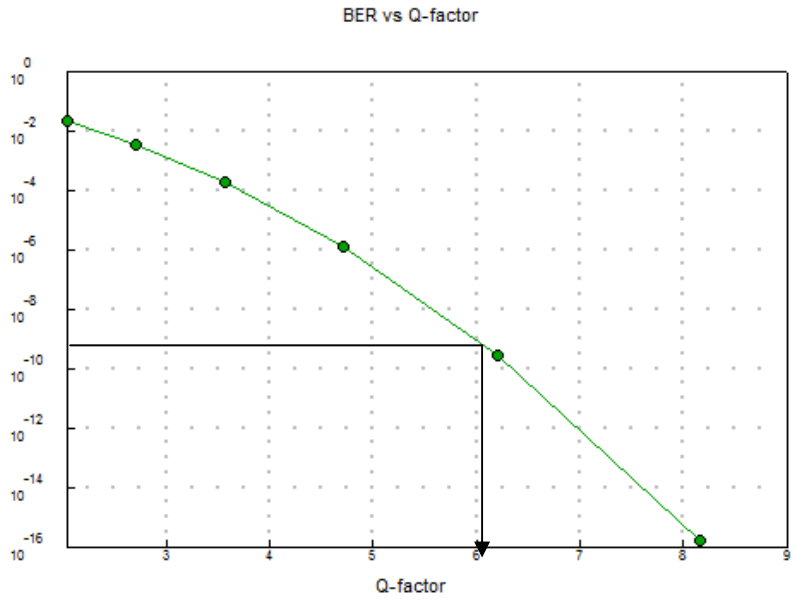

Figure 8.5: A plot of the BER versus the Q factor.

From figure 8.5, the BER = 10^{-9} corresponds to a Q value of 6. This is the most commonly quoted Q value in telecommunication systems. It should be noted that the Q-factor method is used in systems operating in "error free" regions, i.e., below 10^{-13} BER ratios.

8.4 Modulation Format Tolerance with Change in the Transmission Rates

We used a mimicked aerial optical fibre with a DGD equal to 1 ps. The length of this optical fibre was set to 50 km.

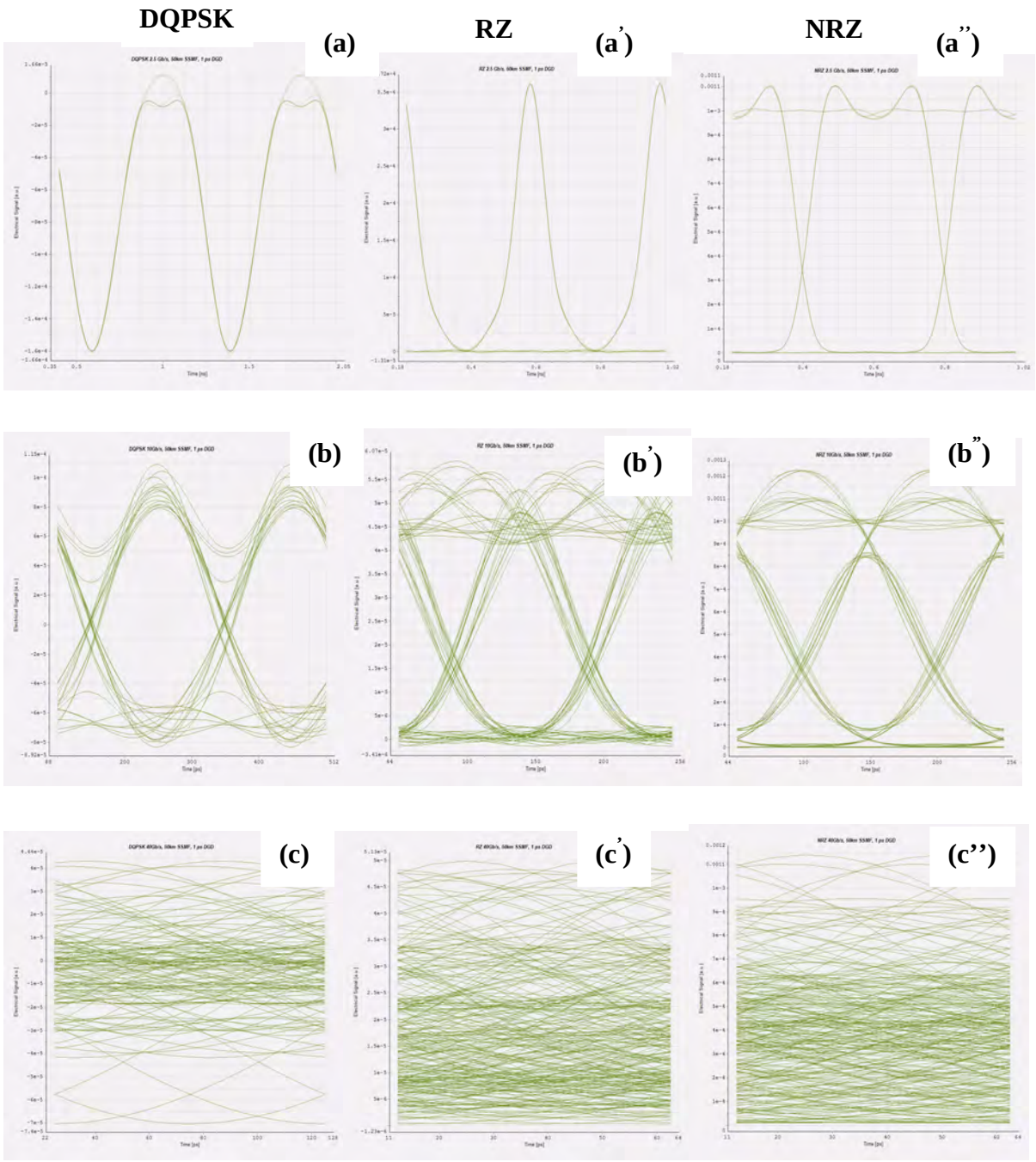

Figure 8.6: Eye diagrams for a simulated aerial optical fibre with 1 ps DGD and 50 km in length. The transmission rates are 2.5 Gb/s for (a), (a') and (a"), 10 Gb/s for (b), (b') and (b") and 40 Gb/s for (c), (c') and (c"). Further, (a), (b) and (c) are for DQPSK modulation format, (a'), (b') and (c') are for RZ modulation format and (a"), (b") and (c") are for the NRZ modulation format.

The polarization controllers in our schematic layout shown in figure 8.2 were set to a coupling angle of 45º between the two 25 km length aerial optical fibres. Figure 8.6 illustrates the output at the receiver using the eye diagrams by use of the BER tester. The transmission rates are 2.5 Gb/s for (a), (a') and (a''), 10 Gb/s for (b), (b') and (b'') and 40 Gb/s for (c), (c') and (c''). Further, (a), (b) and (c) are for DQPSK modulation format, (a'), (b') and (c') are for RZ modulation format and (a''), (b'') and (c'') are for the NRZ modulation format.

Generally, as the transmission rates increase from 2.5 Gb/s to 40 Gb/s, the eye diagrams start closing gradually for all the modulation formats. In other words, the eye diagrams in (a), (a') and (a'') are more open compared to those of (b), (b') and (b'') which in turn are more open compared to those of (c), (c') and (c''). It should be noted in fact that the eye diagrams in (c), (c') and (c'') are too distorted. Simulations for transmission rates of 60 Gb/s, 80 Gb/s and 100 Gb/s were also performed, though not shown, but the distortions were enormous and no constructive information could be obtained from them for reporting.

At transmission rates of 2.5 Gb/s, 10 Gb/s and 40 Gb/s, the eye openings are biggest in the DQPSK followed by RZ and lastly NRZ modulation formats as shown in figure 8.6. Therefore, using the eye diagrams, one is able to make a qualitative analysis of the output signal at the receiver and for this case; the DQPSK modulation format is more tolerant in a PMD-induced aerial optical fibre compared to the RZ modulation format which in turn is more tolerant compared to the NRZ modulation format.

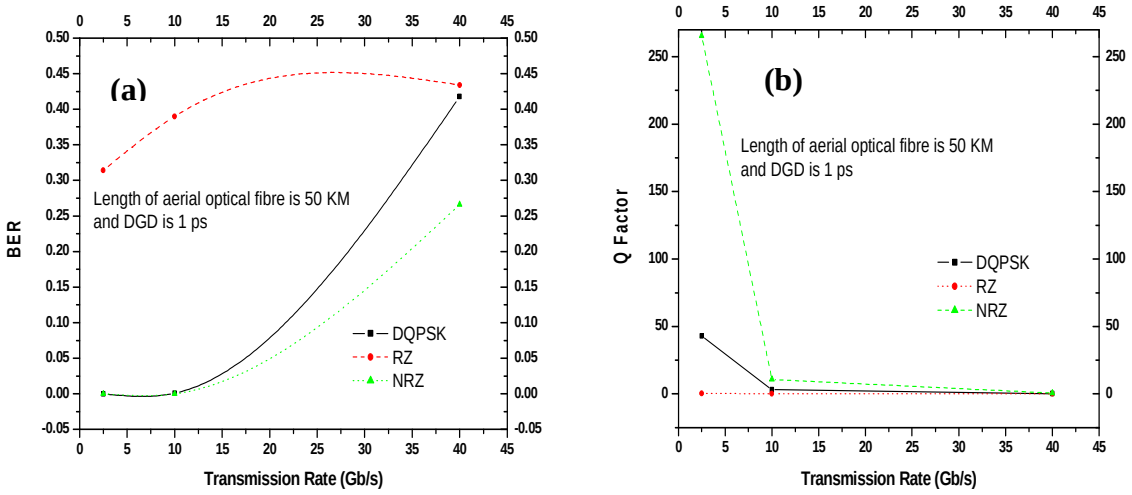

Figure 8.7: (a) shows the BER versus the transmission rate and (b) shows the Q-factor versus transmission rate for a mimicked aerial optical fibre, 50 km long, with a DGD of 1 ps.

Next we used the BER and the Q-factor performance metrics, which are quantitative parameters, to confirm the eye diagram visual displays.

From figure 8.7(a), it is clear that all the modulation formats i.e. DQPSK, RZ and NRZ experience an increase in BER as the transmission rates increase. This implies that the number of errors at the receiver in the output signal increased and from the definition of BER (ratio of number of errors to total number of bits), it increased. This is consistent with the visual displays of the eye diagrams.

However, it should be noted that the BER for the RZ modulation format is higher than that for DQPSK and NRZ modulation formats. It is 0.34 at 2.5 Gb/s and 0.43 at 40 Gb/s while DQPSK and NRZ are both 0 at 2.5 Gb/s and 0.42 and 0.27 respectively at 40 Gb/s. So a trade off has to be made on which modulation format to use for say dense wavelength-division multiplexed (DWDM) systems taking into consideration the peak power and optical spectra widths as was discussed in section 8.1 and the above observation.

From figure 8.6, when one looks at the eye diagrams' openings at a transmission rate of 40 Gb/s, little or no information can be retrieved from them. Therefore, the BER, which is taken to be the best measure of performance of our system (Ip 2010), becomes a handy method together with the Q-factor as shown in figure 8.7. Signal performance information is easily retrievable from these latter methods.

It is also observed from figure 8.7(b) that as the transmission rates increase it generally led to a decrease in the Q-factor. Therefore, as the Q factor decreased as shown in figure 8.7 (b), the BER was also increasing (see figure 8.7(a)).This confirms the discussion we had in section 8.3.3 where the Q-factor increases with the decrease in the BER. In this case, we also observe low Q values for the RZ modulation format compared to the DQPSK and NRZ modulation formats. It should still be noted that the RZ modulation format is usually preferred to the NRZ modulation format in communication systems, because of its advantage of having a low peak power as discussed in section 8.1 and also shown in figure 8.1 for the optical transmission spectra.

8.5 Modulation Format Tolerance with Change in the Optical Fibre Length

The measurement in section 8.4 was repeated here for the mimicked aerial optical fibre with a DGD equal to 1 ps at transmission rates of 10 Gb/s but changing the optical fibre length. Again the polarization controllers were set to a coupling angle of 45º between the two aerial optical fibres. Figure 8.8 illustrates the output at the receiver using the eye diagrams by use of the BER tester. The aerial optical fibre lengths are 250 km for (a), (a') and (a'') and 500 km for (b), (b') and (b''). (a) and (b) are for DQPSK modulation format, (a') and (b') are for NRZ modulation format and (a'') and (b'') are for the RZ modulation format.

In general, as the optical fibre lengths increase from 250 km to 500 km, the eye diagrams start closing gradually for all the modulation formats. That is, the eye diagrams in (a), (a') and (a'') are more open compared to those of (b), (b') and (b'').

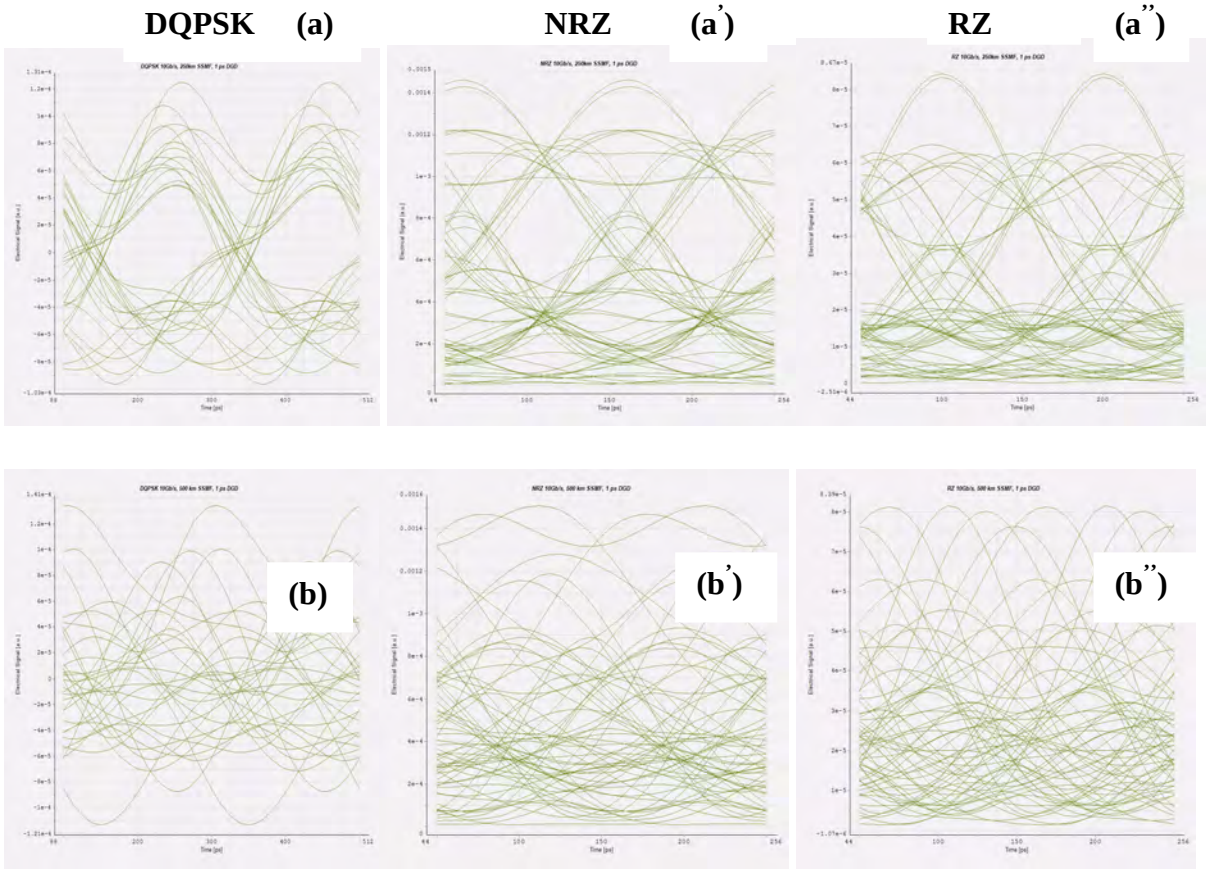

Figure 8.8: Eye diagrams for an aerial optical fibre with 1 ps DGD with a transmission rate of 10 Gb/s. The aerial optical fibre lengths are 250 km for (a), (a') and (a'') and 500 km for (b), (b') and (b''). (a) and (b) are for DQPSK modulation format, (a') and (b') are for NRZ modulation format and (a'') and (b'') are for the RZ modulation format.

At a transmission rate of 10 Gb/s for both 250 km and 500 km aerial optical fibre lengths, the eye openings are biggest in the DQPSK followed by NRZ and lastly RZ modulation formats as shown in figure 8.8. Hence again, as in section 8.4, using the eye diagrams, one is able to make a qualitative analysis of the output signal at the receiver and for this case; the DQPSK modulation format is more tolerant in a PMD-induced aerial optical fibre compared to NRZ modulation format which in turn is more tolerant compared to the RZ modulation format as the aerial optical fibre length is increased.

We then also used the BER and the Q-factor performance metrics to confirm the eye diagram visual displays.

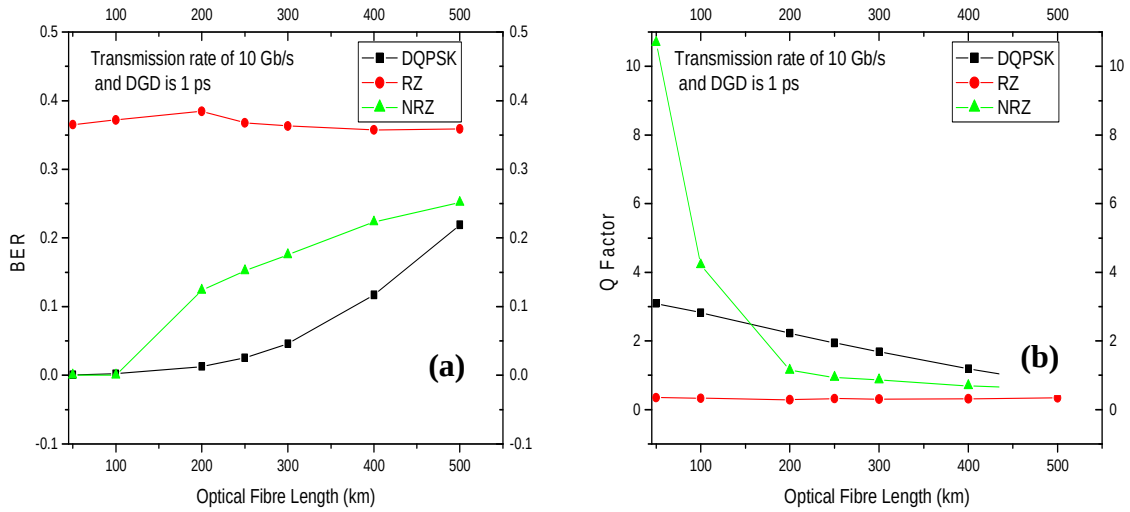

Figure 8.9: (a) shows the BER versus the optical fibre length and (b) shows the Q-factor versus optical fibre length for a mimicked aerial optical fibre with a DGD of 1 ps with a transmission rate of 10 Gb/s.

It is clearly visualized from figure 8.9 (a) that all the modulation formats i.e. DQPSK, RZ and NRZ experience an increase in BER as the length of our mimicked aerial optical fibre is increased. This means that the number of errors at the receiver in the output signal increased. This is consistent with the visual displays of the eye diagrams in figure 8.8.

However, it should also be noted that the BER for the RZ modulation format is higher than that for DQPSK and NRZ modulation formats and also its variations with changing optical fibre length is small compared to the other two. At 10 Gb/s, the DQPSK and NRZ have a

BER of 8.5×10^{-4} and 5.2×10^{-27} at aerial optical fibre length of 50 km, which increases to 0.22 and 0.25 at 500 km lengths respectively. The same reason highlighted in section 8.4 applies here too.

Also, a decrease in the Q factor is observed, as shown in figure 8.9(b), when the aerial optical fibre length is increased for all three modulation formats. Hence, as the Q factor decreased, as shown in figure 8.9(b), the BER was also increasing (see figure 8.9(a)). In this case, it is also observed that the RZ modulation format has low Q values compared to the DQPSK and NRZ modulation formats. The same reason that was given in section 8.4 still holds, i.e., the low peak power of the former modulation format.

8.6 Summary of Results

In making a comparison of the different modulation formats' tolerance to PMD in aerial optical fibres, the different boundary conditions that could favour a given modulation format should be considered. A case in point is the low peak power exhibited by the RZ modulation format compared to the DQPSK modulation format as well as the high spectral efficiency of the latter compared to the former modulation format. This means a trade off between a high spectral efficiency modulation format and one with low peak power.

From sections 8.4 and 8.5, the DQPSK data modulation format is most tolerant to PMD followed by the NRZ and lastly the RZ. This was shown by the use of the three performance metrics; eye diagram, bit-error rate (BER) and the Q-factor. As the transmission rates increased from 2.5 Gb/s to 40 Gb/s, the eye diagram openings closed, the BER increased and the Q-factor decreased. Also, as the aerial optical fibre length was increased from 50 km to 500 km, the Q-factor decreased, the BER increased and the eye diagram openings closed.

CHAPTER 9

CONCLUDING REMARKS

State of polarization (SOP) and polarization-mode dispersion (PMD) monitoring over aerial optical fibres in telecommunication systems have been studied in this thesis. SOP monitoring is important since it is used to determine the rate of PMD compensation in optical fibres. PMD compensation in buried fibres is quite challenging, however, in this study we determined the rate of compensation for an aerial optical fibre link which is more complex considering its random fluctuation because of the environmental conditions to which it is exposed. Also studied in this thesis was the tolerance of modulation formats in PMD-induced aerial optical fibres. The modulation formats considered were the nonreturn-to-zero (NRZ) and return-to-zero (RZ), which are intensity modulation formats, together with the differential quadrature phase shift keying (DQPSK) which is a phase modulated format.

9.1 Bending, Twisting and Environmental Effects on Optical Fibres

PMD being a stochastic quantity, precautions have to be taken before measurements are made in order to stabilize the measurement system. This is very important especially for polarimetric measurement techniques used to determine PMD since even optical fibre patchcords that have small PMD can have a big effect on the measurement noise. Deployed aerial optical fibres, as used in this study, make this even more complicated compared to deployed buried optical fibres. It was shown in section 5.2 that bending an optical fibre induces linear birefringence while optical fibre twisting induces circular birefringence.

Vortex-induced vibrations (3 to 30 km/h wind speed range) led to a slow drift of the normalized Stokes vectors with little noise. A smooth random walk pattern was also observed when these normalized Stokes parameters were analyzed by use of the Poincaré sphere. But rapid white noise-like rotation of the Stokes parameters and a random population of the Poincaré sphere were obtained in the presence of wind gusts in the cable galloping region. The wind speed in the cable galloping region is 25 to 65 km/h. This was investigated in section 5.3.

In section 5.4, we investigated the influence of temperature on the SOP spread of a laser pulse in an aerial optical fibre. It was found that the SOP spread is much more random

during the day compared to the evenings and night times because of the higher temperatures for the former. In addition, on days that had relatively low wind speeds, the SOP spread was not as random as on days that had high wind speeds.

9.2 PMD Monitoring and Compensation

Since PMD and hence SOPs vary randomly due to random variations in the optical fibre birefringence, it becomes very important to measure and characterize the probability density functions (pdfs) of these variable quantities. In section 6.1, a Gaussian pdf was fitted to the FO-PMDs, FO-PMD coefficient values and the SO-PMDs for an aerial optical fibre exposed to severe vortex-induced oscillations on the South African telecommunication network measured using an FTB-5700 single-ended dispersion analyzer. The number of PMD values used here were only 184 compared to the large numbers that had to be used by other researchers using other measurement techniques to achieve the same pdf. Some examples are; Brodsky *et al.* (2003) made 950 while Mudau (2008, p.82) of our research group made 150 000 PMD measurements in order to be able to obtain a Gaussian fit for the PMD statistics. The PMD values we obtained confirmed its accuracy and robustness in unstable polarization conditions. Indeed, the mean PMD of the aerial optical fibre under consideration was measured to be 0.47 ps with a standard deviation of 0.08 ps; this compared well with the manufacturer's quoted PMD value of 0.46 ps.

In section 6.2, the FTB-5700 and the GINTY were used to measure FO-PMD for the same aerial optical fibre. The FO-PMD values obtained from them were analyzed statistically and fitted with a Gaussian pdf. In our investigations, an 11% and 12% PMD uncertainty was obtained for the FTB-5700 and GINTY, respectively. These two values perfectly fall within the range that was proposed by Gisin *et al.* (1996). However, histograms of the SO-PMD values obtained from both these instruments were better fitted by the Maxwellian distribution compared to the Gaussian and the Foschini *et al.* (2000) distributions. The measured mean SO-PMD value (0.12 ps/nm) obtained was approximately equal to that obtained from the theoretical mean equation proposed by Foschini *et al.* (2000).

An investigation of the variations of FO-PMD, FO-PMD coefficients and SO-PMD with the environment was carried out in section 6.3. The GINTY (FTB-5500B) and FTB-5700 (single-

ended dispersion analyzer) measurement techniques were both used. Environmental changes, especially temperature and wind speed, change the birefringence and mode coupling of the aerial optical fibre and this in turn leads to the fluctuation in the measured PMDs. It was observed that these parameters varied more when the GINTY was used compared to the FTB-5700 measurement instrument. This, hence, confirmed the robustness of the FTB-5700 single-ended dispersion analyzer instrument to accurately measure PMD of an aerial optical fibre.

In sections 6.4 and 6.5, an investigation of the rate at which PMD compensation can be achieved in aerial optical fibres was carried out. It is important to note that the compensator has to track the changing PMD vector and this is the same as tracking the changing SOPs though the PMD vector fluctuations are normally slower. With the determination of the 50% decorrelation time of the laser light, the time scale over which the polarization effects occur for PMD compensation to be made accurately is then known. The time for PMD compensation should be slightly higher than the 50% decorrelation time since SOP changes are always faster than PMD vector changes. The response times for accurate PMD compensation for the aerial fibre were determined and the maximum was found to be slightly higher than 390 s on a windy and hot day.

9.3 Output SOP Statistical Characterization

One of the polarimetric measurement techniques, the Jones matrix eigenanalysis method, was used to measure the FO-PMD and SO-PMD of deployed buried optical fibre links as shown in section 7.1. We were able to fit the Maxwellian distribution and the Foschini *et al.* (2000) distribution very well onto the histograms of the FO-PMD and SO-PMD statistics obtained respectively. This was only true if the optical fibre link under consideration was long enough to possess numerous random mode-coupled sites since random coupling is responsible for the significant variations of FO-PMD and PSPs as a function of wavelength (Foschini and Poole 1991).

The distributions of the statistics of the relative changes in SOP angles per unit wavelength (for a deployed buried optical fibre) and per unit time (for deployed aerial optical fibre) were found to be skewed towards the low values side just like for the theoretical SO-PMD and FO-PMD statistical distributions. In section 7.4, we found out that fast SOP fluctuations

occurred during the daytime (around noon) and the slow SOP changes were experienced in the morning and in the evening. The SOP variations in aerial fibres are due to environmental fluctuations, while SOP variations in buried fibres are due to random mode coupling and the distribution of birefringence along the fibre. The statistical distributions of the rate of change of SOP angles approached the statistical distribution first derived by Foschini *et al*. (2000) better, compared to the Weibull and Rayleigh distributions as shown in section 7.2. It should be noted that having a statistical distribution of the rates of change of SOP angles helps one know the time scale over which the polarization effects occur to enable accurate PMD compensation.

9.4 Modulation Format's Tolerance to PMD

For some time now, a fierce debate regarding which modulation format is the "optimum" for optical communication systems has continued. The debate started with nonreturn-to-zero (NRZ) vs. return-to-zero (RZ), later the advanced modulation formats such as CS-RZ, SSB-RZ and duobinary, and now more recently the phase modulated formats such as DPSK and DQPSK. In this study, we investigated the tolerance of some of these modulation formats in aerial optical fibres by simulation. In these investigations, we used different transmission rates (2.5 Gb/s, 10 Gb/s and 40 Gb/s) as well as different lengths of the aerial optical fibre (50 km, 100 km, 200 km, 250 km, 300 km, 400 km and 500 km).

The modulation formats used for our analyses were NRZ (because this is what is currently being used on the South African telecommunication network and also since it is easy to implement because of its low cost), the RZ (due to its lower peak power) and the DQPSK (well known from radio communication where multilevel signalling is frequently used to enhance the spectral efficiency). The RZ modulation format has other advantages over the NRZ modulation format such as; (a) it is less susceptible to intersymbol interference, as well as the fact that its receiver has a 2 dB better performance compared to the latter as shown by Pfennigbauer *et al.* (2002), (b) the RZ pulse shape benefits from a "soliton-like effect" in optical fibres that makes it suffer less distortion from optical fibre nonlinearity compared to NRZ, as described by Hayee and Willner (1999).

The different boundary conditions that could favour a given modulation format should be considered in making a comparison of the tolerance of the different modulation formats to PMD in deployed aerial optical fibres. A case in point is the low peak power exhibited by the

RZ modulation format compared to the DQPSK modulation format as well as the high spectral efficiency of the latter compared to the former modulation format. This implies the need for a trade off between a high spectral efficiency modulation format and one with low peak power.

In sections 8.4 and 8.5, the DQPSK data modulation format was found to be the most tolerant to PMD, followed by the NRZ and lastly the RZ modulation formats. This comparison was achieved by using the three performance metrics; eye diagram, bit-error rate (BER) and the Q-factor. As the transmission rates increased from 2.5 Gb/s to 40 Gb/s, the eye diagram openings closed, the BER increased (BERs for RZ, NRZ and DQPSK were 0.34, 0 and 0 respectively at 2.5 Gb/s and 0.43, 0.27 and 0.42 respectively at 40 Gb/s) and the Q-factor decreased. Also, as the aerial optical fibre length was increased from 50 km to 500 km, the Q-factor decreased, the BER increased (BERs for DQPSK and NRZ were 8.5×10^{-4} and 5.2×10^{-27} with 50 km, respectively, and 0.22 and 0.26 with 500 km, respectively) and the eye diagram openings closed.

In summary, the findings in this thesis show an extensive investigation of the statistical distributions of PMDs (FO-PMD, FO-PMD coefficient and SO-PMD), and for the first time a distribution for the rate of change of SOP angles for a deployed aerial optical fibre. The rate of PMD compensation on deployed aerial optical fibres for the South African network was also determined and hopefully Telkom SA will use it in the near future as they upgrade their network. We also showed that the DQPSK modulation format is the most suitable for optical telecommunication systems even for PMD-induced deployed aerial optical fibres. If also implemented in future by Telekom SA, it will allow for ultra-high capacity spectrally efficient optical telecommunication systems.

APPENDIX A
NOTATION

The following is the abbreviation listing we have used in the thesis.

x, y, z	Optical fibre coordinates: the direction of propagation is in the z direction while x and y are the transverse coordinates i.e. those of Jones space.
$e^{j(\omega_o t-\beta z)}$	Represents a continuous wave travelling in the z direction with j being the imaginary unit, ω_o the angular carrier frequency, t is the time, and β is the propagation constant.
$\Delta\omega$	The deviation from the angular carrier frequency ω_o of the propagating light. $\omega_o+\Delta\omega$ is the optical frequency.
$\lvert s\rangle$	2D complex Jones ket vector, $$\lvert s\rangle=\begin{pmatrix} s_x \\ s_y \end{pmatrix} \quad \text{(A.1)}$$ The bra $\langle s\rvert$ in contrast represents the corresponding complex conjugate row vector, i.e. $\langle s\rvert=\left(s_x^*, s_y^*\right)$. The bra-ket notation is used to distinguish Jones vectors from Stokes vectors. Our Jones vectors are all of unit magnitude, i.e., $\langle s\rvert s\rangle = s_x^* s_x + s_y^* s_y = 1$ assuming coherent light is used.
$\hat{s}$	3D Stokes vector of unit length indicating the polarization of the light field and it corresponds to $\lvert s\rangle$. The Stokes parameters are the components of $\hat{s}$: $$\begin{aligned} s_1 &= s_x s_x^* - s_y s_y^* \\ s_2 &= s_x s_y^* + s_x^* s_y \\ s_3 &= j\left(s_x s_y^* - s_x^* s_y\right). \end{aligned} \quad \text{(A.2)}$$ From this definition, $s_1=1$ for linear polarization aligned with the x axis, $s_2=1$ for linear polarization at 45^o to this axis, and $s_3=1$ for right circular polarized light $\left(s_y = j s_x\right)$ which

	conforms to the traditional optics definition.
I	2×2 or 3×3 identity matrix.
T	2×2 unitary transmission matrix in Jones space. It relates the output to the input through $\|t\rangle = T\|s\rangle$ (A.3) The symbols s and t designate respective input and output quantities as shown in figure A1.
A	2×2 Jones matrix, with $\det(A)=1$. It is related to T by $T = e^{-j\phi_o}A,$ (A.4) with ϕ_o being the common phase.
R	3×3 orthogonal rotation matrix in Stokes space isomorphic to A. It also relates the output to the input via $\hat{t} = R\hat{s}.$ (A.5)
$\vec{\beta}$	3D birefringence vector in Stokes space that describes the local optical fibre properties.
$\vec{\tau}$	The output PMD vector in Stokes space. $\Delta\tau$ is the differential group delay (DGD) which is the magnitude of $\vec{\tau}$ and its direction is that of the Stokes vector of the slow principal state.
$\overline{\Delta\tau}$	Mean DGD of the optical fibre, $\overline{\Delta\tau} \triangleq \langle\Delta\tau\rangle$.
$\hat{p}, \hat{r}$	Unit Stokes vectors: $\hat{p}$ is at times used to describe the polarization of the slow principal state while $\hat{r}$ is used for a rotation axis.
Subscript ω	Represents differentiation, i.e., $ds/d\omega = s_\omega$.

Figure A1: Block diagram of optical fibre under test (FUT).

APPENDIX B
PROBABILITY DENSITIES

Probability densities of a component of first-order PMD (τ_i), the magnitude of the first-order PMD ($|\vec{\tau}|$), a component of second-order PMD ($\tau_{\omega i}$), the magnitude of second-order PMD ($|\vec{\tau}_\omega|$), the second-order PMD component associated with PCD ($|\vec{\tau}|_\omega = \Delta\tau_\omega$), the perpendicular second-order component ($|\vec{\tau}_{\omega\perp}|$), and the depolarization ($|\hat{p}_\omega|$) all scaled to the mean DGD, $\overline{\Delta\tau}$, denoted here by τ. Catalan's constant, G, is 0.915965..., J_o is the zero-order cylindrical Bessel function, and ${}_1F_1$ is the standard hypergeometric function

Density $p_X(x) \geq 0, \quad \int_{-\infty}^{\infty} dx\, p_X(x) = 1$

X	$p_X(x)$	$E(X) \triangleq \int_{-\infty}^{\infty} dx\, xp(x)$	$E\left(X^2\right) \triangleq \int_{-\infty}^{\infty} dx\, x^2 p(x)$
τ_i	$\frac{2}{\pi\tau} e^{-(2x/\tau)^2/\pi}$, Gaussian	**0**	$\frac{\pi}{8}\tau^2 = \sigma^2$
$\|\vec{\tau}\| \triangleq \Delta\tau$	$\frac{8}{\pi^2\tau}\left(\frac{2x}{\tau}\right)^2 e^{-(2x/\tau)^2/\pi};\ x \geq 0,$ Maxwellian $0;\ x < 0$	τ	$\frac{3\pi}{8}\tau^2 = 3\sigma^2$
$\tau_{\omega i}$	$\frac{4}{\pi\tau^2}\sec h\left(\frac{4x}{\tau^2}\right),$ soliton amplitude	**0**	$\left(\frac{\pi}{8}\right)^2 \tau^4 = \sigma^4$
$\|\vec{\tau}_\omega\|$	$\frac{8}{\pi\tau^2}\frac{4x}{\tau^2}\tanh\left(\frac{4x}{\tau^2}\right)\sec h\left(\frac{4x}{\tau^2}\right);\ x \geq 0$ $0;\ x < 0$	$\frac{2G}{\pi}\tau^2$	$3\left(\frac{\pi}{8}\right)^2 \tau^4 = 3\sigma^4$
$\|\vec{\tau}\|_\omega \triangleq \Delta\tau_\omega$	$\frac{2}{\tau^2}\sec h^2\left(\frac{4x}{\tau^2}\right),$ soliton intensity	**0**	$\frac{1}{3}\left(\frac{\pi}{8}\right)^2 \tau^4 = \frac{1}{3}\sigma^4$

$\left\|\vec{\tau}_{\omega\perp}\right\|$	$x\left(\frac{8}{\pi\tau^2}\right)^2 \int_0^\infty d\alpha J_o\left(\frac{8\alpha x}{\pi\tau^2}\right)$ $\times \sec h(\alpha)(\alpha \tanh \alpha)^{1/2}$		$\frac{8}{3}\left(\frac{\pi}{8}\right)^2 \tau^4 = \frac{8}{3}\sigma^4$
$\left\|\hat{p}_\omega\right\|$	$x\left(\frac{24}{\pi\tau^2}\right) \int_0^\infty d\beta \frac{\sinh^{3/2}\beta}{\sqrt{\beta}.\cosh^{5/2}\beta^1}$ $\times {}_1F_1\left(\frac{5}{2};1;-\frac{x^2.4.\beta}{\pi\tau^2}\tanh\beta\right)$		$\frac{4}{3}\frac{\pi}{8}\tau^2 = \frac{4}{3}\sigma^2$

APPENDIX C

ACRONYMS

AMI	Alternate-mark inversion
ASE	Amplified spontaneous emission
BER	Bit error rate
CD	Chromatic dispersion
CSRZ	Carrier-suppressed return-to-zero
CW	Continuous wave
DB	Duobinary
DFB	Distributed Feed Back
DGD	Differential group delay, $\Delta\tau$.
DMF	Data modulation format
DOP	Degree of polarization
DPSK	Differential phase-shift keying
DQPSK	Differential quadrature phase-shift keying
DWDM	Dense Wavelength-division multiplexing
EDFA	Erbium-doped fibre amplifier
FWHM	Full width at half maximum
FWM	Four-wave mixing
ISI	Intersymbol interference
JME	Jones matrix eigenanalysis method
MMM	Müller matrix method
MZM	Mach-Zehnder modulator
NRZ	Non-return-to-zero modulation
OADMs	Optical add/drop multiplexers
OOK	On-off-keying
OSNR	Optical signal-to-noise ratio

OTDR	Optical time-domain reflectometry
P-OTDR	Polarization optical time-domain reflectometry
PBS	Polarization beam splitter
PC	Polarization controller
PCD	Polarization-dependent chromatic dispersion
pdf	Probability density function
PDL	Polarization-dependent loss
PDG	Polarization-dependent gain
PM	Phase modulator
PMF	Polarization-maintaining fibre, also called high-birefringence fibre
PMD	Polarization-mode dispersion
Pol. sk	Polarization shift keying
PSK	Phase shift keying
PSP	Principal state of polarization, $\left\vert p\right\rangle$, $\hat{p}$
RF	Radio frequency
RZ	Return-to-zero modulation
SOP	State of polarization
SSB	Single sideband
VSB	Vestigial sideband
WDM	Wavelength-division multiplexing
XPM	Cross-phase modulation

APPENDIX D

RESEARCH OUTPUTS OF THE AUTHOR

2010

Winston T. Ireeta, Vitalis Musara, Lorinda Wu, and Andrew W. R. Leitch, "Statistical Characterization of the Output State of Polarization in Deployed Single Mode Fibres," Optics Letters, vol. 35, issue 12, pp. 2049-2051, June 2010.

Winston T. Ireeta, Vitalis Musara, Samuel K. Fosuhene, Lorinda Wu, and A.W.R. Leitch, "Determining the Rate of PMD Compensation in Deployed Aerial Optical Fibres Through SOP Monitoring," Proc. 12th Southern African Telecommunication Network and Applications Conference (SATNAC), Spier Estate, Stellenbosch, South Africa (5th to 8th September 2010). Published in the Conference Proceedings, pp. 261-265, ISBN: 978-0-620-47934-9.

Winston T. Ireeta, Vitalis Musara, and A.W.R. Leitch, "A Comparison of the Tolerance of DQPSK, NRZ and RZ Modulation Formats in a PMD-induced Environment", Oral presentation at the 55th South African Institute of Physics (SAIP) Conference, CSIR, Pretoria, South Africa (27th September to 1st October 2010). Published in the Conference Proceedings, ISBN: 978-0-620-46211-2.

Winston T. Ireeta, V. Musara, L. Wu, and A.W.R. Leitch, "SOP and PMD monitoring on deployed aerial optical fibres," submitted to the Optics Communications Journal (November 2010).

Vitalis Musara, **Winston T. Ireeta**, Samuel K. Fosuhene, Lorinda Wu, and A.W.R. Leitch," The Influence of High first-order Polarization Mode Dispersion Sections on Optical Network System Performance," Proc. 12th Southern African Telecommunication Network and Applications Conference (SATNAC), Spier Estate, Stellenbosch, South Africa (5th to 8th September 2010). Oral presentation by Winston Tumps Ireeta. Published in the Conference Proceedings, pp. 273-276, ISBN: 978-0-620-47934-9. (*Awarded prize for 2nd best paper at conference*)

Vitalis Musara, **Winston T. Ireeta**, L. Wu, and A.W.R. Leitch, "The General Interferometry Technique: Interferogram Analysis in The Presence of a High Polarization Mode Dispersion Segment," Winston Tumps Ireeta is the corresponding author. Submitted to AFRICON 2011 (March 2011).

Vitalis Musara, **Winston T. Ireeta**, Samuel K. Fosuhene, Lorinda Wu, and A.W.R. Leitch, "The impact of a High Polarization Mode Dispersion Section on the Output State of Polarization of Propagating Light," submitted to Optical Fibre Technology Journal (May 2010).

Vitalis Musara, **Winston T. Ireeta**, Samuel K. Fosuhene, Lorinda Wu, and A.W.R. Leitch, "Tuneable Polarization Mode Dispersion Emulator: Fixed Polarization Maintaining Fibre Sections and Rotatable Polarization Orientations," Optik: International Journal of Light and Electron Optics (In Press).

Vitalis Musara, Samuel Fosuhene, **Winston T. Ireeta**, Andrew Leitch, and Lorinda Wu, "Emulator With Inverse Trend in First-Order and Second-Order Polarization Mode Dispersion," Optics Communications Journal (In Press).

Samuel K. Fosuhene, Vitalis Musara, **Winston T. Ireeta**, and Andrew W. R. Leitch, "Forward and Single-ended Polarization Mode Dispersion (PMD) Measurements on a Tunable PMD Emulator", Poster presentation at the 55th South African Institute of Physics (SAIP) Conference, CSIR, Pretoria, South Africa (27th September to 1st October 2010). Published in the Conference Proceedings, ISBN: 978-0-620-46211-2.

2009

V. Musara, **W.T. Ireeta**, L. Wu and A.W.R. Leitch, "Detecting the Dominance of PMD from a Fibre Segment on an Optical Network System Through State of Polarization Monitoring", Proc. 11th Southern African Telecommunication Network and Applications Conference (SATNAC), Royal Swazi Spa, Swaziland (30th August to 2nd September 2009). Oral presentation by Winston Tumps Ireeta. Published in the Conference Proceedings, pp. 461-462. ISBN: 978-0-620-44106-3.

REFERENCES

A

Agarwal, A., S. Chandrasekhar, and R.-J. Essiambre. 2004. "42.7 Gb/s CSRZ-VSB for spectrally efficient meshed networks," *Proc. European Conference on Optical Communication, ECOC'04.* Paper We3.4.4.

Agrawal, G. P. 2007. "Nonlinear Fiber Optics," *Academic Press, New York.*

Allen, C. T., P. K. Kondamuri, D. L. Richards, and D. C. Hague. 2003. "Measured temporal and spectral PMD characteristics and their implications for network-level mitigation approaches," *IEEE J. Lightwave Technol*. 21:79-86.

B

Bakhshi, B., J. Hansryd, P. A. Andrekson, J. Brentel, E. Kolltveit, B. K. Olsson, and M. Karlsson. 1999. "Measurement of the differential group delay in installed optical fibres using polarization multiplexed solitons," *IEEE Photon. Technol. Lett.* 11:593-595.

Betti, S., G. D. Marchis, and E. Iannone. 1992. "Polarization modulated direct detection optical transmission systems," *IEEE J. Lightwave Technol*. 10:1985-1997.

Bigo, S., Y. Frignac, G. Charlet, W. Idler, S. Borne, H. Gross, R. Dischler, W. Poehlmann, P. Tran, C. Simonneau, D. Bayart, A. J. G. Veith, and J.-P. Hamaide. 2001. "10.2 Tbit/s (256 × 42.7 Gb/s PDM/WDM) transmission over 100 km Teralight fiber with 1.28 bit/s/Hz spectral efficiency," *Proc. Optical Fiber Communication Conference, OFC'01*. Paper PD25.

Bigo, S. 2004. "Multiterabit DWDM terrestrial transmission with bandwidth-limiting optical filtering," *IEEE J. of Selected Topics in Quantum Electronics.* 10:329-340.

Bohn, M., W. Rosenkranz, P. M. Krummrich, F. Horst, B. J. Offrein, and G. L. Bona. 2004. "Experimental verification of combined adaptive PMD and GVD compensation in a 40 Gb/s transmission using integrated optical FIR filters and spectrum monitoring," *Optical Fiber Communication Conference, OFC'04.* Technical Digest. Paper TuG3.

Born, M. and E. Wolf. 1980. "Principles of optics," *Pergammon Press, Oxford*.

Bosco, G., R. Gaudino, and P. Poggiolini. 2001. "An exact analysis of RZ versus NRZ sensitivity in ASE noise limited optical systems," *Proc. European Conference on Optical Communication, ECOC'01*. 4:526-527.

Brodsky, M., P. Magill, and N. J. Frigo. 2003. "Long–term PMD characterization of installed fibres-How much time is adequate?," *OSA Annual Meeting 2003.* Paper F12.

Bruyere, F. 1996. “Impact of first- and second-order PMD in optical digital transmission systems,” *Opt. Fiber Technol.* 2:269-280.

Buchali, F., H. Bülow, W. Baumert, R. Ballentin, and T. Wehren. 2000. “Reduction of the chromatic dispersion penalty at 10 Gb/s by integrated electronic equalizers,” *Optical Fiber Communication Conference, OFC’00.* Technical Digest. Paper ThS1: 268-270.

Bülow, H. 1998. “System outage probability due to first- and second-order PMD,” *IEEE Photon. Technol. Lett*. 10:696-698.

Bülow, H. 2000. “PMD mitigation techniques and their effectiveness in installed fiber,” *Proc. Optical Fiber Communication Conference, OFC’01*. Paper ThH1.

C

Cameron, J., L. Chen, X. Bao, and J. Stears. 1998a. “Time evolution of polarization mode dispersion in optical fibres,” *IEEE Photon. Technol. Lett*. 10:1265-1267.

Cameron, J., X. Bao, and J. Stears. 1998b. “Time evolution of polarization mode dispersion for aerial and buried cables,” *Proc. Optical Fiber Communication Conference, OFC’98.* Technical Digest. 240-241.

Cavallari, M., C. R. S. Fludger, and P. J. Anslow. 2004. “Electronic signal processing for differential phase modulation formats,” *Proc. Optical Fiber Communication Conference, OFC’04*. Paper TuG2.

Charlet, G., J.-C. Antona, S. Lanne, P. Tran, W. Idler, M. Gorlier, S. Borne, A. Klekamp, C. Simonneau, L. Pierre, Y. Frignac, M. Molina, F. Beaumont, J.-P. Hamaide, and S. Bigo. 2002. “6.4 Tb/s (159 × 42.7 Gb/s) capacity over 21 × 100 km using bandwidth-limited phase-shaped binary transmission,” *Proc. European Conference on Optical Communication, ECOC’02.* Paper PD4.1.

Chikama, T., S. Watanabe, T. Naito, H. Onaka, T. Kiyonaga, Y. Onoda, H. Miyata, M. Suyama, M. Seino, and H. Kuwahara. 1990. “Modulation and demodulation techniques in optical heterodyne PSK transmission systems,” *IEEE J. Lightwave Technol*. 8:309–321.

Cho, P. S., V. S. Grigoryan, Y. A. Godin, A. Salamon, and Y. Achiam. 2003. “Transmission of 25 Gb/s RZ-DQPSK signals with 25 GHz channel spacing over 1000 km of SMF-28 fiber,” *IEEE Photon. Technol. Lett*. 15:473-475.

Corsi, F., A. Galtarossa, and L. Palmieri. 1999. “Beat length characterization based on backscattering analysis in randomly perturbed single-mode fibers,” *IEEE J. Lightwave Technol.* 17:1172-1178.

Costello, D. J., J. Hagenauer, H. Imai, and S. B. Wicker. 1998. “Applications of error-control coding,” *IEEE J. Transactions Information Theory*. 44:2531-2560.

Curti, F., B. Daino, G. De Marchis, and F. Matera. 1990. “Statistical treatment of the evolution of the principal states of polarization in single mode fibres,” *IEEE J. Lightwave Techno*l. 8:1162-1166.

Cyr, N., A. Girard, and G. W. Schinn. 1999. “Stokes parameter analysis method, the consolidated test method for PMD measurements,” *Proc. National Fiber Optics Engineers Conference, NFOEC’99*. Paper 23.

Cyr, N. 2004a. “Polarization mode dispersion measurements: Generalization of the interferometric method to any mode coupling regime,” *IEEE J. Lightwave Technol*. 22:794-805.

Cyr, N., R. Roberge, J. Bradley, G. Amice, F. Audet, and G. W. Schinn. 2004b. “Interferometric PMD measurement of a transatlantic 5512-km fiber link including 119 EDFAs,” *Proc. Optical Fiber Communication Conference, OFC’04*. Session MF.

D

Dahan, D. and G. Eisenstein. 2002. “Numerical comparison between distributed and discrete amplification in a point-to-point 40-Gb/s 40-WDM-based transmission system with three different modulation formats,” *IEEE J. Lightwave Technol.* 20:379–388.

De Angelis, C., A. Galtarossa, G. Gianello, F. Matera, and M. Schiano. 1992. “Time evolution of polarization mode dispersion in long terrestrial links,” *IEEE J. Lightwave Technol*. 10:552-555.

De Lignie, M. C., H. G. J. Nagel, and M. O. Van Deventer. 1994. “Large polarization mode dispersion in fiber optic cables,” *IEEE J. lightwave Technol*. 12:1325-1329.

Derickson, D. 1998. “Fiber Optic Test and Measurement,” *Prentice Hall*. New Jersey.

Desurvire, E., D. Bayart, B. Desthieux, and S. Bigo. 2002. “Erbium-Doped Fiber Amplifiers, Device and System Developments” *Wiley*. Hoboken, NJ.

Djupsjöbacka, A., A. Berntson, J. Mårtensson, and D. Källgren. 2009. “Measured temporal statistics of the DGD RMS-value in buried optical fibers,” *IEEE Photon. Technol. Lett*. 21:1801-1803.

E

ECI Telecom. 2008. “40G transmission in metro and long-haul networks,” White Paper. *http:\\nxtcommnews.com/images/ECI_40G_Transmission_in_Metro_and_Long-haul_Networks.doc*

Eickhoff, W., Y. Yen, and R. Ulrich. 1981. “Wavelength dependence of birefringence in single mode fibre,” *Appl. Opt*. 20:3428-3435.

Eyal, A., W. Marshall, M. Tur, and A. Yariv. 1999. “Representation of second-order PMD,” *Elect. Lett*. 35:1658-1659.

F

Forestieri, E. 2003. “A fast and accurate method for evaluating joint second-order PMD statistics,” *IEEE J. Lightwave Technol.* 21:2942-2952.

Foschini, G. J. and C. D Poole. 1991. “Statistical theory of polarization dispersion in single mode fibres,” *IEEE J. Lightwave Technol*. 9:1439-1456.

Foschini, G. J., R. M. Jopson, L. E. Nelson, and H. Kogelnik. 1999. “The statistics of PMD-induced chromatic fibre dispersion,” *IEEE J. Lightwave Technol*. 17:1560-1565.

Foschini, G. J., L. E. Nelson, R. M. Jopson, and H. Kogelnik. 2000. “Probability densities of second-order polarization mode dispersion including polarization dependent chromatic fiber dispersion,” *IEEE Photon. Technol. Lett*. 12:293-295.

Foschini, G. J., L. E. Nelson, R. M. Jopson, and H. Kogelnik. 2001. “Statistics of second-order PMD depolarization,” *IEEE J. Lightwave Technol.* 19:1882-1886.

Fukuchi, K. 2002. “Wideband and ultra-dense WDM transmission technologies toward over 10-Tb/s capacity,” *Proc. Optical Fiber Communication Conference, OFC’02*. Paper ThX5.

G

Galtarossa, A. and L. Palmieri. 1998. “Relationship between pulse broadening due to polarization mode dispersion and differential group delay in long single mode fibres,” *Elect. Lett.* 34:492-493.

Galtarossa, A., L. Palmieri, M. Schiano, and T. Tambosso. 1999. “Single-end polarization mode dispersion measurement using backreflected spectra through a linear polarizer,” *IEEE J. Lightwave Technol*. 17:1835-1842.

Galtarossa, A., L. Palmieri, M. Schiano, and T. Tambosso. 2000a. “Statistical characterization of fiber random birefringence,” *Opt. Lett.* 25:1322-1324.

Galtarossa, A., L. Palmieri, A. Pizzinat, M. Schiano, and T. Tambosso. 2000b. “Measurement of local beat length and differential group delay in installed single-mode fibres,” *IEEE J. Lightwave Technol*. 18:1389-1394.

Galtarossa, A. and L. Palmieri. 2004a. “Reflectometric measurements of polarization properties in optical-fiber links,” *IEEE J. Trans. on Instrumentation and Measurement*. 53:86-94.

Galtarossa, A. and L. Palmieri. 2004b. “Spatially resolved PMD measurements,” *IEEE J. Lightwave Technol*. 22:1103-1115.

Galtarossa, A., L. Palmieri, and D. Sarchi. 2004c. “Measure of spin period in randomly birefringent low-PMD fibres,” *IEEE Photon. Technol. Lett*. 16:1131-1133.

Galtarossa, A. and C.R. Menyuk (Eds.). 2005. “Optical Fibre Communication Reports,” *Springer*. New York.

Galtarossa, A., L. Palmieri, A. Pizzinat, and L. Schenato. 2006a. “PMD management in unidirectionally spun fiber links,” *Proc. European Conference on Optical Communication, ECOC’06.* Paper We3.P.28.

Galtarossa, A., M. Guglielmucci, L. Palmieri, A. Pizzinat, L. Schenato, and C. G. Someda. 2006b. “Experimental justification of a method for low-PMD measurements,” *IEEE Photon. Technol. Lett*. 18:1228-1230.

Galtarossa, A., P. Griggio, L. Palmieri, A. Pizzinat, and L. Schenato. 2006c. “Polarization properties of randomly-birefringent spun fibers,” *Opt. Fiber Technol*. 12:205-216.

Galtarossa, A., D. Grosso, L. Palmieri, and L. Schenato. 2008a. "Reflectometric measurement of birefringence rotation in single mode optical fibers," *Opt. Lett*. 33:2284-2286.

Galtarossa, A., D. Grosso, L. Palmieri, and L. Schenato. 2008b. "Distributed polarization mode dispersion measurement in fiber links by polarization-sensitive reflectometric techniques,' *IEEE Photon. Technol. Lett*. 20:1944-1946.

Galtarossa, A., D. Grosso, and L. Palmieri. 2009a. "Accurate characterization of twist-induced optical activity in single-mode fibers by means of polarization sensitive reflectometry," *IEEE Photon. Technol. Lett*. 21:1713-1715.

Galtarossa, A., D. Grosso, L. Palmieri, and M. Rizzo. 2009b. "Spin-profile characterization in randomly bire-fringent spun fibers by means of frequency domain reflectometry," *Opt. Lett*. 34:1078-1080.

Gamatham, R. R. G. 2008. "Investigation of polarization mode dispersion measurement performance in optical fibre with a focus on the fixed analyzer technique," *MSc. Thesis, Nelson Mandela Metropolitan University (NMMU).*

Gavioli, G., E. Torrengo, G. Bosco, A. Carena, V. Curri, V. Miot, P. Poggiolini, F. Forghieri, S. J. Savory, L. Molle, and R. Freund. 2010. "NRZ-PM-QPSK 16 ×100 Gb/s transmission over installed fiber with different dispersion maps," *IEEE Photon. Lett*. 22:371-373.

Gené, J. M. and P. J. Winzer. 2010. "First-order PMD outage prediction based on outage maps," *IEEE J. Lightwave Technol*. 28:1873-1881.

Gibbon, T. B. 2007. "Polarization mode dispersion compensation in an optical fibre,' *PhD Thesis, Nelson Mandela Metropolitan University (NMMU).*

Gibbon, T. B., L. Wu, D. W. Waswa, A. B. Conibear, and A. W. R. Leitch. 2008. "Polarization mode dispersion compensation for the South African optical-fibre telecommunication network," *South African J. Sci*. 104:119-123.

Gisin, N., J. P. Von der Weid and J. P. Pellaux. 1991. "Polarization mode dispersion of short and long single-mode fibers," *IEEE J. Lightwave Technol*. 9:821-827.

Gisin, N. and J. P. Pellaux. 1992. "Polarization mode dispersion: Time versus frequency domains," *Opt. Comm*. 89:316-323.

Gisin, N., B. Gisin, J. P. Von der Weid, and R. Passy. 1996. “How accurately can one measure a statistical quantity like polarization-mode dispersion?” *IEEE Photon. Technol. Lett.* 8:1671-1673.

Gisin, N. and R. Huttner. 1997. “Combined effects of polarization mode dispersion and polarization dependent loss in optical fibers,” *Opt. Comm*. 142:119-125.

Gleeson, L., E. Sikora, and M. J. O’Mahoney. 1997. “Experimental and numerical investigation into the penalties induced by second order polarization mode dispersion at 10 Gb/s,” *Proc. European Conference on Optical Communication, ECOC’97.* 15-18.

Gnauck, A. H., P. J. Winzer, S. Chandrasekhar, and C. Dorrer. 2004a. “Spectrally efficient (0.8 b/s/Hz) 1-Tb/s (25 × 42.7 Gb/s) RZ-DQPSK transmission over 28 100-km SSMF spans with 7 optical add/drops,” *Proc. Optical Fiber Communication Conference, OFC’04.* Paper Th4.4.1.

Gnauck, A. H., X. Liu, X. Wei, D. M. Gill, and E. C. Burrows. 2004b. “Comparison of modulation formats for 42.7-Gb/s single-channel transmission through 1980 km of SSMF,” *IEEE Photon. Technol. Lett.* 16:909–911.

Gnauck, A. H., and P. J. Winzer. 2005. “Optical phase-shift-keyed transmission,” *IEEE J. Lightwave Technol.* 23:115–130.

Gordon, J. P. and H. Kogelnik. 2000. “PMD Fundamentals: Polarization mode dispersion in optical fibres,” *Proc. National Academy of Sciences USA.* 97:4541-4550.

Griffin, R. A. and A. C. Carter. 2002a. “Optical differential quadrature phase shift key (oDQPSK) for high-capacity optical transmission,” *Proc. Optical Fiber Communication Conference, OFC’02*. Paper WX6.

Griffin, R. A., R. I. Johnstone, R. G. Walker, J. Hall, S. D. Wadsworth, K. Berry, A. C. Carter, M. J. Wale, J. Hughes, P. A. Jerram, and N. J. Parsons. 2002b. “10 Gb/s optical differential quadrature phase shift key (DQPSK) transmission using GaAs/AlGaAs integration,” *Proc. Optical Fiber Communication Conference, OFC’02.* Paper FD6.

H

Hakki, B. W. 1996. “Polarization mode dispersion in a single mode fiber,” *IEEE J. Lightwave Technol*. 10:2202-2208.

Hamaide, J.–P. 2002. “Linear and nonlinear effects in lightwave transmission: Dispersion management in terrestrial and submarine systems,” *Proc. Optical Fiber Communication Conference, OFC’02.* Tutorial paper.

Hayase, S., N. Kikuchi, K. Sekine, and S. Sasaki. 2003. “Proposal of 8-state per symbol (binary ASK and QPSK) 30 Gb/s optical modulation/demodulation scheme,” *Proc. European Conference on Optical Communication, ECOC’03.* Paper Th2.6.4.

Hayee, M. I. and A. E. Willner. 1999. “NRZ vs RZ in 10–40 Gb/s dispersion-managed WDM transmission systems,” *IEEE Photon. Technol. Lett*. 11:991-993.

Headley, C. and G. P. Agrawal (eds.). 2005. “Raman Amplification in Fiber Optical Communication Systems,” *Academic Press*. California.

Hecht, J. 1999. “Understanding Fiber Optics,” *Prentice Hall*. New Jersey.

Heffner, B. L. 1992. “Automated measurement of polarization mode dispersion using Jones matrix eigenanalysis,” *IEEE Photon. Technol. Lett*. 4:1066-1069.

Hirano, A., Y. Miyamoto, K. Yonenaga, A. Sano, and H. Toba. 1999. “40 Gb/s l-band transmission experiment using SPM-tolerant carrier-suppressed RZ format,” *Elect. Lett.* 35:2213–2215.

Hodzic, A., B. Konrad, and K. Petermann. 2002. “Alternative modulation formats in N× 40 Gb/s WDM standard fiber RZ-transmission systems,” *IEEE J. Lightwave Technol.* 20:598–607.

Hodzic, A., B. Konrad, and K. Petermann. 2003. “Improvement of system performance in N ×40-Gb/s WDM transmission using alternate polarizations,” *IEEE Photon. Technol. Lett*. 15:153-155.

Humblet, P. A. and M. Azizoglu. 1991. “On the bit error rate of lightwave systems with optical amplifiers,” *IEEE J. Lightwave Technol*. 9:1576–1582.

I

Idler, W., S. Bigo, Y. Frignac, B. Franz, and D. Veith. 2001. “Vestigial sideband demultiplexing for ultra high capacity (0.64 bit/s/Hz) transmission of 128 × 40 Gb/s channels,” *Proc. Optical Fiber Communication Conference, OFC’01*. Paper MM3.

Ip, E. 2010. “Nonlinear compensation using backpropagation for polarization-multiplexed transmission,” *IEEE J. Lightwave Technol*. 28:939-951.

Ireeta, W. T., V. Musara, L. Wu, and A. W. R. Leitch. 2010a. "Statistical characterization of the output state of polarization in deployed single mode fibres," *Opt. Lett*. 35:2049-2051.

Ireeta, W. T., V. Musara, L. Wu, and A. W. R. Leitch. 2010b. "Determining the rate of PMD compensation in deployed aerial optical fibres through SOP monitoring," *Proc. Southern Africa Telecommunication Networks and Applications Conference, SATNAC'10*. 261-265.

Ireeta, W. T., V. Musara, and A. W. R. Leitch. 2010c. "A comparison of the tolerance of DQPSK, NRZ and RZ modulation formats in a PMD-induced Environment," *Proc. South Africa Institute of Physics Conference, SAIP'10*.

Islam, M. N., (ed.) 2003. "Raman Amplifiers for Telecommunications 1+2," *Springer*. Verlag, New York.

J

Jeunhomme, L. B. 1983. "Single mode fibre Optics: Principles and Applications," *Marcel Dekker*. New York.

Jones, R. C. 1941. "A new calculus for the treatment of optical systems I," *J. Opt. Soc. Am.* 31:488–503.

Jones, R. C. 1947. "A new calculus for the treatment of optical systems VI," Experimental determination of the matrix," *J. Opt. Soc. Am*. 37:110-112.

Jopson, R. M., L. E. Nelson, and H. Kogelnik. 1999a. "Measurement of second-order PMD vectors in optical fibres," *IEEE Photon. Technol. Lett*. 11:1153-1155.

Jopson, R. M., L. E. Nelson, G. J. Pendock and A. H. Gnauck. 1999b. "Polarization-mode dispersion impairment in return-to-zero and nonreturn-to-zero systems," *Proc. Optical Fiber Communication Conference, OFC'99.* Paper WE3.

Jopson, R., L. E. Nelson, H. Kogelnik, and G. J. Foschini. 2001. "Probability densities of depolarization associated with second-order PMD in optical fibres," *Proc. Optical Fiber Communication Conference, OFC'01*. Paper ThA4.

K

Kabal, P. and S. Pasupathy. 1975. "Partial-response signalling," *IEEE J. Trans. Commun.* COM-23:921–934.

Kaminow, I. P. 1981. "Polarization in optical fibres," *IEEE J. Quantum Electron*. QE-17:15-22.

Karlsson, M., J. Brentel, and P. A. Andrekson. 2000. “Long-term measurement of PMD and polarization drift in installed fibers,” *IEEE J. Lightwave Technol.* 18:941-951.

Keiser, G. 2000. “Optical Fiber Communications,” *McGraw-Hill International Eds*.

Khosravani, R. and A. E. Willner. 2000. “Comparison of different modulation formats in terrestrial systems with high polarization mode dispersion,” *Proc. Optical Fiber Communication Conference, OFC’00.* Paper WL5.

Kim, H. and R.-J. Essiambre. 2003. “Transmission of 8 × 20 Gb/s DQPSK signals over 310-km SMF with 0.8-b/s/Hz spectral efficiency,” *IEEE Photon. Technol. Lett.* 15:769–771.

Kogelnik, H., R. M. Jopson, and L. E. Nelson. 2002. “Polarization-mode dispersion,” in Systems *and Impairments, Optical Fiber Telecommunication IVB,* I. Kaminow and T. Li (Eds.) *Academic Press*. New York. 725–861.

Kramer, G., A. Ashikhmin, A. J. V. Wijngaarden, and X. Wei. 2003. “Spectral efficiency of coded phase-shift keying for fibre-optic communication,” *IEEE J. Lightwave Technol*. 21:2438-2445.

L

Lee, J. H., M. S. Kim, and Y. C. Chung. 2003. “Statistical PMD emulator using variable DGD elements,” *IEEE Photon. Technol. Lett.* 15:54-56.

Lee, S., Y. Xie, O. H. Adamczyk, and A. E. Willner. 2000. “Penalty distribution comparison for different data formats under high PMD values,” *Proc. European Conference on Optical Communication, ECOC’00.* 2:93–94.

Lender, A. 1963. “The duobinary technique for high-speed data transmission,” *IEEE J. Trans. Commun. Electron.* 82:214–218.

Lepley, J. J., J. G. Ellison, S. G. Edirisinghe, A. S. Siddiqui, and S. D. Walker. 2000. “Excess penalty impairments of polarization shift keying transmission format in presence of polarization mode dispersion,” *Elect. Lett*. 36:736-737.

Li, J., G. Biondini, W. L. Kath, and H. Kogelnik. 2010a. “Outage statistics in a waveplate hinge model of polarization-mode dispersion,” *IEEE J. Lightwave Technol*. 28:1958-1968.

Li, J., F. Zhang, and Z. Chen. 2010b. “Electrical dispersion compensation for multichip DPSK detection utilizing MISO DFE,” *IEEE Photon. Technol. Lett*. 22:444-446.

Lu, P., L. Chen, and X. Bao. 2002. “System outage probability due to the combined effect of PMD and PDL,” *IEEE J. Lightwave Technol*. 20:1805-1808.

M

Mabrouki, A., M. Gadonna, A. Guoronnec, R. Goarin, and R. Le Naour. 1998. "Analysis of polarization mode dispersion of single mode elliptic-core optical fibers," *Opt. Comm*. 149:255-260.

Madsen, C. K., J. A. Walker, J. E. Ford, K. W. Goossen, T. N. Nielsen, and G. Lenz. 2000. "A tunable dispersion compensating MEMS all-pass filter," *IEEE Photon. Technol. Lett*. 12:651-653.

Mamyshev, P., B. Mikkelsen, F. Liu, S. Dey, J. Bennike, and C. Rasmussen. 2002. "Spectrally efficient pseudo duo-binary modulation formats for high-speed optical data transmission," *Proc. Conf. Lasers and Electro-Optics, CLEO'02*.

Marcuse, D. and C. R. Menyuk. 1998. "Simulation of single-channel optical systems at 100 Gb/s," *IEEE J. Lightwave. Technol.* 17:564–569.

Miyamoto, Y., A. Hirano, K. Yonenaga, A. Sano, H. Toba, K. Murata, and O. Mitomi. 1999. "320-Gb/s (8 × 40 Gb/s) WDM transmission over 367-km with 120-km repeater spacing using carrier-suppressed return-to-zero format," *Elect. Lett.* 35:2041–2042.

Mollenauer, L. F. and J. P. Gordon. 1994. "Birefringence-mediated timing jitter in soliton transmission," *Opt. Lett*. 19:375-377.

Mudau, A. E. 2008. "Characterization of polarization effects on deployed aerial optical fibre in South Africa," *MSc. thesis, Nelson Mandela Metropolitan University (NMMU).*

Musara, V. 2009a. "Polarization mode dispersion emulation and the impact of high first order PMD segments in optical telecommunication systems," *PhD thesis, Nelson Mandela Metropolitan University (NMMU).*

Musara, V., L. Wu, and A. W. R. Leitch. 2009b. "A polarization mode dispersion emulator with tunable first-order PMD and constant second-order PMD," *Opt. Comm.* 282:3270-3274.

Musara, V., L. Wu, G. Pelaelo, and A. W. R. Leitch. 2009c. "PMD emulation using polarization maintaining fibres: Fixed root-mean-square DGD but varying second-order PMD," *Rev. Sci. Instrum.* 80:1-5.

Musara, V., S. Younsi, L. Wu, M. Zghal, and A. W. R. Leitch. 2009d. "Statistical characterization of combined first and second-order polarization mode dispersion in a deployed fibre cable," *Proc. IEEE Africon*. 1-6.

N

Nelson, L. E., R. Jopson, H. Kogelnik, and G. J. Foschini. 1999. “Measurement of depolarization and scaling associated with second-order PMD in optical fibres,” *IEEE Photon. Technol. Lett*. 11:1614-1616.

Nelson, L. E., M. Karlsson, and D. Q. Chowdhury. 2004. “Special issue on polarization mode dispersion,” *IEEE J. Lightwave Technol*. 22:951-952.

Namihira, Y. and J. Maeda. 1992. “Polarization mode dispersion measurements in optical fibres,” *Proc. Symp. Opt. Fiber Measurements, SOFM’92.*145-150.

O

Oberson, P., K. Julliard, N. Gisin, R. Passy, and J. P. Von der Weid. 1996. “Interferometric polarization mode dispersion measurements with femtoseconds sensitivity,” *Proc. Symp. Opt. Fiber Measurements, SOFM’96.*143-146.

Ohm, M. and J. Speidel. 2003. “Quaternary optical ASK-DPSK and receivers with direct detection,” *IEEE Photon. Technol. Lett*. 15:159-161.

Ohm, M. 2004. “Optical 8-DPSK and receiver with direct detection and multilevel electrical signals,” *Proc. IEEE/LEOS Workshop Advanced Modulation Formats*. 45-46.

Olsson, N. A. 1989. “Lightwave systems with optical amplifiers,” *IEEE J. Lightwave Technol.* 7:1071–1082.

Ono, T., Y. Yano, K. Fukuchi, T. Ito, H. Yamazaki, M. Yamaguchi, and K. Emura. 1998. “Characteristics of optical duobinary signals in terabit/s capacity, high-spectral efficiency WDM systems,” *IEEE J. Lightwave Technol.* 16:788–797.

P

Palmieri, L., A. Galtarossa, and T. Geister. 2010a. “Distributed characterization of bending effects on the birefringence of single mode optical fibers,” *Opt. Lett*. 35:2481-2483.

Palmieri, L., T. Geisler, and A. Galtarossa. 2010b. “Distributed characterization of bending-induced birefringence in spun fibers by means of P-OFDR,” *OFC/NFOEC’10*. Paper OWS2.

Pan, S. and J. Yao. 2010. “UWB-over-fiber communications: Modulation and Transmission,” *IEEE J. Lightwave Technol*. 28:2445-2455.

Penninckx, D., L. Pierre, J.-P. Thiery, B. Clesca, M. Chbat, and J. L. Beylat. 1996. “Relation between spectrum bandwidth and the effects of chromatic dispersion in optical transmissions,” *Electron. Lett.* 32:1023–1024.

Pfennigbauer, M., M. Pauer, P. J. Winzer, and M. M. Strasser. 2002. ‘Performance optimization of optically preamplified receivers for return-to-zero and nonreturn-to-zero coding’, *Int. J. Electron. Comm.* 56:261–267.

Phua, P. B. and H. A. Haus. 2002. “Variable second-order PMD module without first-order PMD,” *IEEE J. Lightwave Technol.* 20:1951-1956.

Poole, C. D. and R. E. Wagner. 1986. “Phenomenological approach to polarization dispersion in long single-mode fibres,” *Elect. Lett*. 22:1029-1030.

Poole, C. D. 1988a. “Statistical treatment of polarization dispersion in single mode fibre,” *Opt. Lett*. 13:687-689.

Poole, C. D. and C. R. Giles. 1988b. “Polarization-dependent pulse compression and broadening due to polarization dispersion in dispersion-shifted fiber,” *Opt. Lett*. 13:155-157.

Poole, C. D., N. S. Bergano, R. E. Wagner, and H. J. Schulte. 1988c. “Polarization dispersion and principal states in a 147-km undersea lightwave cable,” *IEEE J. Lightwave Technol*. LT-6:1185-1190.

Poole, C. D., J. H. Winters, and J. A. Nagel. 1991. “Dynamical equation for polarization dispersion,” *Opt. Lett*. 16:372-374.

Poole, C. D. and D. L. Favin. 1994. “Polarization-mode dispersion measurements based on transmission spectra through a polarizer,” *IEEE J. Lightwave Technol*. 12:917-929.

Proakis, J. G. 2001. “Digital Communications,” *4th ed. McGraw-Hill*. New York.

R

Rashleigh, S. C. 1983. “Origins and control of polarization effects in single-mode fibers,” *IEEE J. Lightwave Technol*. LT-1:312-331.

Raybon, G., S. Chandrasekhar, A. Agarwal, A. H. Gnauck, J. S. L. L. Buhl, and A. Adamiecki. 2004. “Limitations of optical add/drop filtering on 42.7-Gb/s transmission with 50-GHz channel spacing,” *Proc. European Conference on Optical Communication, ECOC’04.* Paper Mo4.5.1.

Raybon, G. 2006. “Performance of advanced modulation formats in optically routed networks,” *Proc. Optical Fiber Communication Conference, OFC’06.* Paper OThR1.

Roberge, R. 2009. “Case study: PMD measurement on aerial fibre under wind-induced oscillations and vibrations,” *EXFO Electro-Optical Engineering Inc*. Technical Note 039.

Rogers, A. J. 1981. “Polarization-optical time domain reflectometry: a technique for the measurement of field distributions,” *Appl. Opt*. 20:1060-1074.

S

Schinn, G. W. 2003. “Polarization and the patchcord,” *EXFO Electro-Optical Engineering Inc*. Technical Note 008.

Sekiya, K., T. Ito, H. Sugahara, K. Fukuchi, R. Ohhira, and T. Ono. 2003. “Flexible 40 Gb/s WDM transmission beyond 1000 km enabled by 195 μm^2 *A*eff PSCF and AC-RZ signal format,” *Elect. Lett.* 39:386–388.

Shen, T. S. R., A. P. T. Lau, and G. N. Liu. 2010. “OSNR monitoring for higher order modulation formats using asynchronous amplitude histogram,” *IEEE Photon. Technol. Lett*. 22:1632-1634.

Shieh, W. 1999. “Principal states of polarization for an optical pulse,” *IEEE Photon. Technol. Lett*. 11:677-679.

Shtaif, M. and A. Mecozzi. 2000. “Study of the frequency autocorrelation of the differential group delay in fibres with polarization mode dispersion,” *Opt. Lett*. 25:707-709.

Stark, J. B., J. E. Mazo, and R. Laroia. 1998. “Phased amplitude-shift signalling (PASS) codes: Increasing the spectral efficiency of DWDM transmission,” *Proc. European Conference on Optical Communication, ECOC’98.* 373–374.

Sunnerud, H. 2001. “Polarization-mode dispersion in optical fibres: characterization, transmission impairments, and compensation,” *PhD Thesis, Chalmers University of Technology*.

Sunnerud, H., M. Karlsson, C. Xie, and P. A. Andrekson. 2002. “Polarization-mode dispersion in high speed fibre-optic transmission systems,” *IEEE J. Lightwave Technol.* 20:2204-2219.

Suzuki, K., I. Nakamatsu, T. Shimoda, S. Takaesu, J. Ushioda, E. Mizuki, M. Horie, Y. Urino, and H. Yamazaki. 2004. "WDM tuneable dispersion compensator with PLC ring resonators," *Optical Fiber Communication Conference, OFC'04.* Technical Digest. Paper WK3.

T

Taga, H., M. Suzuki, and Y. Namihira. 1998. "Polarization mode dispersion tolerance of 10Gbit/s NRZ and RZ optical signals," *Elect. Lett*. 34:2098-2100.

TIA/EIA FOTP-122. 1999. "Polarization mode dispersion measurement for single mode optical fibres by Stokes parameter evaluation," *Telecommunications Industry Association (TIA) Std.* Arlington, VA.

TIA/EIA 455-124-A (FOTP-124A). 2004. "Polarization mode dispersion measurement for single mode optical fibres by interferometry," *Telecommunications Industry Association (TIA) Std.* Arlington, VA.

Tokle, T. 2004. "Optimised dispersion management and modulation formats for high speed optical communication systems," *PhD dissertation, Technical University of Denmark.*

Tomita, A. and R. Y. Chiao. 1986. "Observation of Berry's topological phase by use of an optical fiber," *Phys. Rev. Lett*. 57:937-940.

Tomita, S., M. Kawase, T. Shinohara, and H. Fuchigami. 1988. "Suppression of galloping oscillations for a self-supporting optical fibre," *IEEE J. Lightwave Technol*. 6:186-190.

Trischitta, P. R. and W. C. Marra. 1996. "Global undersea communication networks," *IEEE Communication Magazine.* 34:20-21.

Tsuritani, T., A. Agata, I. Morita, K. Tanaka, and N. Edagawa. 2001. "Performance comparison between DSB and VSB signals in 20 Gb/s based ultra-long-haul WDM systems," *Proc. Optical Fiber Communication Conference, OFC'01*. Paper MM5.

U

Ulrich, R. and A. Simon. 1979. "Polarization optics of twisted single-mode fibers," *Appl. Opt*. 18:2241-2251.

V

Vacondio, F., A. Ghazisaeidi, A. Bononi, and L. A. Rusch. 2009. "DQPSK: When is a narrow filter receiver good enough?," *IEEE J. Lightwave Technol*. 27:5106-5114.

Van den Borne, D., S. L. Jansen, G. D. Khoe, H. de Waardt, and E. Gottwald. 2006a. "Line optimization in long-haul transmission systems with 42.8-Gb/s RZ-DQPSK modulation," *Proc. Optical Fiber Communication Conference, OFC'06.* Paper OFD2.

Van den Borne, D., S. L. Jansen, G. D. Khoe, H. de Waardt, and E. Gottwald. 2006b. "A comparison between multi-level modulation formats: 21.4-Gb/s RZ-DQPSK and POLMUX-RZ-DPSK," *Proc. Optical Fiber Communication Conference, OFC'06.* Paper OThR2.

Van Wiggeren, G. D., A.R. Motamedi, and D.M. Baney. 2003. "Single scan interferometric component analyzer," *IEEE Photon. Technol. Lett*. 15:263-265.

W

Waddy, D. S., P. Lu, L. Chen, and X. Bao. 2001. "Fast state of polarization changes in aerial fibre under different climatic conditions," *IEEE Photon. Technol. Lett*. 13:1035-1037.

Waddy, D. S., L. Chen, and X. Bao. 2002. "Theoretical and experimental study of the dynamics of polarization-mode dispersion," *IEEE Photon. Technol. Lett*. 14:468-470.

Waddy, D. S., L. Chen, and X. Bao. 2005. "Polarization effects in aerial fibers," *Opt. Fiber Technol*. 11:1-19.

Walklin, S. and J. Conradi. 1997. "On the relationship between chromatic dispersion and transmitter filter response in duobinary optical communication systems," *IEEE Photon. Technol. Lett.* 9:1005–1007.

Walklin, S. and J. Conradi. 1999. "Multilevel signalling for increasing the reach of 10 Gb/s lightwave systems," *IEEE J. Lightwave Technol*. 17:2235-2248.

Wang, J. and J. M. Kahn. 2004. "Impact of chromatic and polarization-mode dispersions on DPSK systems using interferometric demodulation and direct detection," *IEEE J. Lightwave Technol.* 22:362–371.

Watts, P. M., V. Mikhailov, M. Glick, P. Bayvel, and R. I. Killey. 2004. "Single sideband optical signal generation and chromatic dispersion compensation using digital filters," *Elect. Lett.* 40:958–960.

Williams, P. A. 1999. "Modulation phase-shift measurement of PMD using only four launched polarization states: a new algorithm," *Elect. Lett*. 35:1578-1579.

Williams, P. A. 2004. "PMD measurement techniques and how to avoid pitfalls," *J. Opt. Fibre. Comm.* Rep. 1:84-105.

Willner, A. E., S. M. R. M. Nezam, L. Yan, Z. Pan, and M. C. Hauer. 2004. "Monitoring and control of polarization-related impairments in optical fiber systems," *IEEE J. Lightwave Technol.* 22:106-125.

Winzer, P. J. and A. Kalmar. 1999. "Sensitivity enhancement of optical receivers by impulsive coding," *IEEE J. Lightwave Technol.* 17:171–177.

Winzer, P. J., A. H. Gnauck, G. Raybon, S. Chandrasekhar, Y. Su, and J. Leuthold. 2003a. "40-Gb/s alternate-mark-inversion return-to-zero (RZ-AMI) transmission over 2000 km," *IEEE Photon. Technol. Lett.* 15:766–768.

Winzer, P. J., H. Kogelnik, C. H. Kim, H. Kim, R. M. Jopson, L. E. Nelson, and K. Ramanan. 2003b. "Receiver impact on first-order PMD outage," *IEEE Photon. Technol. Lett.* 15:1482–1484.

Winzer, P. J., R.-J. Essiambre, and S. Chandrasekhar. 2004. "Dispersion tolerant optical communication systems," *Proc. European Conference on Optical Communication, ECOC'04.* Paper We2.4.1.

Winzer, P. J. and R.-J. Essiambre. 2006a. "Advanced optical modulation formats," *Proc. IEEE*. 94:952-985.

Winzer, P. J. and R.-J. Essiambre. 2006b. "Advanced modulation formats for high-capacity optical transport networks," *IEEE J. Lightwave Technol*. 24:4711-4728.

Woodward, S., S. Y. Huang, M. Feuer, and M. Boroditsky. 2003. "Demonstration of an electronic dispersion compensator in a 100 km 10 Gb/s ring network," *IEEE Photon. Technol. Lett.* 15:867-869.

Wooten, E. L., K. M. Kissa, A. Yi-Yan, E. J. Murphy, D. A. Lafaw, P. F. Hallemeier, D. Maack, D. V. Attanasio, D. J. Fritz, G. J. McBrien, and D. E. Bossi. 2000. "A review of Lithium Niobate Modulators for fibre-optic communication systems," *IEEE J. Selected Topics in Quantum Electronics.* 6:69-82.

Wree, C., J. Leibrich, J. Eick, and W. Rosenkranz. 2003. "Experimental investigation of receiver sensitivity of RZ-DQPSK modulation format using balanced detection," *Proc. Optical Fiber Communication Conference, OFC'03.* Paper ThE5.

Wree, C., D. Becker, D. Mohr, and A. Joshi. 2007. "Measured noise performance for heterodyne detection of 10-Gb/s OOK and DPSK," *IEEE Photon. Technol. Lett*. 19:15-17.

Wuttke, J., P. M. Krummrich and J. Rösch. 2003. “Polarization oscillations in aerial fiber caused by wind and power-line current,” *IEEE Photon. Technol. Lett*. 15:882-884.

X

Xie, C., I. Kang, A. H. Gnauck, L. Moller, L. F. Mollenauer, and A. R. Grant. 2004. “Suppression of intra-channel nonlinear effects with alternate-polarization formats,” *IEEE J. Lightwave Technol.* 22:806-812.

Y

Yoshikane, N. and I. Morita. 2005. “1.14 b/s/Hz spectrally efficient 50×85.4-Gb/s transmission over 300 km using co-polarized RZ-DQPSK signals,” *IEEE J. Lightwave Technol.* 23:108–114.

Z

Zalevsky, Z. and V. Eckhouse. 2004. “Polarization-mode dispersion manipulation using periodic polarization modulation,” *J. Opt. A: Pure Applied Optics.* 6:862-864.

Zhang, Z., X. Bao, Q. Yu, and L. Chen. 2007. “Time evolution of PMD due to tides and sun radiation on submarine fibers,” *Opt. Fiber Technol*. 13:62-66.

Zheng, X., F. Liu, and P. Jeppesen. 2001. “Receiver optimization for 40-Gb/s optical duobinary signal,” *IEEE Photon. Technol. Lett.* 13:744–746.